Università degli Studi di Salerno
Facoltà di Scienze Matematiche Fisiche e Naturali

Doctor Thesis in Chemistry

Towards the rational design of new catalysts for organic transformations

Supervisor
Prof. Luigi Cavallo

Candidate
Laura Falivene

Table of Contents

Introduction

Computational chemistry has emerged as a subfield of theoretical chemistry, focused on solving chemically related problems by calculations. Computational chemistry can be considered as a powerful microscope that can help theoreticians and experimentalists to understand the details of a chemical process at molecular level.

Indeed, thanks to modern advanced theoretical methodologies and to the stronger computer power and speed, computer simulations are able to direct calculate mechanical properties, dynamics of reaction processes, conformational changes, and more. Computer simulations connect microscopic length and time scales of the in-silico experiments to the macroscopic world of the laboratory: on one hand calculations could provide a guess at the interactions between molecules and obtain predictions of properties, obviously the accuracy is limited to the computer power (and budget) and to the chosen theory level; on the other hand a theory could be tested by comparing the simulation results with the experiments, after that, if the model works, it can be used to test the behavior of the systems at several conditions or to test structural differences in the systems, adding new data to those available experimentally.

Most of the theoretical methods are applied to isolated molecules, which correspond to the state of an ideal gas phase. Since most chemical processes take place in the condensed phase, and the interaction of the reacting species with its environment it's relevant, for example by coordination to the metal center or by formation of hydrogen bonds, it can be necessary to include solvent molecules in the calculation. Depending on the size of the solvent molecules and the number of solvent molecules needed, the overall size of the system and the resulting computational effort can be significantly increased. Nevertheless, if there are no specific solute-solvent interactions, the main solvent effect of the solvent is electrostatic and it depends on its dielectric constant. This contribution can be

described by continuum solvation models, which allows to have quite reliable solvation energies with minimal computational costs.

Catalysis and the route to new catalysts

Catalysis in its broad term is estimated to contribute to roughly 30% of the global gross world product. Catalysts and catalytic processes are fundamental in many areas, spanning from massive production such as oil refining, energy production and agrochemicals, to high added value applications in the pharma industry and in the synthesis of advanced materials.

In principle most of catalysts were in the solid state, heterogeneous catalysts, but in the last decades homogeneous catalysts become more and more important, thanks to the development of a large range of ligand frameworks that have been used to tune the behavior of various systems. In many cases, the final industrial implementation is associated to a heterogenized catalyst, by grafting the homogenous transition metal complex to an inert support.

Developing better performing catalysts (more selective, stable and active, as well as energetically and environmentally friendly), or catalysts leading to the synthesis of new materials, remains a topic of primary relevance in the academy as well as in the industry.

Nevertheless, the search for new catalysts is often driven by the "trial and error" approach, based on the more or less systematic scanning of the catalytic space to find well performing catalysts by trying out different times practical experiments and experiences without the use of a rational organized theory and methodology; in short, by shooting "blindly" until the good catalyst is found. On one hand, trial and error is an extremely powerful tool that can lead to discovery of really unpredictable catalysts. On the other side, it also has some weaknesses, like the great consumption of time, the waste of money and the absence of a clearly defined route that should be followed to obtain better catalysts.

In this brute force approach to novel catalysts, computational techniques can be of enormous value to screen novel catalyst architectures more rapidly to obtain insights that could help in the design and experimental synthesis of novel and improved catalysts.
DFT-based prediction of the reactivity of new catalysts is not a new approach, and systematic methods are sought for a priori computational prediction to see whether a catalyst will be feasible experimentally, productive and fruitful in the industry.
To improve catalysts, a detailed insight into the reaction pathways and a deep characterization of the catalyst itself is needed. The complete understanding of all steps in a complicated mechanism is rather difficult experimentally, but can be often achieved by computations. Once the mechanism has been clarified and the crucial parameters are found, new hypothesis for more performing catalysts can be deduced and can be tested by calculations.
A completely different approach to the development of new catalysts is based on a rationalization of the catalytic space. Indeed, the catalysts space is perceived as a disorganized space where a limited number of well performing catalysts is spread in a plethora of ineffective catalysts. Reorganizing this chaotic space to have a continuous gradation of catalysts from bad ones to well performing ones is in principle possible, through the development of molecular descriptors.
Probably, the most popular molecular descriptors are the Tolman cone angle and the Tolman electronic parameter, used to quantify steric and electronic effects in
phosphines. Indeed, when a good descriptor is available, an accurate screening of a wide range of structures can be done by calculations, in such way that only the most promising catalysts have to be tested experimentally. In this way the route towards new catalysts can be easier and shorter.

Objectives

This PhD thesis is clearly focused on the "rational" side of the different approaches for developing new catalysts, either by strict collaboration with experimental groups to rationalize the behavior of catalysts in development, or through the development of molecular descriptors for the quantification of steric and electronic effects in transition metal based catalysts.
In particular, the attention has been focused mainly on catalytic systems based on N-heterocyclic carbene (NHC) ligands.
The work has been divided in the two following sections listed below.

- Chapter 3 : Steric and electronic tools to characterize organometallic complexes. Fundamental structural complex properties.

- Chapter 4 : NHC-systems catalytic activity: metathesis of alkenes and alkynes catalyzed by ruthenium complexes; cross coupling reactions catalyzed by palladium complexes; organo-polymerization.

Cap.1 Theoretical background

Computer modeling and simulation are widely accepted as a tool that can help to study the properties of chemical and biological systems and to generate new scientific understandings to move in the right way towards the effective design of catalysts.
The strength of this field is the possibility to rationalize experimental results allowing gain in terms of human time, money (saving on reagents, solvent and disposals) and environmental care.
In general, with computational chemistry it is possible to study the relative stability of molecules, to characterize the species along reaction pathways and the thermodynamics and the kinetic of the reactions, to understand the bond strengths, to rationalize and predict the behavior of some classes of complexes, to obtain spectroscopic information, to quantify intra and inter-molecular forces and more.

1.1 Born-Oppenheimer approximation

The non-relativistic Hamiltonian of a system of n particles contains kinetic (T) and potential (V) energy for all particles, nuclei and electrons.

$$H_{tot}= T_n+T_e+V_{ne}+ V_{ee}+ V_{nn}$$

Where the potential energy operator is the Coulomb potential. In order to solve the complete quantum mechanical problem, the eigenfunctions and eigenvalues of this Hamiltonian have to be sought, which will be given by the solution of the Schrodinger equation. Clearly, an exact solution of this equation is not possible and approximations must be made.
The Born-Oppenheimer approximation can be invoked, considering that there is a strong separation of timescales between the electronic

and nuclear motion, since the electrons are lighter than the nuclei by three orders of magnitude.
The Schrodinger equation can therefore be separated into one part which describes the electronic wave function for a fixed nuclear geometry, and another part which describes the nuclear wave function, where the energy from the electronic wave function plays the role of a potential energy.
As consequence,

$$\Psi(r,R) = \emptyset(x,R)X(R)$$

where R is used to denote the nuclear coordinates and r to denote the electron ones.

It should be noted that nuclei are heavy enough for quantum effects to be almost negligible and that electrons respond instantaneously to the nuclear motion.
As consequence, the main effort is to calculate the electronic Schrodinger for a given nuclear configuration.

1.2 Density functional theory (DFT)

The density functional theory is a method to resolve the electronic structure of a system by using a functional (that is a function of another function), the electron density. This theory is based on one-to-one correspondence that exists between ground-state electronic densities and external potential, as stated by the Hohenberg-Kohn theorems. The ground state density, n_0 (r), is given in terms of the ground-state wave-function by:

$$n_0(\mathrm{r}) = \sum_{s_1,\ldots,s_{N_c}} \int dr_2 \ldots dr_{N_c} \left|\emptyset_0\left(r,s,r_2,s_2,..r_2,s_2\right),\ldots..,s_{N_c}\right|^2$$

where r and s represent a single position and spin variable, respectively.

A consequence of the Hohenberg-Kohn theorems is that the exact ground state energy, ε_0(R), can be obtained by minimizing a certain functional, ε[n], over all electronic densities n(r).

The functional ε(n) is given as a sum, T(n) + W(n) + V(n), where T(n) and W(n) represent the kinetic energy and Coulomb repulsion energies, respectively, and V(n) = $\int d(r)V_{eN}$(r) n (r).

Although the functional T(n) +W(n) is universal for all systems of N_e electrons, its form is not known.

Thus, Kohn and Sham (KS) introduced the idea of a non-interacting reference system with a potential $V_{KS}(r, R)$, such that the ground state energy and density of the non-interacting system equal those of the true interacting system.[1]

Within the KS formulation of DFT, a set of n_{occ} orthonormal single particle orbitals, Ψ_i(r), i = 1,…, n_{occ}, with occupation numbers f_i, where $\sum_{i=1}^{n_{occ}} f_i = N_e$,is introduced. These are known as the KS orbitals.

In term of the KS orbitals, the density is given by

$$n(\mathrm{r}) = \sum_{i=1}^{n_{occ}} f_i \, |\Psi_i(r)|^2$$

And the functional takes the form

$$\varepsilon[\{\Psi_\mathrm{i}\}] = -\frac{h^2}{2m} \sum_{i=1}^{n_{occ}} f_i < \Psi_i|\nabla^2|\Psi_i > \; + \frac{e^2}{2} \int dr \, dr' \, \frac{n(r)n(r')}{|r-r'|} + \varepsilon_{XC}[n] + \int drdn(r)V_{eN}\,(r,R) \equiv \; T_{nonint}[\{\Psi\}] + J[n] + \varepsilon_{XC}[n] + V[n]$$

The first term in the functional represents the quantum kinetic energy, the second is the direct Coulomb term from Hartree-Fock theory, the third term is the exact exchange-correlation energy, whose form is unknown, and the fourth term is the interaction of the electron density with the external potential due to the nuclei. Thus, the KS potential is given by

$$V_{KS}(r,R) = \frac{e^2}{2}\int dr' + V_{eN}(r,R)$$

And the Hamiltonian of the non-interacting system is, therefore,

$$H_{KS} = -\frac{h^2}{2m}\nabla^2 + V_{KS}(r,R)$$

The KS orbitals will be the solutions of a set of self-consistent equations known as the Khon-Sham equations

$$H_{KS\Psi_i}(r) = \varepsilon_i \Psi_i(r)$$

Where ε_i are the KS energies. The last equation constitutes a self-consistent problem because the KS orbitals are needed to compute the density, which is needed, in turn, to specify the KS Hamiltonian. However, the latter must be specified in order to determine the orbitals and orbital energies.

The preceding discussion makes clear the fact that DFT, is in principle, an exact theory for the ground state of system. However, because the exchange-correlation functional, defines as formula, is unknown, in practice, approximations must be made.

One of the most successful approximations is the so called local density approximation (LDA), in which the functional is taken as the spatial integral over a local function that depends only on the density:

$$\varepsilon_{XC}[n] \approx \int dr f_{LDA}(n(r))$$

The LDA is physically motivated by the notion that the interaction between the electrons and the nuclei creates only weak inhomogeneities in the electron density. Therefore, the form of LDA is obtained by evaluating the exact expressions for the

exchange and correlation energies of a homogeneous electron gas of uniform density *n* at the inhomogeneous density *n* (r).
In many instances of importance in chemistry, however, the electron density possesses sufficient inhomogeneities that the LDA beaks down. It could be improved by adding an additional dependence on the lowest order gradients of the density:

$$\varepsilon_{XC}[n] \approx \int dr f_{GGA}\,(n(r), |\nabla^2 n(r|)$$

which is known as the generalized gradient approximation (GGA). Among the most used GGAs are those of Becke, Lee and Parr, Perdew and Wang, Perdew, Becke and Ernzerhof, and Cohen and Handy. Tipically, these can be calibrated to reproduce some set of the known properties. However, GGAs, are also know to understimate transition state barriers and cannot adequately treat dispersion forces. Attempts to incorporate dispersion interactions in an empirical way have recently been proposed. In order to improve reaction barriers, new approximation schemes such as Becke's 1992 functional, which incorporates exact exchange, and the so-called meta-GGA functionals, which include an additional dependence on the electron kinetic energy density

$$\tau(r) = \sum_{i=1}^{n_{occ}} f_i\, |\nabla\, \emptyset_i(r)|^2$$

have been proposed with reasonable success. However, the problem of designing accurate approximate exchange-correlation functionals remains one of the greatest challenges in DFT.

1.3 Basis set

Molecular orbitals are created using set of functions (called basis functions) which are combined in linear combinations (generally as

part of a quantum chemical calculation). Obviously, complete basis would mean that an infinitive number of functions must be used, which is impossible in actual calculations. As consequence, finite set of basis functions are used.

For convenience these functions are typically atomic orbitals centered at each atomic nucleus within the molecule. These atomic orbitals are well described with Slater-type orbitals (STOs), as STOs decay exponentially with distance from the nuclei, accurately describing the long-range overlap between atoms, and reach a maximum at zero, well describing the charge and spin at the nucleus. STOs are computationally difficult, for this reason they are approximated as linear combinations of Gaussian orbitals instead. This leads to huge computational savings because it is easier to calculate overlap and other integrals with Gaussian basis functions.

The most important factor is the number of functions to be used. Today, there are hundreds of basis sets composed of Gaussian-type orbitals (GTOs). The smallest of these are called minimal basis sets, and they are typically composed of the minimum number of basis functions required to represent all electrons on each atom.

The minimum basis set is the one in which on each atom in the molecule a single basis function is used for each orbital. However, for atoms such as lithium, basis functions of p type are added to the basis functions corresponding to the 1s and 2s orbitals of the free atom. For example, each atom in the second period of the periodic system (Li - Ne) would have a basis set of five functions (two s functions and three p functions).

The next improvement in the basis set is a doubling of all basis functions, producing a Double Zeta (DZ) type basis, or a tripling of them, Triple Zeta (TZ).

Another common addition to minimal basis set is the addition of polarization functions, denoted by an asterisk,*. Two asterisks,**, indicate that polarization functions are also added to light atoms (hydrogen and helium). These are auxiliary functions with one additional node.

Another common addition is the diffuse function, denoted by a plus sign +, or by "aug" (from "augmented"). Two plus signs indicate that diffuse functions are also added to light atoms (hydrogen and helium). These are very shallow Gaussian basis functions, which more accurately represent the "tail" portion of the atomic orbitals, which are distant from the atomic nuclei. These additional basis functions can be important when considering anions and other large, "soft" molecular systems.

During most molecular bonding, it is the valence electrons which principally take part in the bonding. In recognition of this fact, it is common to represent valence orbitals by more than one basis function (each of which can in turn be composed of a fixed linear combination of primitive Gaussian functions). Basis sets in which there are multiple basis functions corresponding to each valence atomic orbital are called valence double, triple, quadruple-zeta, and so on, basis sets (zeta, ζ, was commonly used to represent the exponent of an STO basis function).

The notation for the split-valence basis sets arising from the group of John Pople is typically X-YZg. In this case, X represents the number of primitive Gaussians comprising each core atomic orbital basis function. The Y and Z indicate that the valence orbitals are composed of two basis functions each, the first one composed of a linear combination of Y primitive Gaussian functions, the other composed of a linear combination of Z primitive Gaussian functions.

Other split-valence basis sets often have rather generic names such as: SVP, DZV, TZV, TZVPP, QZVPP.

For systems involving elements from the third row or higher in the periodic table there is a large number of core electrons which in general are unimportant for the chemical reactivity. However, it is necessary to use a large number of basis functions to expand the corresponding orbitals, otherwise the valence orbitals will not be well described due to a bad description of the electron-electron repulsion. The common approach used is the introduction of an Effective Core Potential (ECP), also called pseudopotential, to

represent all the core electrons. In other words, the core electrons are modeled as a suitable function, and only the valence electrons are treated explicitly.
In addition to localized basis sets, plane-wave basis sets can also be used in quantum-chemical simulations. Typically, a finite number of plane-wave functions are used, below a specific cutoff energy which is chosen for a certain calculation. These basis sets are popular in calculations involving periodic boundary conditions. In practice, plane-wave basis sets are often used in combination with an 'effective core potential' or pseudopotential, so that the plane waves are only used to describe the valence charge density. This is because core electrons tend to be concentrated very close to the atomic nuclei, resulting in large wave-function and density gradients near the nuclei which are not easily described by a plane-wave basis set unless a very high energy cutoff, and therefore small wavelength, is used. This combined method of a plane-wave basis set with a core pseudopotential is often abbreviated as a PSPW calculation.

1.4 Programs

Gaussian

In this thesis the Gaussian suite program has been used has the primary tool to locate structures along reaction pathways. Gaussian is a computer program initially released in 1970 by John Pople and his research group at Carnegie-Mellon University as Gaussian 70. It has been continuously updated since then.
The name originates from Pople's use of Gaussian orbitals to speed up calculations compared to those using Slater-type orbitals, a choice made to improve performance on the limited computing capacities of then current computer hardware.
The current version of the program is Gaussian 09.[2] Originally available through the Quantum Chemistry Program Exchange, it was later licensed out of Carnegie Mellon University, and since 1987 has been developed and licensed by Gaussian, Inc.

ADF

The ADF program has been used in this work thesis to perform a detailed energy bond decomposition analysis when needed.

Amsterdam Density Functional (ADF) is a program for first-principles electronic structure calculations that makes use of density functional theory (DFT).

ADF was first developed in the early seventies by the group of E. J. Baerends from the Vrije Universiteit in Amsterdam, and by the group of T. Ziegler from the University of Calgary. Nowadays many other academic groups are contributing to the software. Scientific Computing & Modelling (SCM), a spin-off company from the Baerends group, coordinates the development and distribution of ADF since 1995. Together with the rise in popularity of DFT over the last decade, ADF has become a popular computational chemistry software package used in the industrial and academic research. The ADF program 10 was used.[3,4]

Computational recipe

DFT calculations. The DFT static calculations were performed at the GGA level with the Gaussian 09 set of programs, using the BP86 functional of Becke and Perdew.[5,6,7] The electronic configuration of the molecular systems was described with the standard split-valence basis set with a polarization function of Ahlrichs and co-workers for H, B, C, N, O, Cl, P, F, Si (SVP keyword in Gaussian).[8] For metal atoms the small-core, quasi-relativistic Stuttgart/Dresden effective core potential, with the associated triple-ζ valence basis set (standard SDD keywords in Gaussian)[9,10,11] was used. The geometry optimizations were performed without symmetry constraints, and the characterization of the located stationary points was performed by analytical frequency calculations. The potential energies have been obtained via single point energy calculations with M06[12,13] functional with the triple-ζ basis set of Ahlrichs for main atoms (TZVP keyword in Gaussian09), augmented with a diffuse d function for Cl and O atoms when anionic ligands are involved.[14] Free energies have been obtained including to these electronic energies zero point energy and thermal corrections from the gas-phase frequency

calculations at the BP86/SVP level. Solvent effects have been estimated in single point calculations on the gas phase optimized structures, based on the polarizable continuous solvation model PCM.[15, 16]

Energy decomposition analysis has been performed using the Amsterdam Density Functional (ADF) program. The electronic configuration of the molecular systems was described by a triple–ζ STO basis set with a polarization function (ADF basis set TZP). In these calculations the Gaussian09 geometries were used. The local exchange-correlation potential by Vosko et al., augmented in a self-consistent manner with Becke's exchange gradient correction and Perdew's correlation gradient correction was used in this analysis.

$\%V_{Bur}$ and Topographic steric maps. Calculating the $\%V_{Bur}$ requires the definition of the metal M centre to which the ligand is coordinated. If the structure to be examined is a transition metal complex, it can be natural to use the coordinates of the metal centre as in the structure. In the case of phosphines, for examples, it is the P atom that is coordinated to the putative metal centre.

The M centre is located on the line passing through the point to be coordinated and the centre of mass of the atoms chosen.

Once the position of the M centre is defined, a sphere of radius R, centred on M, is built. This sphere is sectioned by a regular 3D cubic mesh of spacing s, which defines cubic voxels v_{xyz} of volume s^3. The distance between the centre of each voxel with all the atoms in the ligand is tested to check if any of the atoms is within a van der Waals distance from the centre of the examined voxel.

If no atom is within a van der Waals distance, the volume s^3 of the examined voxel is assigned to the free volume V_{Free} .

Conversely, if a single atom is within a van der Waals distance, the volume s^3 of the examined voxel is assigned to the buried volume V_{Bur}.

With this description, Eq 1 holds:

$$1)\ V_{Sphere} = \Sigma v_{xyz} = V_{Free} + V_{Bur} = \Sigma v_{xyz(Free)} + \Sigma v_{xyz(Buried)}$$

While the V_{Bur} already indicates the amount of the coordination sphere that is occupied by the considered ligand, we prefer the more intuitive $\%V_{Bur}$ descriptor of
Eq. 2, which simply simply is:

$$2)\ \%V_{Bur} = 100*V_{Bur}/V_{Sphere}$$

After all the voxels in the first coordination sphere have been marked as free or buried, for each (x,y) point within the first coordination sphere the program scans the sphere from the top (i.e. away from the ligand) to find at which z value there is the first buried voxel.
This procedure results in a surface, defined as S(x,y) = zB. Positive values of zB indicate that the ligands protrudes in the z > 0 half-sphere, which is the half-
sphere where the reacting groups are placed.
Finally, the maps are a simple 2D isocontour representation of the interaction surface S(x,y) = zB.

Cap. 2 N-Heterocyclic carbenes

2.1 Historical background

Carbenes are compounds with a neutral di-coordinate carbon atom featuring either two singly-occupied non-bonding orbitals (a triplet state), or alternatively both a lone pair and an accessible vacant orbital (a singlet state).

Since the pioneering work of Curtius and Staudinger, carbenes have played a prominent role as transient intermediates. Introduced by Doering into organic chemistry in the 1950s, and by Fischer into organometallic chemistry in the1960s, these fascinating species are involved in many reactions of great synthetic interest. Although attempts to prepare the parent carbene (CH_2) by dehydration of methanol had been reported as early as in the 1830's, the quest for stable carbenes has, for a long time, been an unreasonable target.

Between the carbenes, N-Heterocyclic carbenes (NHCs) have become an incontrovertible class of molecules for Transition-Metal (TM) and organo-catalysis.

Inception of the field dates back almost a century ago when Tschugajeff (Chugaev) and co-workers reacted potassium tetrachloroplatinate with methyl isocyanide, followed by the addition of hydrazine. Contrarily to the authors' expectations, this reaction does not lead to a dimeric species composed of tetracyanide platinum moieties bridged by hydrazine molecules, but leads to a compound that is probably the first diamino carbene complex isolated in pure form. The structure of this salt **1**, and the one of its biscarbene derivative **2**, were only solved decades later (Scheme 1). It was later shown that this methodology is applicable to the synthesis of NHC complexes when functionalized isocyanides are used.

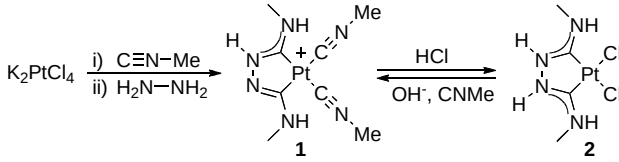

Scheme 1. Tschugajeff's (Chugaev) carbene complexes

In the early 1960s, the first real investigations on NHC were conducted by Wanzlick.

He couldn't isolate any carbenes but he postulated their existence, assuming that a carbon carbenic center can be stabilized if it is localized between two nitrogen atoms in a imidazole ring. This was followed by the first description of NHCs as ligands for metal complexes.

However, it is only in the 1990s that this new class of ligands was brought under the spotlight thanks to the work of Arduengo and co-workers. They were able to isolate and characterize the first stable free NHC. The isolated carbene proved to be a solid crystalline compound, thermally stable, the structure of which was experimentally confirmed by crystallographic analysis.

These findings ignited the curiosity of researchers as the possible role of NHCs as ligands was revealed, an interest that has seen an incredible research activity (Figure 1).

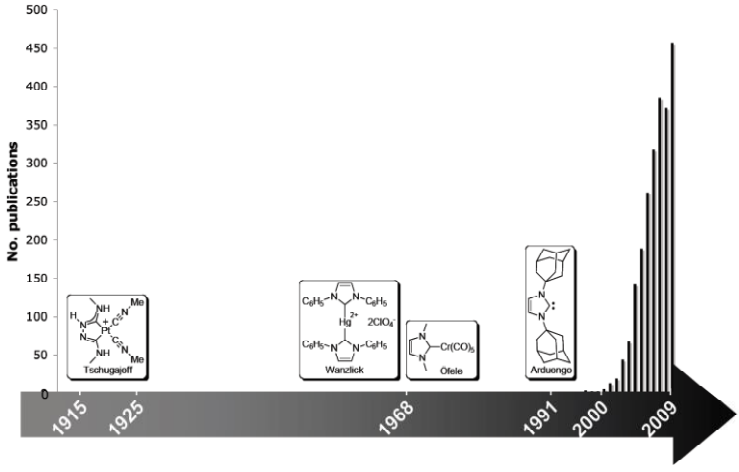

Figure 1. Number of publications (NHC as research topic)

2.2 Features

NHCs are stable singlet carbenes that can act as excellent two electron donor ligands towards any element in the periodic table. They coordinate strongly to late transition metals and heavy main group elements, but are also know to bind to early transition metals and the lanthanoids.

NHCs derive their excellent stability from their unique electronic structure. The carbene carbon atom is sp^2-hybridised featuring two σ-bonds with the adiacent nitrogen atoms and an electron lone pair in the other sp^2-hybrid orbital. The NHC stability is increased by two π N – π C donor interactions from the electron ione pairs on nitrogen into the "empty" p-orbital of the carbene carbon atom.

NHCs are usually referred as mimes of phosphanes, but NHCs are stronger σ-donor and only weak π-acceptor ligands: this makes them better donor ligands than phosphanes and bind stronger to many transition metals than those. Moreover, recent studies have revealed that the electronic features of the NHCs can be also more complicated, with different kind of electron interactions between the metal and the ligand.

N-heterocyclic carbenes can be structurally very different.

It has been estimated that 90% of the studies on NHCs are those based on 5-membered heterocycle compounds, in which the carbene center is linked to two nitrogen atoms, this is based on the versatility of these species with respect to carbenes from other N-heterocycles or acyclic diamino carbenes form. Figure 2 summarizes these heterocycles and the associated name of the corresponding NHC.

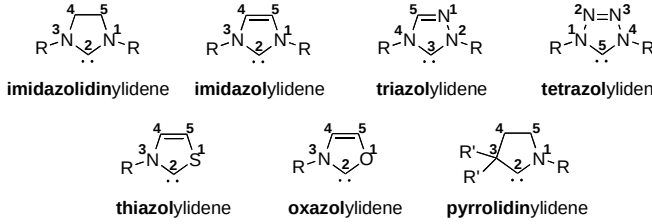

Figure 2. Common 5-membered heterocyclic carbenes

2.3 NHCs in organometallic chemistry

After less than twenty years from Arduengo's first isolation of a stable NHC, [17] the impact of these ligands in organic and organometallic catalysis has become enormous.

A lot of NHC based catalysts are already used in industrial scale for a number of different chemical transformations such as Ru-mediated olefin metathesis, [18, 19, 20, 21, 22, 23, 24, 25, 26, 27, 28, 29, 30] Pd-catalyzed cross-coupling reactions of various type, [31, 32, 33, 34, 35] hydrosilation, [8, 36] Cu-catalysed reduction of ketones, [37, 38] C-H activation, [8,39,40] Hydrogenations, [41,42] Au-mediated transformations, [43, 44] as well as free NHCs organocatalysts, etc, see Figure 3.

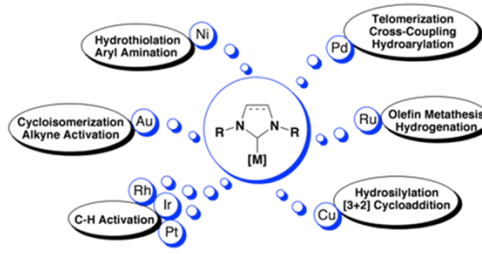

Figure 3. Some of NHC complexes reaction activities

This impressive number of applications is possible thanks to the NHCs rather flexible architectures whose stereoelectronics can be largely modified, thus giving the possibility to tune their catalytic activity.

This explains why several groups have dedicated remarkable efforts to deep characterize this class of ligands.[45, 46, 47, 48, 49, 50, 51, 52, 53, 54, 55]

Cap.3 Steric and Electronics of NHCs

3.1 Introduction

A remarkable amount of research has been done to understand the details of the M−NHC bond,[56, 57, 58, 59, 60, 61, 62, 63, 64] and the way this bonding influences catalytic behavior.[65, 66] As typical in organometallic chemistry, most of the work in this field has been focused on rationalizing chemical/catalytic behavior using molecular descriptors able to capture different features imparted from the ligands.

Indeed, it is a common and useful procedure to decompose the chemical behavior of transition metal complexes in terms of the steric and electronic properties of the various ligands coordinated to the same metal center.

In this context, we will assume the classical definition of Tolman that electronic effects are those effects that are transmitted along the bonds, whereas steric effects result from forces (usually nonbonding) between parts of the system that are topologically distant. This separation allows the property of interest to be decomposed according to the following equation,

$$\text{Property} = a + b \cdot S + c \cdot E$$

in which S and E are measures of the steric and electronic characteristics, respectively, of a given ligand, whereas a, b and c are constants that should be fitted to reproduce a given set of training data.

The main handles for tuning steric and electronic are the substituents on N atoms, the nature of the C4-C5 bridge (either saturated or unsaturated), the substituents on the C4 and C5 atoms, see Figure 4.

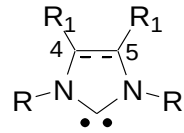

Figure 4. Schematic representation of a 5-membered NHC ligand

3.2 Steric Effects in NHC ligands

The initial intuition that steric properties of NHCs could be modulated and could impact catalytic behaviour stimulated the development of steric descriptors to quantify the steric requirement of different NHCs and, possibly, to compare them with phosphines.
Tolman proposed to measure the size of a ligand by the cone angle θ defined with the metal at the vertex and the atoms at the perimeter of the cone.[67] Tertiary phosphines are commonly classified using this parameter. The Tolman cone angle and related descriptors [68, 69, 70, 71, 72, 73, 74, 75] could not be used for NHCs since they are not cone shaped.
After some initial attempts, like the fence model,[76] work in the field mostly converged on the work of Nolan and Cavallo, the per cent of buried volume, $\%V_{Bur}$, as a standard and intuitive descriptor (in line with the main philosophy used by Tolman to develop the cone angle) able to describe reasonably well the steric bulkiness of NHCs.[50, 77, 78, 79, 80]
The $\%V_{Bur}$ is the fraction of the volume of a sphere centered on the metal occupied by a given ligand. The volume of this sphere represents the space around the metal atom that must be shared by the different ligands upon coordination (first coordination sphere), see Figure 5.
One of the advantages of the $\%V_{Bur}$, as a molecular descriptor characterising the steric properties of ligands, is its generality, which means that it can be applied also to quantify the steric property of ligands other than NHC. Indeed, extensive testing on a

large series of phosphane ligands demonstrated that the $\%V_{Bur}$ correlates well with the Tolman cone angle, allowing thus to move between the two scales.[81]

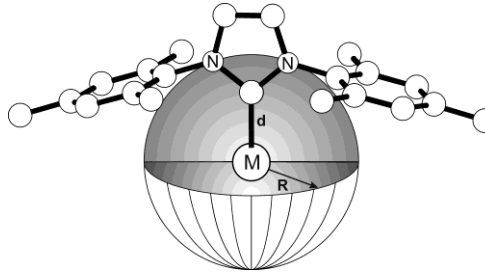

Figure 5. Representation of the sphere used to calculate the $\%V_{Bur}$

The $\%V_{Bur}$ was initially introduced to rationalise the trend in the bond dissociation energy of NHC ligands in a series of [RuClCp*(NHC)] and [Ni(CO)$_3$(NHC)] complexes. [65, 82] The almost linear correlation between the experimental bond dissociation energy and the $\%V_{Bur}$ indicated clearly that for NHCs, similarly to phosphines, steric bulkiness is a key parameter determining their binding ability to transition metal systems.
The $\%V_{Bur}$ values of a series of related NHC ligands obtained by analysing the steric bulk of the NHC ligand in the DFT optimised structure of the model [IrCl(CO)$_2$(NHC)] complexes are reported in Figure 6.

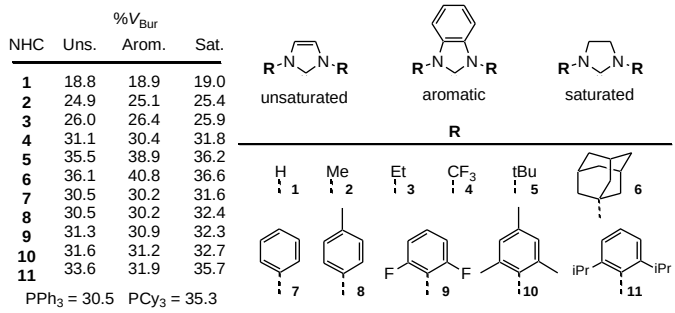

Figure 6. %V_{Bur} of frequently encountered NHC ligands from the quantum mechanically optimised structure of (NHC)Ir(CO)$_2$Cl complexes. For comparison, the %V_{Bur} of two popular phosphines, PPh_3 and PCy_3, as obtained from optimisation of (PR_3)Ni(CO)$_3$ complexes, is also reported

Analysis of the data reported in Figure 6 indicates that the saturated NHCs are slightly more bulky than that the unsaturated analogues, an effect ascribed to the different nature of the NHC skeleton that results in the N-C-N angle being consistently 4-5° greater in the saturated NHCs, thus bending slightly the *N*-substituent toward the metal.

Generally speaking, the bulkiest NHCs present a tri-substituted sp^3 C atom, like *tert*-butyl or adamantyl *N*-substituents. This effect can be further enhanced by appropriate NHC design, as in the bioxazoline derived NHC complex shown in Figure 7. The tricyclic rigid skeleton places the *N*-substituents in close proximity to the metal atom, which results in a very high %V_{Bur}, see Figure 7. On the other hand, also very bulky substitutents in the ortho positions of the N-aromatic ligand can increase remarkably the %V_{Bur}, relative to the prototype SIMes and IMes ligands, see again Figure 7.

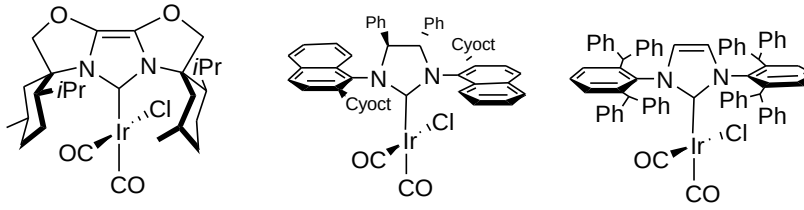

$\%V_{Bur}$ = 40.7 $\%V_{Bur}$ = 38.4 $\%V_{Bur}$ = 38.9

Figure 7. $\%V_{Bur}$ from the quantum mechanically optimised structures of the $[IrCl(CO)_2(NHC)]$

As aforementioned, the generality of the $\%V_{Bur}$ has allowed to place tertiary phosphines and NHCs on the same scale, and the values reported in Figure 6 for the classical PPh_3 and PCy_3 phosphines indicate that the less bulkier PPh_3 compares with NHCs of intermediate bulkiness, such as those presenting *p*-tolyl *N*-substituents, while the more bulky PCy_3 compares with IPr and SIPr. Finally, is worth mentioning that have been proposed other descriptors to measure the steric bulkiness of NHCs ligands, such as methods based on the molecular electrostatic potential. However, these methods require quantum mechanical calculations to be performed, a task not easily accessible to all research groups, whereas the $\%V_{Bur}$ can be calculated also using crystallographic data as input, and a freely available web tools has been developed to this end.

3.2.1 Steric maps

In this section a new steric tool developed during this thesis work to better characterize NHCs (but in general any ligands) will be described.

Despite the increasing understanding of the steric properties of NHC ligands, a clear limitation of the $\%V_{Bur}$ descriptor was emerging. Indeed, the $\%V_{Bur}$ –like the Tolman's cone angle – only measures an average property, while catalysis can be determined by

a non-homogeneous distribution of the ligands in the first coordination sphere of the metal.

This issue was solved by us introducing topographic steric maps, as a natural evolution of the $\%V_{Bur}$.

Topographic steric maps can be considered as a chemical analogue of geographical physical maps, which indicate the location of landforms like deserts, mountains and plains. In the case of transition metal complexes, topographic steric maps can be used to highlight the surface of interaction between the catalytically active transition metal and the substrate. The steric maps of Figure 8 report the value along the z-axis at which the NHC ligand starts to bury space in the coordination sphere around the Ru center. Positive values of the isocontour lines refer to the top half-sphere, which is the half sphere where the heterocyle ring of the NHC ligand is placed.

Focusing on the complex containing the prototype SIMes ligand, the mesityl group opposite to the Ru-methylidene bond shields the vacant coordination position on the Ru center, see the deep blue area on the left two quadrants in Figure 8a. The impact of the mesityl group laying above the Ru-methylidene bond, in the right quadrants of the steric map, is less relevant since it has to compete with the methylidene group for space. Nevertheless, the broad pale yellow area at 1.00-1.25 Å indicates that the mesityl ring is able to impart a noticeable steric pressure on the Ru-methylidene bond. The major impact is through the *ipso* and *ortho* C atoms of the mesityl ring, see their green imprints in Figure 8a. Finally, the *ortho* methyl groups of the mesityl ring have a small impact at the borders of the coordination sphere.

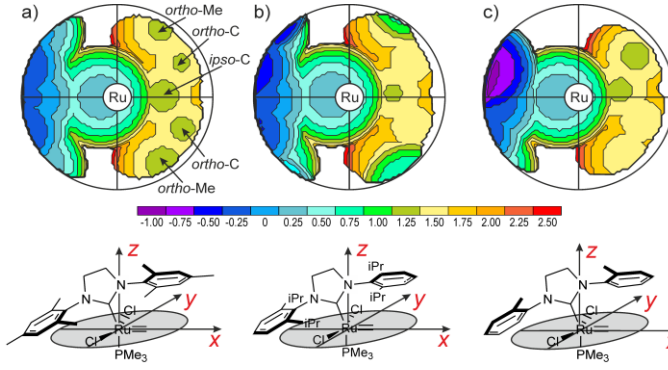

Figure 8. Steric maps of the NHC ligands in the optimized geometries of selected Ru complexes. The colouring scale of the isocontour levels, in Å, is also reported

Comparison between the SIMes and the SIPr ligands, see Figures 8a and 8b, indicates that the bulkier *ortho i*-Pr groups of the N-substituent above the Ru-methylidene bond have a much stronger influence at the border of the coordination sphere, see the pale blue areas, introducing steric clashes with the Cl ligands. To relieve this steric interaction the SIPr ligand is slightly pushed away, and the steric pressure on the central zone, where the Ru-methylidene bond is placed, is relieved. This is indicated by the absence of the green spots corresponding to the *ortho* C atoms of the mesityl ring in Figure 8b. In short, analysis of the topographic steric maps evidences that, despite the similar $\%V_{Bur}$, the SIMes and SIPr ligands shape remarkably different reactive pockets. Quite flat and with a constant pressure the SIMes ligand, vault shaped with higher steric pressure at the border the SIPr ligand.

Comparison between the steric maps of the *o*-tolyl NHC and of the classical SIMes complex highlights differences between these two systems. First, the space available on quadrant opposite to the Ru-methylidene bond, and corresponding to the unsubstituted side of the *o*-tolyl ring (top-left quadrant in Figure 8c), is more hindered than the quadrant corresponding to the substituted side of the ring

(bottom-left quadrant in Figure 8c). Further, the top-left quadrant is also more hindered that the analogous quadrant in the SIMes system. Similar asymmetry can be appreciated in the right quadrants, and again the top quadrant is more buried with the imprint of the *ortho* C atom visible, whereas in the bottom quadrant, which corresponds to the substituted side of the *o*-tolyl ring, there is no trace of the *ortho* C atoms and of the Me substituent.

As a final remark, we can note that adding groups at positions C4 and C5 of the heterocycle can be also used to modify the steric properties of the NHC ligand, though the C4 and C5 substituents are pointing well away from the metal center. The reason is that this modification restricts rotation around the N-substituent bond, thus preventing large rotation of the N-aryl ligands that can trigger C-H (de)activation of the ortho C-H bonds. [83, 84, 85, 86]

Further, this modification can be also used to develop chiral NHC ligands to be used in asymmetric catalysis, [87, 88 , 89, 90] see Figure 9 for representative examples. In this case, the main challenge resides in placing stereocontrol elements near the metal center without affecting the overall reactivity of the catalyst. Rotation of the N-substituents can be restricted to afford ligands that efficiently transfer their chiral information, using unsymmetrically substituted aryl side chains in connection with substitution on the NHC bridge,[91] see again Figure 9.

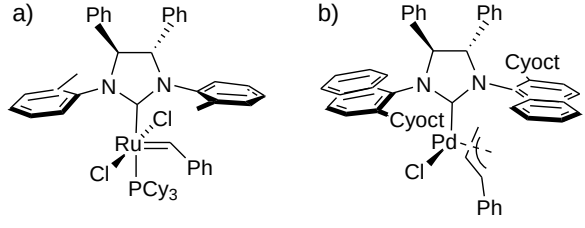

Figure 9. Example of chiral NHC ligands effective in asymmetric synthesis

3.2.2 Web Application Implementation

The SambVca program was modified to implement the user friendly generation of topographic steric maps.
The modified SambVca server has been made freely available to the chemical community through a graphical interface on a web application at the URL http://www.molnac.it/OM-2.0/2.0. The user interface combines several client-side technologies such as HTML, CSS and Java, running on an Apache web server. The background program to perform the buried volume calculations has been implemented in Fortran. The main interface is shown in Chart 2.

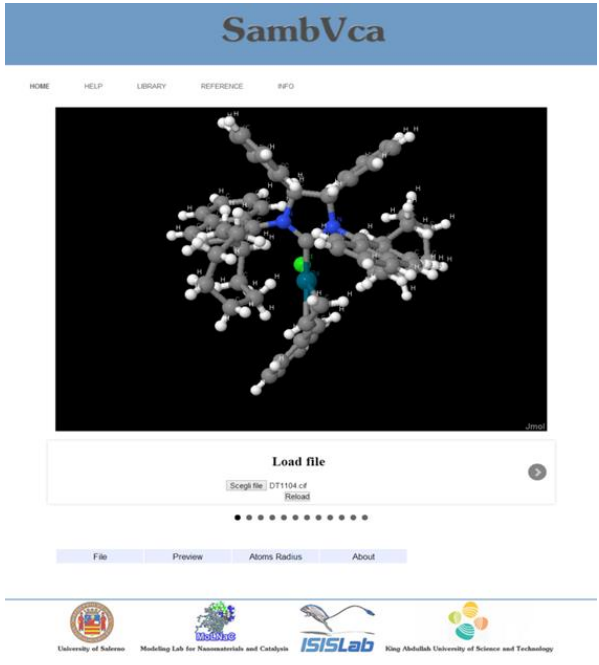

Chart 2.

Following a user friendly interface, the user can upload the coordinates file as classical XYZ format files, or as PDB, CIF, MOL files. A 3D visualization of the complex in JMol (http://www.jmol.org/) is provided. After uploading of the

coordinates, the user needs to provide the following structural parameters, using the interactive jmol window:

- The atom/s that should be used to define the centre of the sphere
- The atom/s that should be used to define the coordination axis (Z-axis)
- The atom/s that should be used to define the XZ-plane
- The atom/s that should be removed, i.e. the atom/s of the complex that are not part of the ligand whose steric properties you want to analyse

At this point, the user can choose to accept or to change the default settings (Bondi radii scaled by 1.17 for the atoms, a radius of 3.5 Å for the sphere centered on the metal, a distance of 2.10 between the coordinated atom and the putative metal centre, and the mesh spacing value of 0.10 Å for the numerical integration). Finally, if H atoms are to be included in the %VBur calculation, it is necessary to active the corresponding option.

After the input has been defined, the user has to Click on the button "SUBMIT" to run the program and visualize the results on the HTML page (see Chart 3) and the steric map is also downloadable.

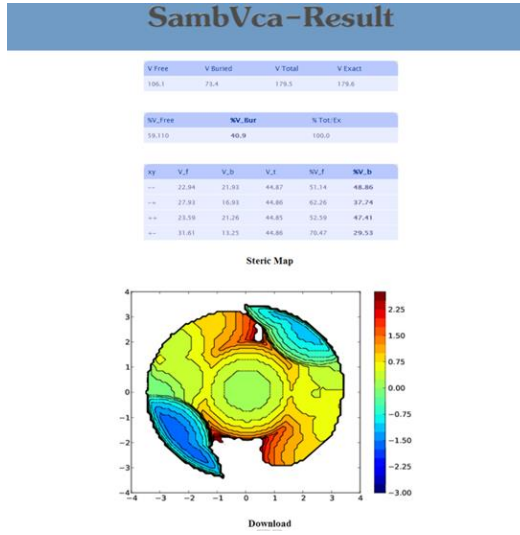

Chart 3.

On the web site is also available a section named Library, where the user can find a large numbers of popular organometallic complexes pre-loaded. The structural parameters are already set and user can directly visualize the steric map.

3.3 Electronic effects in NHC ligands

NHCs can be classified as typical strong σ-basic/π-acid ligands,[52, 92 , 93] although they have been also shown to exhibit reasonable π-basic properties.[94] This electronic modularity allows NHC ligands to adapt flexibly to different chemical environments represented by a transition metal and the other ligands.

The σ-basic capability of NHCs is consequence of a lone electrons pair in a high energy σ orbital, localized on the carbene C atom, which confers NHC σ-donor properties clearly stronger than those of basic phosphines, such as PCy_3. [52, 95] For this reason, the principal interaction between a NHC and the metal center is σ-donation from the HOMO of the NHC ligand, centered on the

carbene C atom, to empty d orbitals of the metal, see Figure 10. Donation from the NHC to the metal can be reinforced by donation from filled π orbitals on the NHC ligand to empty d orbitals, this transfer being particularly effective in electron-deficient metals.[96] As any σ-basic/π-acid ligand, NHCs can act as acceptor from electron-rich metals that can back-donate electron density from filled d orbitals to empty low energy π orbitals of the NHC as in a classical d → π* back-donation. [31, 97]

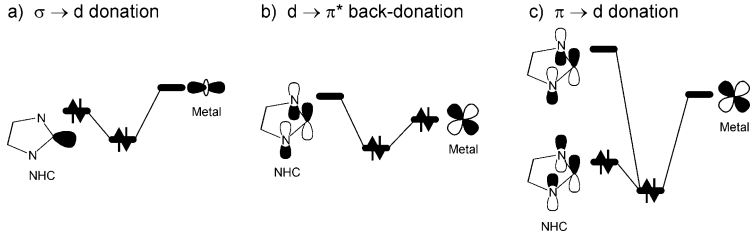

Figure 10. Diagram illustrating the σ → *d* (a), the *d* → π* (b), and the π → *d* (c) bonding modes occurring between NHCs and transition metals

Controlled tuning of the electronic properties of the NHC ligand can result in drastic consequences on the catalytic efficiency of the corresponding metal complexes. The key structural handles that can be modified to tune the electronic properties in classical 5-membered NHCs are again the C4-C5 bridge of the imidazol or imidazoline skeleton, the substituents on the C4 and C5 carbon atoms and the *N*-substituents.

Similarly to phosphines, the key experimental parameter to assess the electronic properties of NHCs is the average CO stretching frequency, ν_{av}, by IR spectroscopy.[34, 40, 41, 98, 99] The quite generally accepted model system for this measurement is $[IrCl(CO)_2(NHC)]$.

Focusing on the bridge of the NHC skeleton, no strong effects have been noticed by comparing transition metal complexes bearing strictly related imidazolin - and imidazole - based NHCs, see Figure 11a, with the average CO stretching frequency ν_{av} varying by

usually less than 2-3 cm^{-1}. [34, 65, 87] This suggests that these two skeletons transfer similar amounts of electron density to the metal.
The conclusion that changes in the bridge of the NHC skeleton have such a small effect on the electronic properties of the NHC is quite surprising, considering that SIMes and IMes based catalysts often show remarkably different catalytic behaviour. Of course, changing the nature of the NHC cycle, like in the abnormal NHC ligand of Figure 11b, has a strong impact on the ν_{av} value, which can reach values as low as 2003 cm^{-1}. [40]

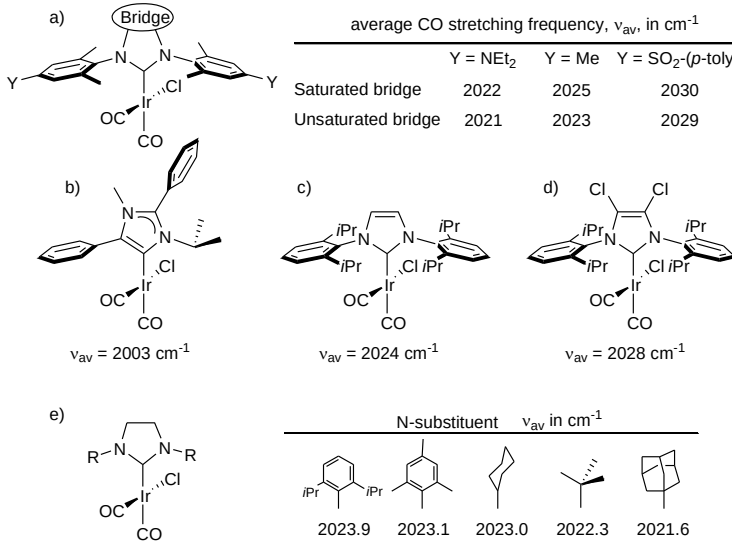

Figure 11. Variation in the average CO stretching frequency as consequence of a modification of the NHC ligand

More impact has been instead observed when the C4 and C5 substituents are modified. Remaining in the class of $[IrCl(CO)_2(NHC)]$ complexes, replacing the H atoms on the C4 and C5 atoms by Cl atoms in a IPr complex resulted in the rather high shift of the average CO stretching frequency from 2023.9 to 2028.3 cm^{-1}, see Figure 11c-d. [34] Impact on the electronic properties of the metal can be also achieved by changing the nature of the N-

substituents, see Figure 11e. As general rule, alkyl *N*-substituents are better electron donors that aryl N-substituents, but the range spanned by the average CO stretching frequency remains relatively small (less than 5 cm^{-1}). [34, 86]

Similar effects have been measured for the saturated analogues. Interestingly, stronger effects can be obtained by placing an electron-withdrawing or electron-donating group in the *para*-position of an aromatic *N*-substituent of the NHC ligand. As shown in Figure 11a, on going from a strongly electron-donating group, such as NEt_2, to a strongly electron-withdrawing group, such as SO_2-(*p*-tolyl), the average CO stretching frequency of $[IrCl(CO)_2(NHC)]$ complexes increases by 8 cm^{-1}. [86]

As for steric effects, comparison between NHCs and tertiary phosphines is quite instructive also in the case of electronic effects. The ν_{av} of a series of NHCs ligands discussed above is plotted versus the Tolman electronic parameter (TEP) in Figure 12, together with some of the most typical tertiary phosphines. Visual inspection indicates that quite low TEP values correspond to standard NHCs, and that they are clustered in the relatively small range of 3-5 cm^{-1}. Phosphines, instead, span over the much larger range of roughly 12 cm^{-1}, and consistently at higher TEP values. Nevertheless, with appropriate modification of the heterocycle ring and of its substituents, it is possible to connect the TEP of NHCs to phosphines.

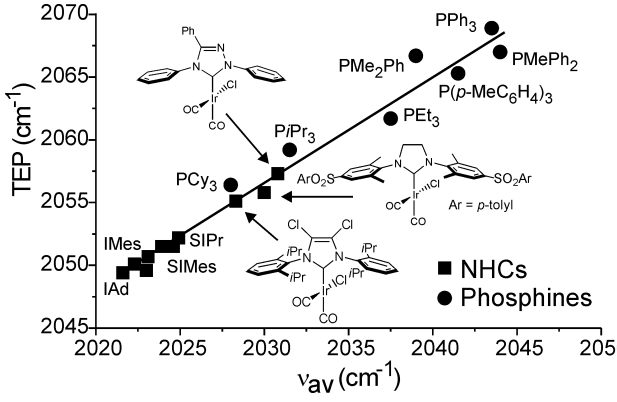

Figure 12. Tolman electronic parameter, TEP, *versus* the average CO stretching frequency, ν_{av}, for selected NHCs and phosphines. For the sake of readability, only the most popular NHCs are labeled

At this point, it is worth to note that beside heavy modification of the heterocycle ring, such as in abnormal carbenes or in triazol based carbenes, changing the substituents on the N, C4 and C5 atoms of the NHC has not a strong impact on the electronic properties of the metal, as measured by the CO stretching frequency.

3.3.1 Through space donation from NHC ligands to the metal

In this section an analysis of the M−NHC interaction in complexes presenting groups with different electronic properties in the para position of the aryl N-substituent is presented.

Recently, Plenio et al. demonstrated that the redox potential of several Ru, Pd, Ir, and Rh NHC-based complexes depends on the nature of the substituents at the para position of the N-xylyl rings.

This was found puzzling because communication through the σ-bonds is unlikely, seven bonds separate these substituents from the redox-active metal center, and communication through the π-orbitals is equally unlikely, as the aromatic ring of the Nsubstituent

is orthogonal to the NHC ring. Based on these considerations, Plenio and co-workers suggested that communication between the NHC ligand and the metal center could occur through π-face donation.[35, 39, 86, 100, 101]

To provide a theoretical support to this experimental evidence that communication between the para-substituent and the metal could occur "through space", specifically between the π-system of the N-substituent and the metal, a computational work has been performed.[102, 103]

To tune the computational protocol, we first tried to reproduce the experimental redox potential, $E_{1/2}$, of the Ir and Ru complexes shown in

Chart 4.

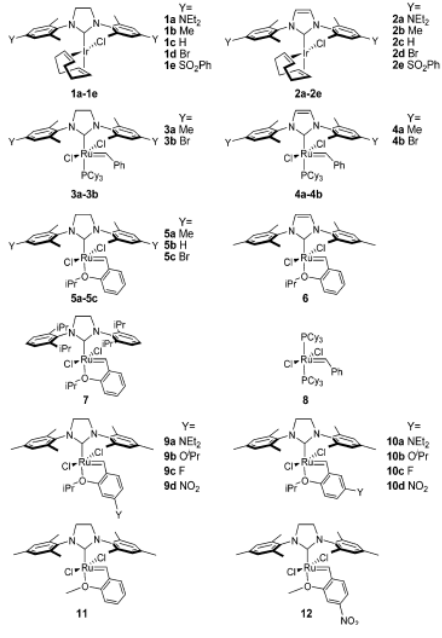

Chart 4. Systems investigated in the present study

The DFT calculated redox potentials for the systems of Chart 4 are plotted against the experimental $\Delta E_{1/2}$ in Figure 13. The data reported in Figure 13 show that higher redox potentials correspond to NHC ligands presenting an electron-withdrawing group in the para position of the N-xylyl substituent, whereas a reduction in the redox potential is found when an electron-donating group is present in the para position of the N-xylyl substituent. From a quantitative point of view, the calculated redox potentials reproduce well the absolute experimental $\Delta E_{1/2}$ values, with a R^2 equal to 0.92. The mean unsigned error and the root-mean-square deviation between the calculated redox potentials and the experimental $\Delta E_{1/2}$ are equal to 45 and 58 mV, respectively, which gives an indication of the accuracy that can be expected when the protocol we developed is used to predict the $\Delta E_{1/2}$ in newly developed Ru-catalysts. Further, the very good agreement between the calculated redox potential and the experimental $\Delta E_{1/2}$ indicates that DFT calculations can be used to characterize the electronic properties of NHC ligands for which the experimental $\Delta E_{1/2}$ is not available, thus adding to the set of molecular descriptors used to classify NHC ligands in terms of steric and electronic properties.

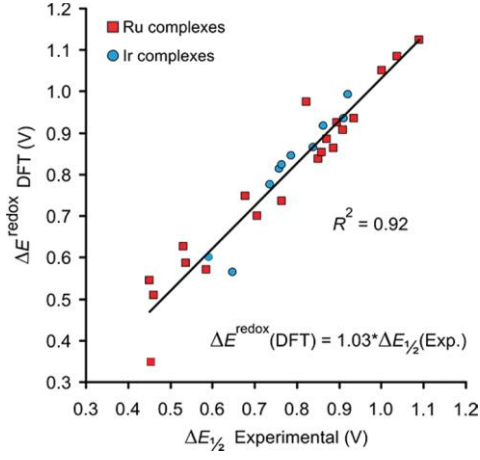

Figure 13. Plot of the DFT redox potentials versus the experimental $\Delta E_{1/2}$ for the Ir and Ru complexes shown in Chart 4

After the calculation protocol has been validated, we moved to clarify if the Y group in the para position of the N-substituent influences the stability of the neutral species or of the cationic oxidized species. To this end, we examined if the $\Delta E_{1/2}$ correlates with the energy of the highest occupied molecular orbital (HOMO) of the neutral species, because the first ionization energy can be approximated with the HOMO in the framework of the Koopman's theorem. This plot is reported in Figure 14. Inspection of the plot clearly shows an almost linear and quantitative relationship between the energy of the HOMO, which is strongly centered on the Ir and the Ru atoms, and the experimental $\Delta E_{1/2}$ for both Ir and Ru complexes. This finding indicates that one effect of the Y group is to destabilize the neutral species by raising the energy of the HOMO.

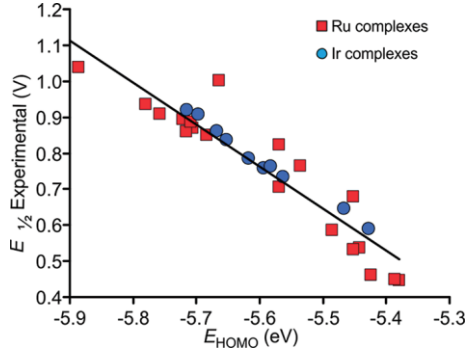

Figure 14. Plot of the experimental $\Delta E_{1/2}$ versus the DFT calculated HOMO energy for the systems of Chart 4

Next, we examined selected M−NHC distances, because a change in the σ/π donicity from the NHC ring to the metal, possibly induced by the para Y groups, should influence the M−NHC bonding with a variation of the M−NHC distance. Analysis of the values indicates that the para Y groups do not influence the Ir −NHC distance both in the neutral and in the cationic species.

To shed light on the mechanism through which the Y group in the para position of the N-substituents is able to destabilize the neutral species and to stabilize higher oxidation states, we analysed the electron density in selected systems.

Specifically, the electron density of two prototype systems bearing electron donating NMe_2 or electron withdrawing Br para-groups on the N-aryl substituents was compared in the neutral (reduced) and in the cationic (oxidized) state.

First, we compared the difference in the electron density, $\rho^+ - \rho^0$, between the cationic and the neutral species of a reference system. This plot indicates which is the redistribution of the electron density after oxidation. The electron density difference $\rho^+ - \rho^0$ is plotted in the plane of the NHC ring as well as in the plane orthogonal to it, Figure 15a and b, respectively. Within this definition, red and blue lines (corresponding to positive and negative isocontour lines) indicate zones where the electron density is higher or lower in the cationic species, respectively. Inspection of Figure 15a clearly shows the unexpected result that electron density at the metal, in the plane of the NHC ring, is higher in the cationic form rather than in the neutral form (see the red full lines around the Ru center in Figure 15a).

Indeed, in agreement with the HOMO composition described above, the plot of Figure 15b clearly indicates that upon oxidation electron density is mainly removed from the metal center as well as from the chloride ligands (see the blue dashed lines around the Cl atoms in Figure 15b).

Focusing on a more detailed level, inspection of Figure 15a indicates that, to alleviate the electron deficiency at the metal center in the cationic species, electron density is accumulated on and transferred from the C(ipso) atoms directly to the Ru center via a classical π to d donation, see left side of Figure 15a, as well as to the alkylidene C atom via a π C(ipso) to π^* C(alkylidene) donation, see right side of Figure 15a. The electron density donated from the C(ipso) to the C(alkylidene) allows the alkylidene group to transfer electron density to the metal center, as indicated by the blue dashed

lines around the alkylidene C atom in Figure 15a. Within this scheme, the effect of the Y groups in the para position of the N-substituents becomes easily rationalized. Electron-donating groups reinforce electron density at the C(ipso) of the NHC ligand, thus enhancing their ability to donate to both the metal center and the alkylidene group, whereas electron-withdrawing groups deplete electron density at the C(ipso) of the NHC ligand, thus reducing their ability to donate electron density. Support to this analysis is given by a comparison of the electron density in the neutral and in the cationic systems presenting NMe_2 and Br Y groups, $\rho^{NMe2}-\rho^{Br}$, see Figure 15c,d. Within this definition, positive and negative isocontour lines (full and dashed lines in Figure 15c,d) indicate zones where the electron density is higher or lower in the species presenting an electron-donating NMe_2 group in the para position of the N-aryl ring. Inspection of Figure 15c shows that in the neutral species electron density at the metal as well as at the alkylidene group is substantially the same in 15a and 15c; the main difference (beside the area around the Y groups) is at the C(ipso). The electron density at the C(ipso) is higher in the presence of the NMe_2 group.
Differently, in the cationic species, the electron density in the plane of the NHC ring is quite higher around the metal center and around the alkylidene moiety in 15a, while there is a reduction of excess density around the C(ipso). Further, in the cationic species 15a, there is increased amount of electron density between the two C(ipso) and the metal center on one side, and the alkylidene moiety on the other side.

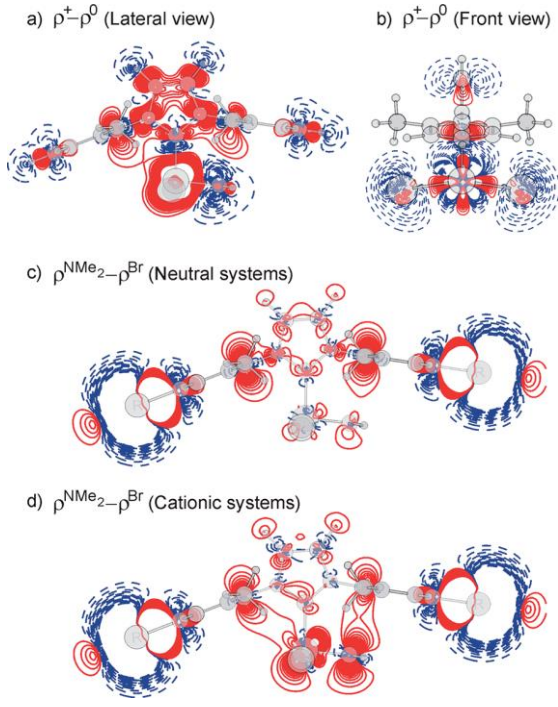

Figure 15. Plots of the electron density difference between the cationic and the neutral species of the Ru-system 15b, $\rho^{+}-\rho_0$, parts a,b, and between the neutral and cationic species of the Ru-systems 15a and 15c, $\rho^{NMe2}-\rho^{Br}$, part c neutral systems, part d cationic systems. Red full and blue dashed lines indicate positive and negative isodensity lines, drawn between −0.01 and 0.01 au with a spacing of 0.0005 au

Cap. 4 Reactivity

4.1 Metathesis - Introduction

Metathesis reaction is a molecular process involving the exchange of bonds between the two reacting chemical species. The chemical species involved can either be ionic or covalent: a general scheme of the metathesis reaction can be represented by the following equation

$$AX + BY = BX + AY$$

This kind of reaction has had a profound impact in the last quarter of century, especially for olefins, alkynes and enynes.
In fact in 2005 Yves Chauvin, Robert H. Grubbs and Richard R. Schrock received the nobel prize in chemistry for the development of the metathesis method in organic synthesis.
The history of alkene metathesis began with its serendipitous discovery at the end of 1960's. The name metathesis was given for the first time to this reaction by Calderon in 1967, [104, 105] but the first observation of the metathesis of propene at high temperature was reported in 1931. The first catalyzed metathesis reactions were found in the 1950's when industrial chemists at Du Pont, Standard Oil and Phillips reported that propene let to ethylene and 2-butenes when it was heated with molybdenum, in the form of the metal oxide or $[Mo(CO)_6]$ on alumina.[106, 107]
The first catalytic systems were either oxides such as WO_3/SiO_2 or Ziegler Natta derived systems such as $WCl_6 + AlX_nR_{3-n}$.
The elucidation of the mechanism pathway took two decades of extensive research by numerous groups, and debate is still active about some fine details.
The accepted mechanism is the one proposed by Y. Chavin in 1971 supported and validated subsequently by the experimental results of Casey,[108] Katz[109] and Grubbs[110,111] groups.

The Chauvin mechanism requires the coordination of the olefin to the metal atom of the metal-alkylidene species, followed by the shift of the coordinated olefin to form the metallocyclobutane intermediate. The metallacyclobutane produced can then cyclorevert to give either the original species or a new alkene and alkylidene.

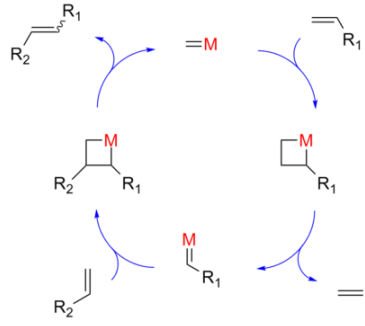

Chart 5.

The fundamental key result was the demonstration of Katz and co-workers in 1976 that a single, well-defined tungsten carbene, for example $Ph_2C=W(CO)_5$, could initiate the metathesis without added co-activators.[112,113]

Like most chemical reactions, the metathesis pathway is driven by the thermodynamic; that is, the final distribution of products is proportional to the exponential of their respective energy values. In olefin metathesis, where all the possible products have similar energy values, the product mixture can be tuned by reaction conditions, such as gas pressure and substrate concentration.

The alkene-metathesis reaction has developed into one of the most powerful tool for the synthesis of new C-C bonds, with applications spanning different size scales, from the academic lab to the industrial plant, and fields, from pharmaceutical synthesis to polymer production.

This versatility indicates a still unexplored potential for this reaction, which calls for the synthesis of innovative and/or better performing catalysts.

Up to now is possible to distinguish three main classes of such catalysts:

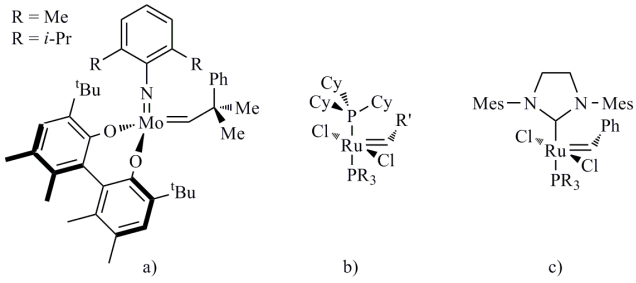

Figure 16. Olefin metathesis (pre)catalysts ordered chronologically: (a) Schrock biphenyl catalysts; (b) Grubbs's first generation; and (c) NHC-based second-generation catalysts (Cy=Cyclohexyl; Mes=Mesityl).

Catalyst **a** was introduced by Schrock's group in 1990, it has a high activity with a wide variety of possible alkene substrates, also sterically crowed. The main problem of this catalyst is its high sensitivity to oxygen, moisture, polar or protic functional group due to the electrophilicity of the high-oxidation state of the metal center.

Afterwards, Grubbs and co-workers introduced ruthenium-based carbene complexes. The first generation of these (pre)catalysts is characterized by the use of phosphine ligands $P(Cy)_3$, **b** in figure 16. These systems exhibits much greater functional-group tolerance but the phosphine ligand suffers from P-C degradation at elevated temperatures, for this reason the use of sterically demanding phosphines often is required in order to stabilize reactive intermediates.[114]

Almost simultaneously, Nolan [115] and Grubbs [5] reported the synthesis of related ruthenium complexes, with an N-heterocyclic carbene ligand instead of one of the phosphine ligands, leading to the class of system **c**. This class of catalysts is addressed as the second generation catalyst and its activity and stability depends a lot on the nature of the N-heterocyclic ligand.

4.1.1 Regioselective Ring Expanding Ene-Yne Metathesis

In this section a computational study on an ene-yne ring expanding metathesis reaction will be presented.
The enyne metathesis is a type of metathesis taking place between an alkyne and an alkene.[116] In particular the reaction considered in this section occurs between a cycloalkene and an alkyne, leading to a ring expanded by two atoms of carbon,[117] see Chart 6.

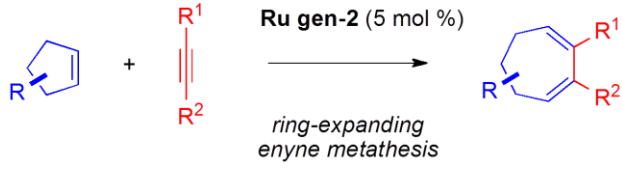

Chart 6.

The reaction considered was investigated experimentally by the group of the Prof. Steven T. Diver, University of Buffalo, USA,[118, 119, 120, 121, 122] see Chart 7.

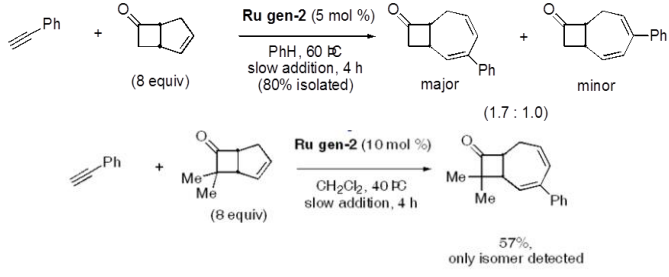

Chart 7.

A point unclear of this reaction is the mechanism of regioselctivity when the gem-methyls groups are present on the cycloalkane, and specifically whether a yne-then-ene or an ene-then-yne reaction pathway is followed.

Better knowledge of the mechanism involved would provide valuable clues for rational design and synthesis of new catalysts with bulk at the appropriate position(s). This would offer a catalyst-based solution rather than a substrate modification, which is not desirable in organic synthesis.

To this aim a complete computational study on the complex cascade metathesis process occurring will be presented here.

First of all, we explored the ene-then-yne pathway.[123, 124, 125]

We concentrated on the starting reaction of the ene substrate leading to intermediates **a** and **b**, and then to **c** and **d** ones. The two pathways basically correspond to the opposite regiochemistry of ene attack to Ru-alkylidene bond. The elementary steps and the relative labeling are shown in Chart 8.

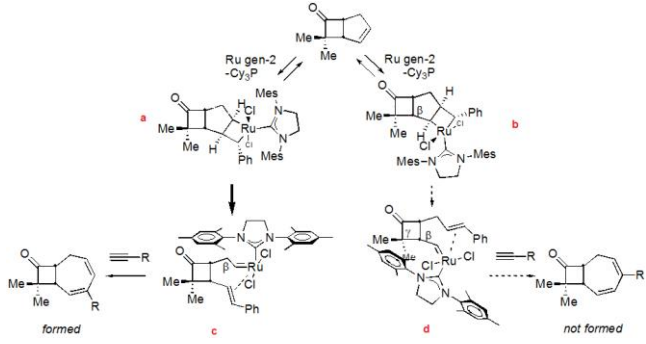

Chart 8.

Figure 17 displays the energy profile of the steps shown in Chart 8, up to intermediates **c** and **d**. The red profile corresponds to that favored experimentally.

Focusing on the first metathesis step, i.e. on the formation of metallacycle, the transition state leading to **a** (**ts1** in Figure 17) is higher in energy relative to the transition state leading to **b** (**ts1'** in Figure 17). Both metallacycles **a** and **b** are rather strained, and can be opened easily to the metathesis products **c** and **d** through transition states **ts2** and **ts2'**. Overall, the energy profiles in Figure

17 are rather smooth, with all transition states are well below in energy relative to the naked 14e species plus the uncoordinated alkene.

In other words, the ene-then-yne pathway is an easy pathway, but the selectivity between the a → c and the b → d pathways is not in agreement with experimental results. In fact all structures along the a → c pathway, which leads to the only product experimentally observed, is higher in energy.

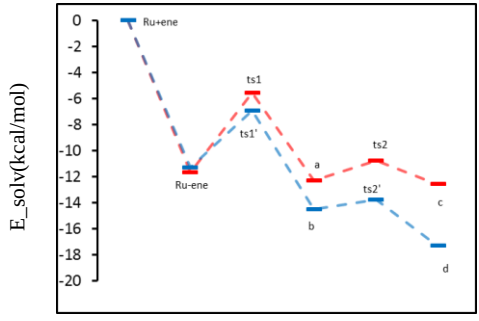

Figure 17. Energy profile of the ene-then-yne pathway

At this point we decided to investigate if the yne-then-ene pathway of Chart 9 could rationalize the experimental data. The first part of the mechanism involves alkyne reactivity to form a vinyl carbene species, the second part involves reactivity of the formed vinyl carbene species with the ene substrate. The former involves competition between the ene and yne functionalities for the initial Ru-alkylidene bond, the latter is the part where selectivity can occur.

The energy profile of the alkyne reactivity is shown in Figure 18, while the energy profile of the metathesis of the ene substrate with the vinyl Ru-carbene bond is shown in Figure 19.

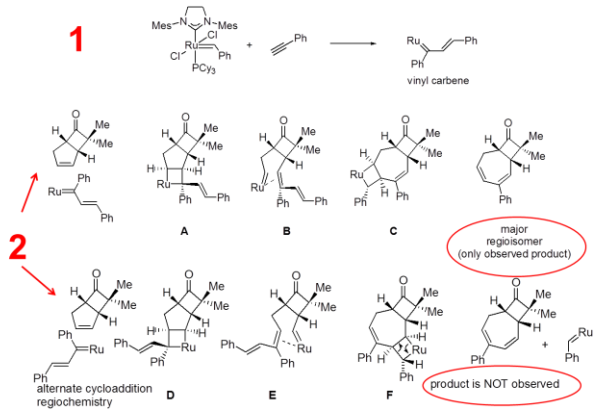

Chart 9.

Focusing on alkyne metathesis, the substrate capture step from the naked 14e species is energetically favored, see Figure 18, though ene coordination is quite stronger, see Figure 17. Overall, ene coordination is favored relative to yne coordination by 5.6 kcal/mol. However, metathesis from the yne coordinated intermediate is a very easy reaction with an almost negligible energy barrier (**ts1** in Figure 18). **Ts1** evolves directly to the very stable vinyl carbene intermediate and the reaction becomes irreversible.

Overall, the yne-then-ene versus ene-then-yne selectivity, determined by a competition between transition states **ts1** in Figures 17 and 18 indicates that the two pathways are very competitive.

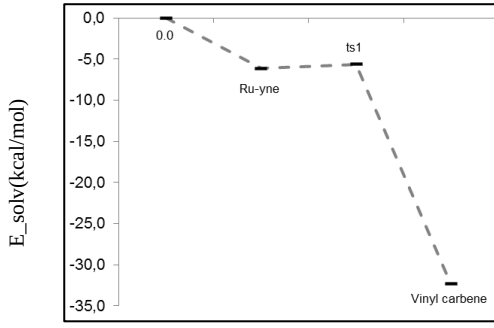

Figure 18. Energy profile for yne metathesis

Having clarified that the yne-then-ene pathway can be competitive with the ene-then-yne pathway, we decided to explore ene reactivity with the formed vinyl carbene species, considering the two possible regiochemistries shown in Chart 9. The corresponding energy profiles are shown in Figure 19.

Both pathways start from the vinyl carbene Ru species with the ene substrate coordinated, the red profile corresponding to that favored experimentally. The profiles of Figure 19 clearly indicate that metallacycle **A**, leading to the experimentally observed product, is higher in energy of metallacycle **D**. This preference for the unflavored pathway is even higher at the level of intermediates **B** and **E**. However, in the final step, corresponding to formation of the seven atom cycles **C** and **F**, the transition state leading to the product observed experimentally (**ts3** in Figure 19) is lower in energy than the transition state leading to the product not observed experimentally (**ts3'** in Figure 19) by 4.0 kcal/mol. Considering that the transition states for closure of the seven membered ring are also the highest in energy along the reaction profile, this indicates that selectivity occurs at this point and is in agreement with the experiments.

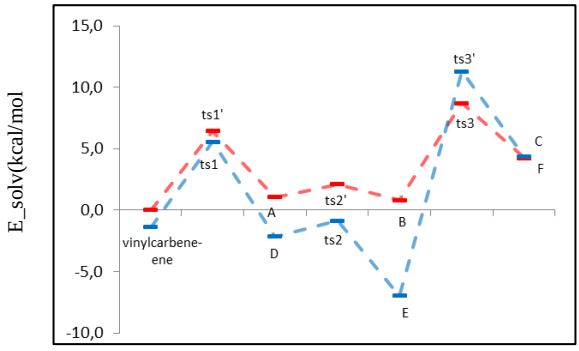

Figure 19. Energy profile for ene metathesis with a vinyl carbene Ru-species

Finally, we tested the same mechanism on the reaction with the alkene substrate without the gem-methyl substituents, see Chart 7. The energy difference between the determining transition states of the two regiodifferent pathways decreases from 4.0 kcal/mol with methyls to 1.9 without them. This is in agreement with the absence of regioselectivity (1.7:1.0) in these experimental conditions.
In conclusion, our results suggest that the only viable pathway to rationalize the observed regioselectivity is the "yne-then-ene" pathway, and the selectivity determining step is the closure of the seven membered ring.

4.1.2 Asymmetric NHC TM-Complexes: steric properties and activity in olefin metathesis.

In this section the characterization and the activity of a new kind of non-symmetrical Ru-NHC complex will be presented.
While a plethora of N-substituents (chiral or achiral) have been proposed for non-symmetrical (saturated or insaturated) NHCs, the case of dissymmetrical unsaturated NHCs was drastically limited to trivial N-substituent moieties. [126] Indeed, accesses of their corresponding imidazolium salt precursors based on the alkylation

of N-substituted imidazoles were mainly restricted to simple alkyl-halides; the cases of hindered alkyl or aryl-halides were more problematic or impraticable.[127,128,129]

Regarding the widely-used and inexpensive Arduengo's one-pot synthesis of symmetrical N,N-bis-aryl (or alkyl) imidazolium salts by reacting anilines (or alkylamines), glyoxal and formaldehyde, the process appeared not suitable for unsymmetrical imidazolium salts.[130]

Recently, Dr. Marc Manduit from ENSCR in Rouen disclosed a one-step procedure affording in good yields and excellent selectivities a wide range of (a)chiral dissymmetrical 1-aryl-3-cycloalkyl-imidazolium salts from sterically congested anilines and cycloalkylamines, and the corresponding transition-metal NHC complexes have been synthetized.

It is well note that the steric properties play an important role in influencing the catalytic activity of NHC/TM complexes.

As consequence, a steric analysis of different TM/asymmetrical NHC complexes have been performed.

The 1-mesityl-3-cyclododecyl-imidazol-2-ylidene Ag, Cu and Au complexes have been considered and their corresponding percent buried volumes ($\%V_{Bur}$) have been calculated using the geometry from single-crystal X-ray analyses. The resulting $\%V_{Bur}$ for Cu and Au, which present the cyclododecyl substituent pointing away from the metal, indicated that, despite the presence of the large cycloalkyl group, the overall steric demand is slightly less pronounced than that of the symmetrical IMes analog in similar NHC-M-Cl complexes, see Table 1.

Differently, for Ag, which presents the cyclododecyl substituent pointing towards the metal, the overall steric demand is more pronounced than that of IMes in the IMes-Ag-Cl complex, see Table 1.

In all cases, the 1-mesityl-3-cyclododecyl-imidazol-2-ylidene ligand has a $\%V_{Bur}$ clearly higher than the ICy ligand, see again Table 1.

Table 1: Comparison of the $\%V_{Bur}$ of different NHCs in (NHC)-M-Cl complexes.[a]

NHC	%VBur (Cu)	%VBur (Ag)	%VBur (Au)
IMes[b]	36.3	36.1	36.5
ICy[b]	28.8	27.7	27.4
Mes-C12	33.6	37.6	34.5

[a] NHC structures extracted from crystal structures (d=2.0)

[b] T. Droge, F. Glorius, Angew. Chem. Int. Ed. 2010, 49, 6940 – 6952

Interestingly, the steric map views presented in Figure 20 evidenced a high steric discrimination between the flexible aliphatic and bulky aromatic groups and outlined the unsymmetrical environment around the metal center. Moreover, the difference in conformation observed between the silver and the gold complexes strikingly demonstrated the highly modular coordination mode of these new-NHC ligands, with a cycloalkyl group able to either shield or liberate a face of the metal center. Therefore, monodentate unsymmetrical 1-aryl-3-cycloalkyl-imidazol-2-ylidene NHCs are able to combine high steric discrimination and flexibility in opposition to traditional C2-symmetric ligands.

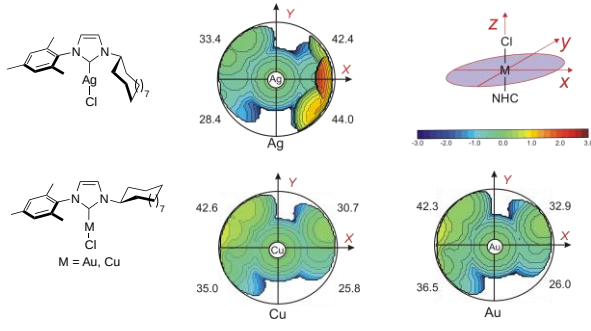

Figure 20. Steric Map views of 1-mesityl-3-cyclododecyl-imidazol-2-ylidene transition-metal complexes Ag, Cu and Au

Since the rapid and efficient protocol to synthesize this unsymmetrical carbene precursors, the corresponding Ru-complexes have been tested as catalysts for olefin metathesis.

Indeed, the introduction of this kind of unsymmetrical-NHC ligands afforded experimentally efficient synthesis of cationic bis-NHC benzylidene ether based ruthenium complexes with abnormal structures and interesting reactivities.

The deprotonation of the trifluoroborate imidazolium salt with potassium bis(trimethylsilyl)amide (KHMDS) followed by the addition of the Hoveyda-Grubbs I complex afforded a brownish solution, which yielded a green ruthenium complex after silica gel purification. The absence of signal in ^{31}P NMR confirmed the success of the phosphine displacement. On the other hand, the ^{1}H and ^{13}C

NMR spectrum evidenced the diagnostic signals of the benzylidene-ether moiety, while suggesting an unexpected double incorporation of the unsymmetrical NHC ligand. Moreover, the detection of a sharp signal in ^{11}B NMR pleaded for a cationic form with BF_4^- as counter anion. X-ray diffraction analysis unambiguously confirmed the structure of the cationic ruthenium complex **2**, which displayed a square pyramidal geometry with trans-NHC ligands. The ethereal fragment occupied a position trans to the chloride, indicating displacement of one halogen ligand and its exchange for the non-coordinated BF_4^- anion (Scheme 2).

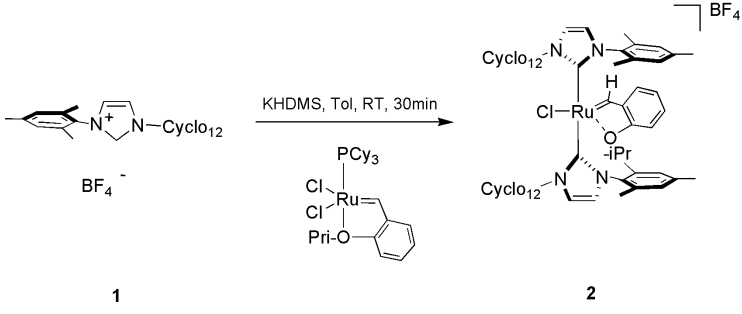

Scheme 2. Cationic ruthenium complex 2 synthesis

Complex 2 represents a unique example of double NHC incorporation on Hoveyda-Grubbs type complex, leading to a unique cationic structure.

This abnormal behavior should certainly be attributed to the special electronic and steric properties of the newly developed unsymmetrical-NHC ligands.

In order to gain a better understanding of the cationization process, theoretical calculations were then undertaken. Starting from the neutral bis-NHC complex **4**, three possible pathways were evaluated (Scheme 3).

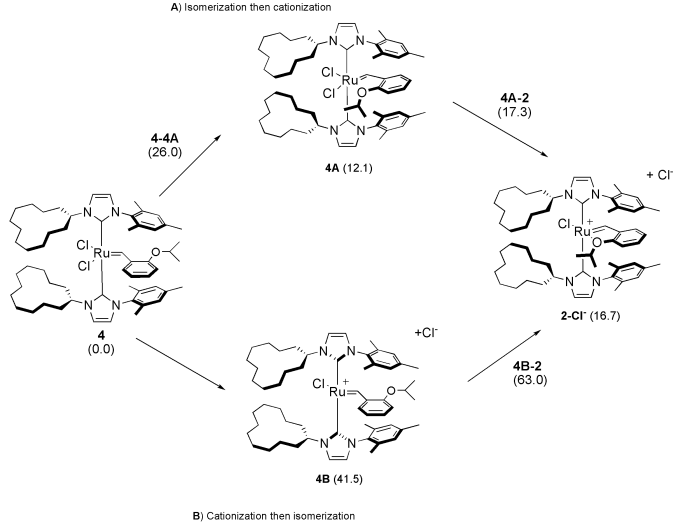

Scheme 3. Proposed cationization patways

The reaction pathway of Scheme 3A consists of an isomerization of the isopropoxy-arylidene group of **4** through a concerted rotation around the Ru=alkylidene and C(carbene)-C(aryl) bonds, and an energy barrier of 26.0 kcal/mol, to achieve isomer **4A**, 12.1 kcal/mol above **4**, in which the isopropxy group is properly oriented to coordinate the Ru center. The cationization step is in this case concerted with isopropoxy coordination to the metal, and occurs through the relatively low energy transition state **4A-2**, at 17.3

kcal/mol above the starting complex **4**. Transition state **4A-2** collapses into complex **2**, 16.7 kcal/mol above **4**. The second pathway considered, instead, starts with the cationization of **4**, followed by isomerization, see Scheme 3B. However, the cationic species **4B**, with a highly unsaturated cationic Ru center, lies 41.5 kcal/mol above **4**. Further, the following rotation around the Ru=alkylidene bond of **4B**, to allow isopropoxy coordination to the Ru center occurs through transition state **4B-2**, 21.5 kcal/mol higher in energy relative to the cationic species **4B**.

Based on these results, the simple cationization-then-isomerization pathway **B** can be excluded. The pathway **A** can be operative, since the energy barriers are accessible.

These numbers also indicate that in presence of any species in solution able to precipitate or simply stabilize the extracted Cl^- anion (like $AgBF_4$ or KBF_4), would allow both complete conversion of the parent complex and easy removal of the side product.

Moving to the activity of this new bis-NHC complexes, it is note that bis-NHC systems are generally recognized as highly stable species with modest catalytic activities.[131,132]

Indeed, the strong bond association between the NHC ligand and the ruthenium center should disfavor the dissociative substitution by an olefin, which considerably diminishes the (pre)catalyst initiation rate.[133] Nevertheless, this class of complexes can still display interesting reactivity at elevated temperature.[134, 135]

In this concern, ruthenium complexes bearing two non-identical NHCs have recently demonstrated capacity to respond under milder reaction conditions.[136, 137, 138]

For this reason, a computational study on the metathesis reaction of the 1,7-octadiene with the new non-symmetric system has been considered. The attention has been focused on the key intermediates, i.e. the 14e system **1**, the olefin coordinated intermediate **2**, the metallacycle **3**, and the key transition state leading to the latter intermediate, Figure 21 displays the energy profile.

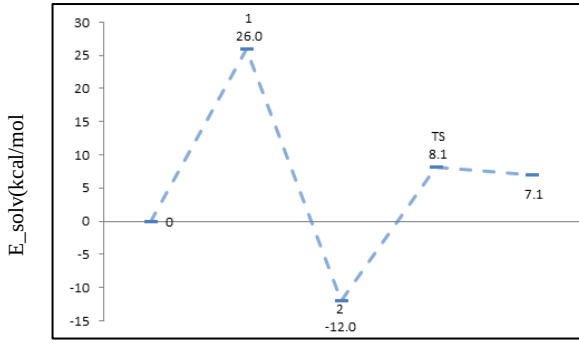

Figure 21. Energy profile of 1,7-octadiene metathesis

The active species is formed by dissociation of the ether ligand (**1** in Figure 21), a step that costs only 26.0 kcal/mol, while dissociation of the NHC costs 60 kcal/mol.

Focusing on the next steps of Figure 21, the substrate coordination to **1**, leading to **2**, is favored of 12.3 kcal/mol. The coordination intermediate **2** evolves to the metallacycle **3** with an energy barrier of 20.0 kcal/mol respect to the intermediate **2** (**TS** in Figure 21). Interestingly, the metallacycle is only slightly more stable than the previous **TS**. All these steps occurs with olefin coordination trans to the Ru-Cl bond.

Considering that a prominent catalytic activity was noticed experimentally after HCl addition in the reaction media, what happens adding HCl has been considered in the calculations too. We first focused our attention on the pathway shown in Chart 10.

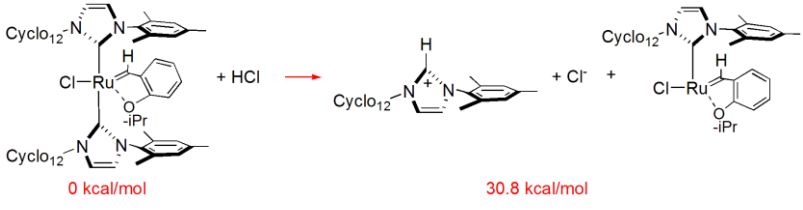

Chart 10.

In presence of HCl one NHC ligand can be protonated, making its lability more favored respect to that of the NHC alone (30.8 kcal/mol vs 60.0 kcal/mol). In this way a new $14e^-$ species is formed, without one NHC and with the styrenylether function still coordinated to the metal.
Anyway the reaction reported in Chart 10 is not so favored, i.e. the products showed are 30.8 kcal/mol higher in energy respect to the cationic (pre)catalyst system.
Then alternative pathway has been considered, see Chart 11.

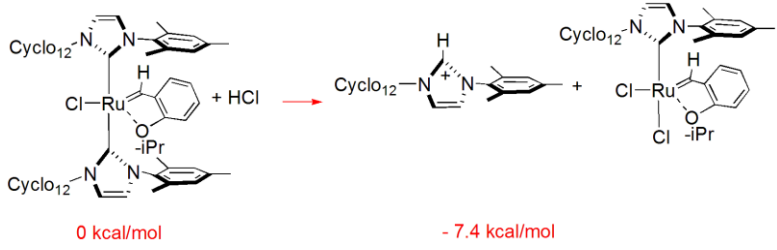

Chart 11.

In this pathway, after the protonation and the release of the NHC ligand, the chlorine atom coordinates to the electron poor metal of the cationic system, leading to an Hoveyda kind system not more cationic (-7.4 kcal/mol).
Based on these results, the pathway showed in Chart 11 seems the favored one.
Moving to the metathesis reaction of the 1,7-octadiene in presence of HCl, a new energy profile has been calculated (Figure 22) involving the $14e^-$ species **1**, the olefin coordinated intermediate **2**, the metallacycle **3**, and the key transition state leading to the latter intermediate.

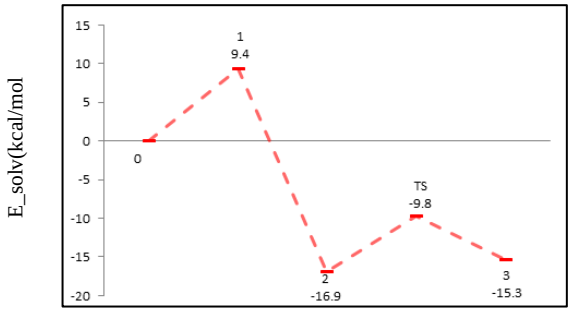

Figure 22. Energy profile of 1,7-octadiene metathesis in presence of HCl

The active species is formed by dissociation of the ether ligand (**1** in Figure 22), a step that costs only 9.4 kcal/mol. Focusing on the next steps of Figure 22, the substrate coordination to **1**, leading to **2**, is favored of 16.9 kcal/mol. The coordination intermediate **2** evolves to the metallacycle **3** with a quite low energy barrier of 7.1 kcal/mol respect to the intermediate **2** (**TS** in Figure 22). The metallacycle is more stable than the previous **TS** of 5.2 kcal/mol. All these steps occurs with olefin coordination trans to the Ru-NHC bond.

From the energetics reported in Figure 21 and in Figure 22, it's clear that, in presence of HCl in the reaction media, the activity of the cationic (pre)catalyst is increased a lot, due to the formation of a neutral Hoveyda kind system that favors the whole reaction path.

The strong potential for protonolysis could be attributed to the more basic cycloalkylamine moiety.

In conclusion, the incorporation of two unsymmetrical NHC ligands on Hoveyda-Grubbs type complex has led to a unique example of a cationic bis-NHC ruthenium complex bearing a benzylidene ether chelating ligand (3a). This new ruthenium species has demonstrated high chemical stability at room temperature, affording a latent catalyst, which could be activated through protonolysis of the ruthenium-NHC bond upon acid addition.

4.1.3 Strength of the Ru-halide bond in NHC Ru-complexes.

In this section a DFT analysis of the strength of the Ru-halide bond in a class of new phosphite-based olefin metathesis (pre)catalysts [123,139] will be presented.

In the field of Ru-NHC metathesis catalysts, the synthetic manipulation of the ligand coordination sphere around ruthenium has mainly focused on modifications of the N-heterocyclic carbene (NHC) ligand, of the alkylidene group, and of the leaving group L, usually coordinated trans to the NHC ligand (see Scheme 4a). The alkylidene group and the leaving group L can also be tethered (Scheme 4b).[140, 141]

In this scenario, the halide ligands have often been considered rather "innocent".

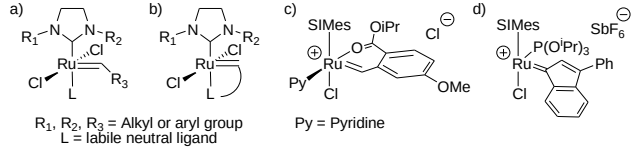

Scheme 4.

However, recently, different works focused on the anionic ligand X: Slugovc and coworkers have reported on a stable cationic Ru (pre)catalyst obtained by abstraction of a chloride ligand from a chelating ester-alkylidene catalyst.[142]

On the other hand, Cazin and coworkers have recently showed that cationic complexes could be readily obtained via chloride abstraction from phosphite derivatives using silver salts allowing the synthesis of a new set of cis-Ru complexes.[143] This cationic (pre)catalyst exhibits excellent performance in metathesis reactions, although high temperatures (superior to 100°C) are needed for its activation. Cazin and coworkers recently observed also the rapid exchange of halide ligands in ruthenium olefin metathesis (pre)catalysts due to this Ru-halide bond lability. More recently, the

heterolysis of the Ru-Cl bond in typical ruthenium olefin metathesis (pre)catalysts was evidenced also by ESI-MS.[144]
Overall, these experiments indicate that the Ru-Cl bond is not a strong and inert moiety and that questions about the strength of the Ru-Cl bonds in Ru-complexes relevant to olefins metathesis is an overlooked area of study.
With the aim to fill this gap, a thermochemical DFT analysis of the Ru-Cl bonds in a series of Ru-complexes has been performed.
In fact DFT has proven quite useful in shedding light on the relative stability of transition metal-ligand bonds.[145] Such fundamental thermodynamic data are often very difficult to obtain experimentally, although they are often key to catalysis.[146, 147, 148, 149]

The analysis was based on the cationic complexes experimental obtained by the group of Cazin and co-workers, Caz-1, 2 and 3 systems, starting from the phosphite-containing olefin metathesis pre-catalysts recently synthetized in the group[123, 128], see Chart 12.

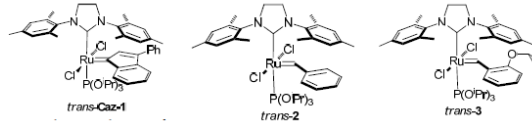

Chart 12.

The $14e^-$ four-coordinate cationic Ru complexes, obtained experimentally with the use of silver salts ($AgBF_4$), displays an unusual sawhorse geometry with the phosphite ligand trans to a probable agostic Ru---H-C bond, suggesting a chloride abstraction occurring trans to the phosphite ligand and not to the N-heterocyclic carbene (NHC), as it would be expected considering the superior trans effect of the latter.
More interestingly, phosphite ligand seemed to be the key feature for a clean chloride abstraction as complex mixtures were obtained starting from phosphine or pyridine derivatives.

The reaction exhibited a noteworthy stereocontrol as only cis cationic species were isolated, regardless of the parent complexes conformation.

To finally elucidate mechanism of chloride abstraction computational data on all the structures corresponding to the cis and trans geometries of the cationic and neutral species of Chart 12 have been considered.

The energetics have been calculated following two computational protocols, i.e. with both BP86 and M06 functional.

The relative stability of the cis and trans isomers of the neutral pre-catalysts is reported in Table 2. It is clear that in CH_2Cl_2 the two isomers are of similar energy both with the BP86 and M06 functionals. However, in terms of free energy the BP86 functional predicts the trans isomer marginally favored in case of Caz-1 and 3, while the cis isomer is slightly favored in case of 2. Differently, the M06 functional predicts the cis isomer to be favored in all cases. Considering that experiments indicate that the cis isomer is thermodynamically favored, these results suggest the M06 functional reproduces better the relative stability of the two isomers.

Moving to the cationic species, both cis^+ and $trans^+$ isomers of Caz-1, 2 and 3 were located. Both for the cis and trans isomers two geometries are possible, depending on which Cl atom is removed (for instance, in case of the cis isomer the Cl atom trans to the NHC or to the phosphite can be removed). We calculated both possibilities but, for the sake of simplicity, we only discuss the one generating the more stable cation.

In case of the cationic species, both the BP86 and M06 functionals predict that the $trans^+$ isomer is remarkably less stable than the cis^+ isomer, see Table 2, which is in qualitative agreement with the stronger experimental preference for the cis+ isomers.

Table 2: Relative potential energy, ΔE, and free energy, ΔG, in kcal/mol, of the cis and trans isomers of the neutral and cationic Caz-1, 2 and 3.

	Cis		Trans		Cis^+		$Trans^+$	
	ΔE	ΔG	ΔE	ΔG	ΔE	ΔG	ΔE	ΔG
Caz-1[a]	0	0	3.3	-0.8	13.9	2.5	22.3	14.0
2[a]	0	0	4.8	0.6	18.1	6.7	25.0	16.9
3[a]	0	0	2.3	-0.5	9.0	1.0	17.6	9.3
Caz-1[b]	0	0	6.5	2.4	23.5	12.1	37.5	29.2
2b	0	0	5.6	1.3	26.3	14.9	37.2	29.4
3b	0	0	4.2	1.5	12.5	4.5	19.2	10.9

[a]BP86 values. [b]M06 values.

Focusing on the energetics of chloride abstraction from the most stable cis isomer of the neutral species, the first remarkable result is the low free energy cost associated to this process whatever system is considered. Indeed, the ΔE of Cl dissociation from Caz-1 is only 13.9 kcal/mol at the BP86 level, a value increasing to 23.5 kcal/mol with the M06 functional. In terms of free energy these values are reduced to 2.5 and 12.1 kcal/mol only, which indicates an extreme lability of the Ru-Cl bond in Caz-1. The energy of Cl dissociation from 2 is somewhat higher, a finding that is probably related to the higher steric hindrance of the indenylidene group in Caz-1, which favors dissociation of another ligand. In case of 3, the extremely low free energy needed to dissociate a chloride ligand, 1.0 and 4.5 kcal/mol at the BP86 and M06 levels, is consequence of the coordination of the isopropoxy group to the ruthenium after Cl dissociation, which clearly stabilizes the cation. Focusing on a comparison between the cis^+ and $trans^+$ isomers, it is clear that the energy cost required to dissociate a Cl ligand form the trans species is higher, still it is not prohibitive considering that these reactions can be run up to 70°C.

Further, these numbers also indicate that in presence of any species in solution able to precipitate or simply stabilize the extracted Cl^- anion, would make Cl dissociation a rather easy process.

We also investigated the energy for the isomerization of trans-Caz-1^+ into cis-Caz-1^+. The corresponding transition state, calculated to be 13.5 and 11.1 kcal/mol above trans-Caz-1^+ at the BP86 and M06 levels, is reported in Figure 23 and it shows an almost tetrahedral geometry around the Ru center. The low energy barrier calculated for the trans-Caz-1^+ to cis-Caz-1^+ isomerization, together with the higher stability of the cis$^+$ isomers, offers an explanation for the experimental high stereoselectivity in favor of the cis$^+$ isomer, whatever starting neutral species is considered.

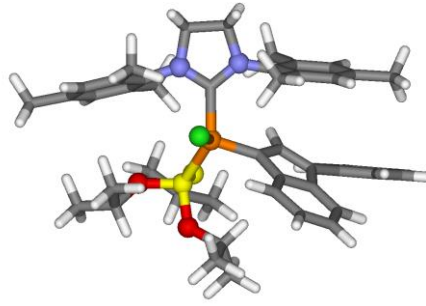

Figure 23. Geometry of the transition state connecting trans-Caz-1^+ and cis-Caz-1^+

To have a better understanding of the relative strength of the various Ru-Cl bonds in the neutral precatalysts, we calculated the Ru-Cl bond snapping energy, which is the energy required to rigidly separate a Cl^- ligand from the neutral precatalyst. In other words, the Ru-cationic species is not allowed to relax to the optimal geometry after Cl^- dissociation.

The bond snapping energies, summarized in Table 3, clearly indicate that both the Ru-Cl bonds in the cis isomer are weaker than the Ru-Cl bonds in the corresponding trans isomer.

However, the most interesting finding is that the Ru-Cl bond trans to the phosphite in the cis isomer is remarkably weaker than all the other Ru-Cl bonds, indicating this as the Cl ligand most likely to be extracted by the Ag salt. The Ru-Cl bond trans to the phosphite is roughly 10 kcal/mol weaker than the Ru-Cl bonds in the trans

isomer, probably consequence of a strong trans influence of the phosphite. The BP86 and M06 functionals again offer a rather similar picture, although the M06 snapping energies are consistently ~10 kcal/mol higher than the BP86 snapping energies.

Table 3: Bond snapping energy in CH_2Cl_2, in kcal/mol, of the Ru-Cl bonds in the neutral Caz-1, 2 and 3 pre-catalysts

	Cis isomer		Trans isomer
	Cl trans to P	Cl trans to NHC	Ru-Cl
Caz-1b	24.2	30.5	34.2
2b	25.6	30.4	34.5
3b	23.1	28.3	32.6
Caz-1c	34.5	43.2	44.0
2c	34.8	39.8	44.6
3c	32.4	38.0	42.7

[a]Only the bond snapping energy of the weaker Cl bond is reported for the trans isomer. In any case, the difference between the two Cl bonds in the trans isomer is negligible, and it is due to the different disposition of the Cl atom relative to benzylidene and indenylidene ligands. [b]BP86 values. [c]M06 values.

Further, we compared the energy cost required to dissociate the the two Cl ligands in the mixed phosphine/phosphite system shown in Figure 24. According to calculations, the energy of dissociation of the Cl ligand trans to the phosphite is 19.5 and 28.6 kcal/mol at the BP86 and M06 levels, versus values of 26.9 and 36.8 kcal/mol for the dissociation of the Cl ligand trans to the phosphine. Again, these values clearly indicate a quite stronger trans-effect of the phosphite relative to phosphine, and could explain the high stability of the cis species in mixed NHC/phosphite complexes.

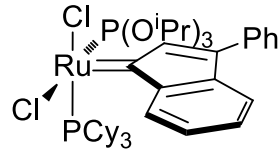

Figure 24. Mixed phosphine/phosphite cis-Ru complex.

Concluding this part, it is clear that the energy data reported in Table 2 and Table 3 are in qualitative agreement with the experimental observations, matching with the complete selectivity of the cationic species formation and with the evidence that in a competition experiment halide abstraction from the cis isomer dominates (i.e. the trans isomer remains mainly unreacted), thus providing a rationalization of the experimental data.
The already assumed strong influence of the phosphite group was unambiguously confirmed by this study and even proved to be stronger than the NHC one. For each complex, the Ru-Cl bond trans to the phosphite ligand was found to be the weakest.
Formation of the cis-cationic species starting from the neutral cis-complex occurred then by a direct chloride abstraction of the chloride trans to the phosphite. Even if the energy required for breaking the Ru-Cl bond in trans isomer were calculated to be notably higher, they were still in order of magnitude with easy abstraction by silver salts.
Formation of the cis cationic species starting from the neutral trans complex was supposed to occur by the first abstraction of one chloride, followed by an instant isomerisation of the trans species thus formed into the more stable cationic cis complex.

Since the Ru-X bonds have demonstrated to be "active", and chloride abstraction using metallic salts has been shown to be possible, this methodology was successfully applied for the synthesis of bromide/iodide,[75, 150] monodentate and bidentate aryloxides,[151,152,153] N,O-, P,O- and O,O-bidentate ligands,[154,155,156] carboxylate and alkylsulfonate derivatives[157, 158] of commercially

available complexes. Precipitation of the silver chloride formed during the reaction allows both complete conversion of the parent complex and easy removal of the side product. Although anionic ligand variation usually leads to species with catalytic activities comparable or lower than the activity of the parent complex (with possible exception of monodentate fluoride bearing aryloxides), recent publications point to the usefulness of these catalysts in particular applications.

Recently Cazin and co-workers used this approach for the anionic ligand exchange involving ligands as Ac, TFA, Bz, Piv, see Scheme 5.

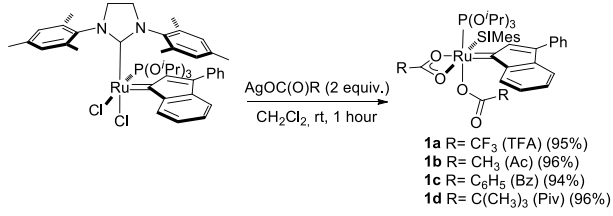

Scheme 6. Synthesis of bis-carboxylato complexes using silver carboxylates

DFT calculations were used to provide a rationalization of the experimental behavior.

The energetics of the anion exchange with respect to the cis-Caz-1 system are reported in Table 4.

Table 4. Relative stability (kcal/mol) of the complexes of Scheme 5 relative to cis-Caz-1.

	1a-d	0.5*(1a-d)	2a-d	3a-d
TFA	-8.8	-4.4	-3.1	-1.8
Ac	-23.4	-11.7	-14.0	-13.1
Bz	-19.6	-9.8	-11.2	-11.2
Piv	-30.8	-15.4	-16.2	-14.5

The data reported in Table 4 show that, in all cases, replacement of the chloride with any of the carboxylates considered is thermodynamically favoured. Comparing the different carboxylates in the bis-substituted complexes 1a-d, TFA is the carboxylate less able to replace the chlorides, with 1a more stable than cis-Caz-1 by 8.8 kcal/mol, followed by the benzoate and by the acetate complexes 1b and 1c favoured by roughly 20-23 kcal/mol, and by the pivalate complex 1d favoured by almost 31 kcal/mol. Focusing on the mono-substituted systems 2 and 3, isomers 2a-b and 2d, with the carboxylate trans to the NHC ligand, are favoured by 1-2 kcal/mol and the isomer 2c is at the same energy of the 3c one. This can be related to steric factors that favour the placement of the bulky carboxylates away from the bulky NHC ligand and to electronic reasons that favour the placement of the more π-donating chloride trans to the π-acidic phosphite.

Considering that in the experiments 1 equivalent of cis-Caz-1 is mixed with 1 equivalent of carboxylate, halving the energies reported in Table 4 for 1a-d allows for a comparison of experiments and calculations. These values are reported in column 3 of Table 4. Comparison of these data indicates that in the case of TFA formation of 0.5 equivalents of 1a is favoured relative to formation of 1 equivalent of 2a or 3a by 1.3 and 2.6 kcal/mol, respectively, and overall formation of 0.5 equivalents of 1a from cis-Caz-1 leads to an energy gain of 4.4 kcal/mol. This is in qualitative agreement with the experimental distribution of products, with a prevalence of 1a. In contrast, for acetate and benzoate, formation of the mixed complexes 2b-c is favoured, with 1b-c 2.3 and 1.4 kcal/mol higher in energy, while 3b-c are 1.4 higher in energy. For pivalate, complex 2d is favoured by 0.8 and 1.7 kcal/mol over 1d and 3d. Finally, as mentioned above, substitution of chlorides by acetate, benzoate or pivalate is clearly favoured. Overall, also these results are in reasonable agreement with experiments, reported in Table 1, which indicate a prevalence of 2b-c, and almost complete disappearance of cis-Caz-1.

The energetics of the reactions shown in Scheme 7 were calculated.

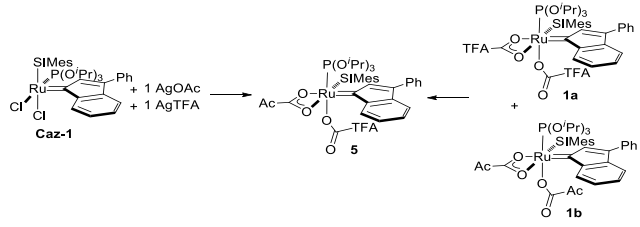

Scheme 7. Preparation of 5 from 1a and 1b.

According to calculations, formation of 5 is favored by 13.8 kcal/mol relative to cis-Caz-1 plus 1 equivalent of TFA and acetate, and by 9.6 kcal/mol relative to 1 equivalent of 1a and 1 equivalent of 1b. Overall, the energetics are in agreement with the experimental evidence that starting from cis-Caz-1 or mixing 1a and 1b leads to formation of 5.

The specific behavior and reactivity displayed by these novel complexes and the possible synthetic routes permitting access (or not) to novel architectures should help further catalyst design effort.

4.1.4 Ru-F phosphite (pre)catalysts for olefin metathesis reactions

The introduction of fluorine atoms in molecules can drastically change their physical and chemical properties.[159] Organofluorine compounds are nowadays employed in agrochemicals and pharmaceutical industries, increasing the demand for this class of compound. Fluorine has been introduced into metal-complexes as fluoride ligand as well.[160, 161, 162, 163] Late-transition-metal fluoride complexes represent a challenge in synthetic organometallic chemistry due to the mismatching of the hard-soft theory (soft cation and hard anion) and the few methods for introducing fluoride ligands.[164,165,166,167,168,169,170]

As a result, only a few examples of Pd,[171] Pt,[172]Ir,[173] Os and Ru fluoride complexes are reported in the literature.[174, 175, 176]

It has been suggested that Ru complexes bearing fluoride ligands would be more active in olefin metathesis reactions compared to their halide counterparts. Kinetic studies by Grubbs and co-workers showed that the overall efficiency of different $[RuX_2(SIMes)(CHPh)]$ complexes (X = Cl, Br, I) decreases in the order Cl > Br > I, hypothesizing an even better efficiency for a Ru-F_2 species.[139] Computational studies claimed the same trend of reactivity for bis-halides complexes (F > Cl > Br > I), predicting the best activity for the bis-fluoride species among olefin metathesis pre-catalysts. Despite this fact, whereas bromide/iodide/carboxylate versions of Grubbs and Hoveyda-Grubbs type complexes have been extensively studied,[75, 146, 147] no fluoride version has been reported to date.

Since the recent growing experimental evidence that halides, and more in general anionic ligands, can be considered mobile ligands that however determine the catalytic behavior, Ru complexes presenting fluoride ligands, have been isolated recently in the group of Dr. Cazin, St. Andrews University, see Chart 13. An analysis similar to that reported in the previous section was performed on these complexes.

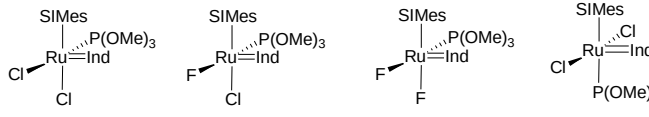

cis-Caz-1 **cis-Caz-1F** **cis-Caz-1F_2** **trans-Caz-1**

Chart 13.

Insights on the stability of the Ru complexes isolated and their corresponding trans-species were obtained with a computational DFT approach (Table 5).

As a remark, the energy values reported in Table 5 are clearly affected by the relative stability of the free chloride and free fluoride anions in solution.

Table 5. Energetics, in kcal/mol, of the halide exchange reactions Caz-1 + F^- -> Caz-1F + Cl^-, and Caz-1F + F^- -> Caz-F_2 + Cl^-.

	Caz-	Caz-1F+F^-	Caz-F_2+2Cl^-
cis-isomer	0.0	-17.9	-31.0
trans-isomer	+3.3	-9.7	-20.3

Focusing on the cis complexes, the replacement of one chloride ligand of Caz-1 by one fluoride ligand, leading to Caz-1F + Cl^-, is favored by 17.9 kcal/mol, see Table 5. In agreement with the experiments, the most stable isomer of Caz-1F presents the fluoride ligand trans to the $P(OiPr)_3$ ligand, the isomer with the fluoride ligand trans to the NHC ligand being 4.5 kcal/mol higher in energy. Substitution of the second considered, the trans isomer, with the $P(OiPr)_3$ ligand trans to the NHC ligand, is less stable than the cis isomer, see Table 5. However, it is worth noting that in Caz-1 the cis isomer is only 3.3 kcal/mol more stable than the trans isomer, while in Caz-1F and Caz-$1F_2$ this preference increases to roughly 10 kcal/mol. Finally, combination of the energy values of the three cis species in Table 5 indicates that formation of 2 mols of Caz-1F by mixing 1 mol of Caz-1 and 1 mol of Caz-$1F_2$ is favored by 4.8 kcal/mol.

Overall, these results are consistent with the experimental evidence that when cis-Caz-1 is reacted with 1 equivalent of AgF, only Caz-1F is formed, and that when cis-Caz-1 is reacted with cis-Caz-$1F_2$ still only Caz-1F is obtained.

In order to provide a rationale for these findings, the relative strength of the different Ru-halide bonds in the considered systems we calculated the bond snapping energy (BSE), already defined in paragraph 4.1.3, see Table 6.

The BSEs of Table 6 indicate that all the Ru-F BSEs are stronger than the BSE for the corresponding Ru-Cl bond, independently from homo or heterolytic fragmentation of the complexes. This allows concluding that the Ru-F bond is stronger than the corresponding Ru-Cl bond.

More specifically, the data reported in Table 6 clearly indicate that the Ru-F bonds in cis-Caz-F_2 are roughly 13 kcal/mol stronger than the corresponding Ru-Cl bonds in cis-Caz-1, compare entries 2 and 10 in Table 6. Further, for the same complexes the Ru-halide bond trans to the $P(OiPr)_3$ ligand is roughly 5 kcal/mol weaker than the Ru-halide bond trans to the NHC ligand, compare entries 1 and 2 as well as entries 9 and 10 in Table 6, suggesting that it is the Ru-halide bond trans to the P atom that undergoes dissociation. Focusing on cis-Caz-1F, the Ru-Cl bond is weaker than the Ru-F bond, compare entries 3 and 4 in Table 5, despite the chloride ligand is trans to the NHC ligand. Finally, the strength of the Ru-Cl bond trans to the NHC ligand is nearly the same in cis-Caz-1 and cis-Caz-1F, compare entries 1 and 3 in Table 6. Focusing on trans-Caz-1, in agreement with our previous work, the calculations indicate that the Ru-Cl bond is stronger when it is trans to another Cl atom rather than to a P atom, compare entries 2 and 5 in Table 6.

Table 6. Ru-X bond snapping energy (BSE) in CH_2Cl_2. Values in kcal/mol.

	Pre-catalyst	Atom	Heterolytic BSE	Homolytic BSE
1	cis-Caz-1	Cl trans to NHC	30.5	83.3
2	cis-Caz-1	Cl trans to P	24.2	81.2
3	cis-Caz-1F	Cl trans to NHC	30.1	84.3
4	cis-Caz-1F	F trans to P	37.4	107.3
5	trans-Caz-1	equivalent Cl	34.2	90.9
6	trans-Caz-F_2	equivalent F	45.3	113.5
7	trans-Caz-1F	F trans to Cl	44.9	111.0
8	trans-Caz-1F	Cl trans to F	35.4	95.1
9	cis-Caz-F_2	F trans to NHC	41.3	108.0
10	cis-Caz-F_2	F trans to P	37.2	110.7

To have a better understanding if the increased strength of the Ru-F bond relative to the Ru-Cl bond is electrostatic in nature or is due to

increased back-donation from the F ligand to the Ru center through a push-pull effect induced by the π-acid phosphite, we performed an energy decomposition analysis (EDA) of the Ru-X bond in in cis-Caz-1 and cis-Caz-$1F_2$, see Table 7.

We briefly recall that the total BSE can be decomposed into three main terms, $-BSE = E_{El} + E_{Pauli} + E_{Orb}$. E_{El} accounts for stabilizing electrostatic interaction between the two fragments, E_{Pauli} accounts for repulsion between doubly filled molecular orbitals on the two fragments, and E_{Orb} accounts for stabilizing interaction between filled orbitals on one fragment with empty orbitals on the other fragment. Since the EDA is performed on the intrinsic strength of the Ru-X bond, which does not depend on the environment that can only stabilize the two fragments, the EDA is performed in the gas-phase. Focusing on cis-Caz-1 and cis-Caz-$1F_2$, the data reported in Table 7 indicate that the increased strength of the Ru-F bond in cis-Caz-$1F_2$ compared to the Ru-Cl bond in cis-Caz-1 is almost 50%-50% shared between the orbital and the electrostatic terms, since both are roughly 14-15 kcal/mol stronger in cis-Caz-$1F_2$ compared to cis-Caz-1. None of the two terms is clearly dominating the other. The repulsive Pauli term is instead rather similar. This suggests that the increased strength of the Ru-F bond is equally consequence of an increased ionic character of the bond, due to the higher electronegativity of the F atom, and to increased orbital interaction, that can be probably correlated to back-donation from the F ligand to the Ru center through a push-pull effect. Comparison between cis-Caz-F_2 and cis-Caz-1F indicates that the halide trans to the NHC ligand has small impact on the Ru-F bond trans to the phosphite.

Table 7. Decomposition analysis of the bond snapping energy of selected Ru-X bonds in the gas-phase. The total bond snapping energy is decomposed as: $-BSE = E_{El} + E_{Pauli} + E_{Orb}$. All values in kcal/mol.

	E_{El}	E_{Pauli}	E_{Orb}	-BSE
Cis-caz-Cl_2	-154.7	117.5	-77.9	-115.0
Cis-caz-F_2	-168.3	122.7	-92.6	-138.1
Cis-Caz-1F	-168.0	119.2	-94.0	-142.8

The computational study reported showed how stable these complexes are compared to cis-Caz-1, with Caz-$1F_2$ being the most stable

The stability of the cis pre-catalysts influences their catalytic activity.

In fact a larger energy barrier was observed for Caz-1F experimentally compared to cis-Caz-1. Caz-$1F_2$ is even less active than the former pre-catalysts due to its higher stability in the cis form and the low amount of active species generated.

4.2 C-C Cross-Coupling - Introduction

Transition metal-catalyzed cross-coupling reactions of organic electrophiles and organometallic reagents have emerged as a powerful synthetic tool to assemble carbon-carbon (C-C) and carbon-heteroatom (C-X) bonds under mild conditions.[177] The impact of the reaction on academic and industrial research, as well as on production, has been immense.

The emergence of cross-coupling as a popular method in synthesis arises from both the diversity of organometallic reagents utilized in these reactions and the broad range of functional groups which can be incorporated into these reagents.

Three of their main developers, Richard F. Heck, Ei-ichi Negishi, and Akira Sizuki, were awarded with the Nobel Prize in Chemistry in 2010 for their work in this field.

The full reaction pathway involves multistep processes with many intermediates and competing equilibria often present. The exact details of all steps are still under investigation.[178, 179, 180, 181]
It is generally accepted that cross-coupling reactions follow a catalytic cycle consisting of three main steps, see Scheme 8.

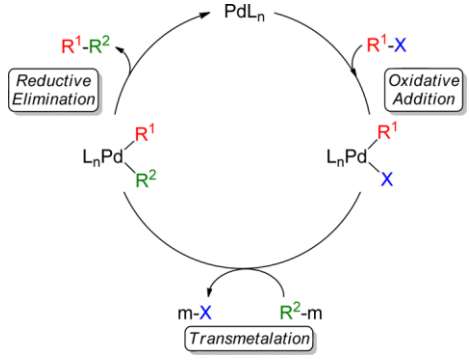

Scheme 8. General catalytic cycle for Pd-catalyzed C_C cross-coupling reactions

The reaction mechanism usually begins with oxidative addition of one organic halide, R^1-X, to the catalyst [M], with the breaking of the organic R group and the heteroatom X bond and the formation of two new bonds with the metal, which increases its oxidation state by two units. This step has been postulated to be rate-limiting in a number of cross-coupling reactions. Subsequently, the organic group R^2 of an organometallic nucleophile, R^2-m, undergoes transmetallation, i.e. is transferred to the catalyst. After this stage both coupling partners are places on the same metal center. The final step is a concerted reductive elimination of the two coupling fragments to regenerate the catalyst and give the organic product.
Despite the fact that the three-step mechanism is generally accepted, each of these main steps has different possibilities and can be quite subtle and specific for each reaction.
C-C cross-coupling reactions are classified on the base of the atom present in the nucleophile species.

For instance, Suzuki-Miyaura [182] is boron-mediated, Stille [183] reaction tin-mediated, Negishi[184] reaction zinc-mediated, etc.
The catalyst most widely used are transition metal complexes from groups 8-10, especially palladium complexes, but also nickel and copper. Palladium catalyzed reactions have several advantages including functional group tolerance, low sensitivity of organo-palladium compounds towards water and air.

4.2.1 NHC-Pd Catalyzed Suzuki-Miyaura Couplings

It is now well accepted that NHC can be excellent ligands also in Pd-catalyzed C-C cross-coupling reactions, which has spurred extensive work in this area.[185, 186, 187, 188]
In line with this trend, this section will report on the effect of using chiral monodentate NHC ligands for metal-catalyzed coupling reaction catalysis. Attention will be focused on the application of these NHCs catalysts in the C-C coupling of bulky aryl compounds.
Between the different kinds of cross-coupling reaction, the Suzuki-Miyaura is the one which displays the widest functional group tolerance, and uses readily available and low toxicity organo-boron nucleophiles.
One of the few challenges remaining in the Suzuki-Miyaura coupling reaction are the transformations involving sterically demanding substrates that lead to tetra-ortho-substituted products. Especially in cases where aryl chlorides are used, the relatively poor nucleophilicity of the arylboron reagents usually results in diminished catalytic activities.
To date, systems that work at room temperature have not been reported for the construction of these important tetra-ortho-substituted biaryl structures via the Suzuki-Miyaura coupling of both aryl chlorides and aryl bromides.
Dr. Dorta and coworkers, university of Zurich, recently reported the synthesis of diastereomerically pure palladium complexes

incorporating a new bulky saturated NHC ligand with a chiral N-heterocycle and a naphthyl side chain with two cyclooctyl groups on the naphthalene moiety, anti-C, see Chart 14.[189]

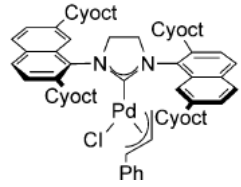

Chart 14.

This asymmetric Pd-catalyzed complex was tested in the palladium-catalyzed Suzuki-Miyaura couplings to give tetra-ortho substituted biaryls. In particular, the reaction studied occurs between 2,4,6-trimethyl phenyl chloride and 2,6-dimethylphenyl boronic acid. Under the mild reaction conditions used (i.e. room temperature), all of the reference catalyst systems did not show good reactivity and lead to product formation in low yield, while the new substructure tested clear shows both high conversions and yields at room temperature. Tetrasubstituted heterobiaryls were also successfully synthesized in good yields.

This uniquely high reactivity prompted to investigate the present catalytic system further in order to understand the subtleties at play.

To gain insight into the subtleties that govern this process, we present computational data on the important catalytic step and on the steric properties of the catalyst system.

To understand the difference between the catalytically preferred new NHC ligand and the more established SIPr ligand, we calculated the buried $\%V_{Bur}$ of the two NHC ligands in these complexes via DFT calculations. The simple $\%V_{Bur}$ of the NHC ligands in the new catalyst (41.5%) and in (SIPr)Pd(cin)Cl (34.9%) show that the new ligand is bulkier than SIPr.

That an overall more bulky NHC ligand behaves better in catalysis involving sterically more demanding substrates is not unusual and the term of flexible steric bulk has been introduced to account for this phenomenon.

At least in a catalytic coupling scheme that follows the classical path (i.e. no secondary reactivity/decomposition), this concept is nevertheless at odds with what one would expect.

For this reason a more detailed analysis by evaluating the $\%V_{Bur}$ in the single quadrants around the Pd center was performed and the corresponding steric contour maps were plotted (Figure 25) for both (SIPr)Pd(cin)Cl (left) and anti-C (right). Splitting the total $\%V_{Bur}$ into quadrant contributions quantifies any asymmetry in the way the ligand wraps around the metal. Within this approach, the quadrant $\%V_{Bur}$ of SIPr is rather constant ($\%V_{Bur}$ ~35%), while the quadrant $\%V_{Bur}$ values of anti-(2,7)-SICyoctNap are largely different. Two quadrants heavily hindered (top left and bottom right, $\%V_{Bur}$ ~53%), two quadrants clearly more open (top right and bottom left, $\%V_{Bur}$ ~30%), creating a groove that is better suited to host bulky substrates as ortho-disubstituted aryl rings.

With these results in mind, we turned our attention to the catalytic step where sterics play the crucial role, namely the transmetallated (NHC)Pd(Ar)(Ar') [where Ar = 2,4,6-trimethylphenyl and Ar' = 2,6-dimethylphenyl] intermediate and the following reductive elimination that leads to the coupled organic product.

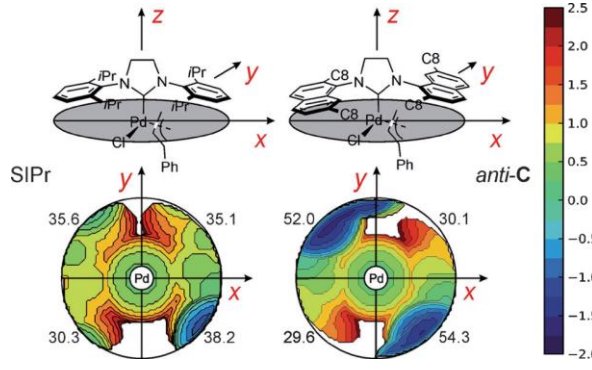

Figure 25. Steric maps of the NHC ligands in the X-ray structure of the (SIPr)Pd(cin)Cl and anti-C complexes. Structures are oriented as shown in the sketches. The number close to each quadrant is the $\%V_{Bur}$ of this quadrant

We first calculated the total energy of the system when going from the starting naked (NHC)Pd(0) species (set at 0 kcal/mol), to the transmetallated (NHC)Pd(Ar)(Ar') intermediate according to equation **1**.

$$(NHC)Pd + ArCl + Ar'B(OH)_2 + KOtBu \rightarrow (NHC)Pd(Ar)(Ar') + KCl + tBuOB(OH)_2 \quad \textbf{(1)}$$

This approach eliminates the specific way the two aryl moieties are loaded on the metal, allowing to concentrate on the crucial step that will be present whatever reaction conditions are chosen or reaction pathways are followed leading to the transmetallated intermediate. The first result is that loading of the two aryls onto the (NHC)Pd(0) species (eq 1), is favored for both (SIPr)Pd (by 23.8 kcal/mol) and [anti-(2,7)-SICyoctNap]Pd (by 30.7 kcal/mol). This in turn means that the special steric environment groove created by the anti-(2,7)-SICyoctNap ligand is able to more readily accommodate (by 6.9 kcal/mol) the bulky aryl fragments than SIPr. An identical preference (6.9 kcal/mol) is also calculated at the level of the following transition state (overall 15 kcal/mol higher in energy) leading to the coupled Ar-Ar' product. Representations of these transition states for both complexes show a distorted T-shaped geometry (Figure 26).

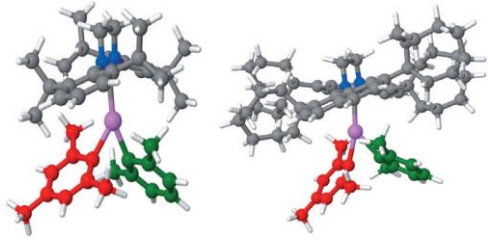

Figure 26. Geometries for the transition state of the reductive elimination for (SIPr)Pd(Ar)(Ar') (left) and [anti-(2,7)-SICyoctNap]Pd(Ar)(Ar') (right)

As already evidenced by the steric contour map of Figure 25, the structures shown in Figure 26 perfectly illustrates that the open quadrants in [anti-(2,7)-SICyoctNap] are able to host the ortho methyl groups of the aryl substituent cis to the NHC ligand. Differently, in presence of the SIPr ligand the same ortho methyl groups interact repulsively with the NHC ligand.
In other words, the special steric characteristics of the this new catalyst is the introduction of a C_2-symmetric NHC ligand with appropriately substituted naphthyl side chains. The 'flexible steric bulk' of this ligand is inherently given by its symmetry, which leaves two of the four quadrants relatively open, thus enhancing the reactivity of the system with respect to the crucial, sterically demanding NHC-Pd(Ar)(Ar') intermediate and the following reductive elimination step.
Together with the overall very bulky nature of this ligand, this translates into the clearly superior catalytic performance that we see in these Suzuki-Miyaura couplings.

4.2.2 Asymmetric catalysis

Despite the use of monodentate N-heterocyclic carbene ligands has become ubiquitous in organometallic chemistry and catalysis, the development of chiral NHC ligands that induce high selectivity in asymmetric metal catalysis is still at an early stage with relatively few reports detailing enantioselectivities of 90% ee and higher.[190,191]
The main difficulties in designing efficient ligands of this type reside in placing stereocontrol elements at positions near the metal center without affecting the overall reactivity of the catalysts.
Chiral NHCs can be mainly classified into two types according to the position of the chiral structural in relation to the donor unit: one has chirality in the N-substituents and the other contains chiral elements within the N-heretocycle (chiral backbone). The latter which is prepared from commercially available chiral diamines has

chirality at the imidazole ring which is quite far away from the metal center.

Prof. Dr. Dorta and coworkers, university of Zurich, recently reported the synthesis of a palladium complex incorporating a bulky NHC ligand with a chiral N-heterocycle and with 2-alkyl-substituted naphthyl side chains, RaRa-C, see Chart 15. In this way, replacing the frequently used symmetric phenyl group (e.g. mesityl or 2,6-diisopropylphenyl group) substituted at nitrogen with mono-ortho-substituted aryl group, the steric effect will potentially transfer the chirality from the backbone to the metal center.[192]

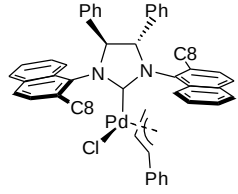

Chart 15.

This asymmetric Pd-catalyzed complex was tested in the intramolecular α-arylation of amides to obtain enantiomerically enriched 3-aryl-3-methyl/allyl fluorine-oxindoles.

Owing to the often attractive properties of such fluorinated compounds for pharmaceutical applications,[193, 194, 195] incorporation of fluorine into organic molecules via enantioselective catalytic processes has been extensively investigated in the past decade and fluorinated oxindole products can be obtained via the catalytic enantioselective fluorination reaction, employing an electrophilic source of fluorine.

However, up to now, no attempts at developing direct α-arylation reactions to gain access to these or other enantioenriched fluorinated compounds have been documented.

Results indicated that the RaRa-C complex of Chart 15 demonstrated the highest enantioselectivity out of all transformations catalyzed by monodentate NHC ligands, see Scheme 9.

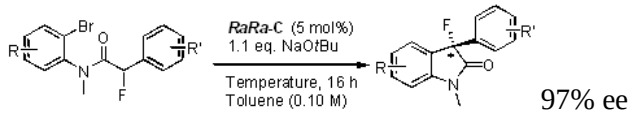

Scheme 9. NHC/Pd-catalyzed α arylation

To rationalize this experimental behavior and visualize any asymmetry in the way the ligand wraps around the metal, the steric demand of the NHC ligand was quantified with the buried volume $\%V_{Bur}$ in the single quadrants around the Pd center, and with the construction of the steric contour maps shown in Figure 27.

The steric map of Figure 27 clearly indicates that two quadrants are heavily hindered (top left and bottom right, $\%V_{Bur}$ ~ 46%), while the other two quadrants are clearly more open (top right and bottom left, $\%V_{Bur}$ ~ 34%), creating a groove that is suited to host bulky substrates.

The ligand wraps around the Pd center with an almost C_2-symmetry, with the naphtyl group syn to the phenyl substituent of the imidazole ring bent toward the metal. This arrangement effectively transfers the stereochemistry of the chiral phenyl substituents to the palladium center to induce a strong chiral environment around it.

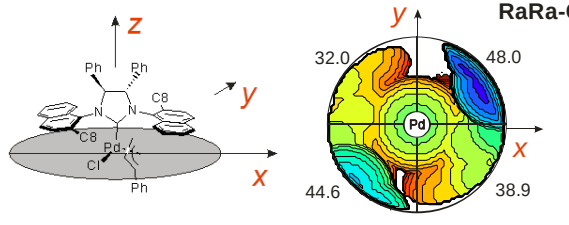

Figure 27. Steric map of the NHC ligand in the X-ray structure of RaRa-C complex. Structure are oriented as shown in the sketch.

To evaluate how this chiral environment is able to induce an energy difference between the products, attention was focused on the key

intermediates, shown in Chart 16, preceding the final reductive elimination of the oxindole product.

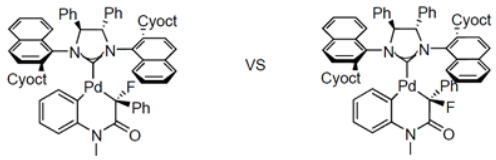

pro-(S) pro-(R)

Chart 16.

The optimized geometries are reported in Figure 28.
Structural analysis indicates that in the most stable intermediate of Figure 28a, leading to the experimentally favored S enantiomer, the aromatic ring that will form the skeleton of the oxindole product, and the Ph substituent on the final chiral C atom of the product are placed below the naphtyl ring, which is in the less buried quadrants highlighted by the steric map of Figure 27. Differently, in the key intermediate of Figure 28b, leading to the experimentally less favored R enantiomer, the Ph substituent on the final chiral C atom of the product is placed below the cyclooctyl ring, which is in a buried quadrant highlighted by the steric map of Figure 27.

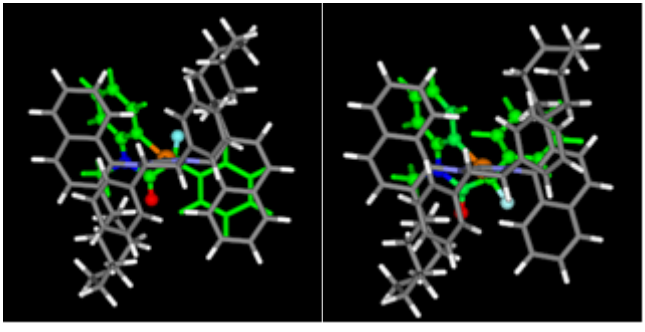

Figure 28. Optimized structure of the key intermediate before final reductive elimination of the products. The intermediates leading to the major S and minor R products are shown in parts a and b, respectively. C atoms of the NHC are colored in grey, C and H atoms of the substrate are colored in green

The relative energy of the two chiral intermediates was calculated. In agreement with the experimental results, the pro-S intermediate, which would lead to a S oxindole, is calculated to be more stable than the pro-R intermediate, which would lead to a R oxindole, by about 4 kcal/mol in toluene.

4.3 Metal free catalysis - Introduction

Organocatalysis[196,197,198] using small-molecule organic compounds as catalysts has risen to prominence over the last decade in organic synthesis, polymer synthesis and other areas, thanks to several advantages it can offer, as compared to other modes of catalysis.
First, many small-molecule organic catalysts are commercially available, inexpensive, and air and moisture stable. Second, small-molecule organic catalysts are readily available from renewable resources and relatively nontoxic and thus "greener" than other types of catalysts. Third, asymmetric catalysis can be achieved by chiral organic reagents, many of which are naturally available from biological sources as single enantiomers.
The term organocatalysis was used for the first time in 2000 from MacMillan and co-workers . They reported the first highly enantioselective
organocatalytic Diels-Alder reaction between cinnamaldehyde and cyclopentadiene using a chiral amine as catalyst.[199]
The general organocatalytic mode of activation involves the cooperation between ion pairs through the formation of covalent bonds or non-covalent interactions like hydrogen bonds or Bronsted acid/base interaction.
Organocaltalytic reactions can be divided in several classes considering the organic molecule involved: amines-enamines-dienamines; hydrogen bonding catalysts, like derivatives of BINOL or catalysts based on thioureas; triazolinium salts; phosphines; N-heterocyclic carbenes.

4.3.1 Organocatalytic Polymerization of Linear and Cyclic Acrylic Monomers by NHCs.[200]

In this section the use of NHCs as organocatalysts in the polymerization of acrylic monomers will be presented.

Thanks to the pioneering work of Waymouth, Hedrick and their co-workers, the utility of the NHC-mediated reactions has been expanded to polymer synthesis,[201, 202,203,204] via predominantly the ring-opening polymerization (ROP) of heterocyclic monomers, such as lactides,[205,206,207] lactones,[208,209,210,211] epoxides,[212,213] cyclic carbonates, [214] cyclic siloxanes, [215 , 216] and N-carboxyl-anhydrides.[217,218]

Although the NHC-mediated ROP of heterocyclic monomers has been highly successful, the NHC-mediated conjugate-addition polymerization of conjugated polar alkenes, such as acrylic monomers, still required the use of a nucleophilic initiator or a Lewis acid catalyst.[219]

Chen and co-workers recently discovered that an NHC alone initiates extremely rapid conjugate-addition polymerization of cyclic acrylic monomers—renewable methylene butyrolactones, including the naturally occurring α-methylene-γ-butyrolactone (MBL) and the biomass-derived γ-methyl-α-methylene-γ-butyrolactone (MMBL). The polymerization achieves quantitative monomer conversion in 1 min with a low NHC quantity loading at room temperature (RT), affording medium or high molecular weight (MW) polymers.

The rate of the polymerization is strongly affected by the relative nucleophilicity of the NHC catalysts employed, with the most nucleophilic ItBu in the series exhibiting the highest activity, the less nucleophilic IMes displaying a much lower activity, and the least nucleophilic TPT often showing no activity at all.

Intriguingly, there exists a remarkable selectivity of the NHC for the substrate structure, thus leading to three different modes of reaction involving acrylic substrates (Figure 29): TPT promotes dimerization of methacrylates such as MMA (pathway A); IMes

selectively forms the single-addition product with methacrylates such as MMA (pathway B); and ItBu mediates rapid polymerization of methylene butyrolactones such as MMBL (pathway C). [220]

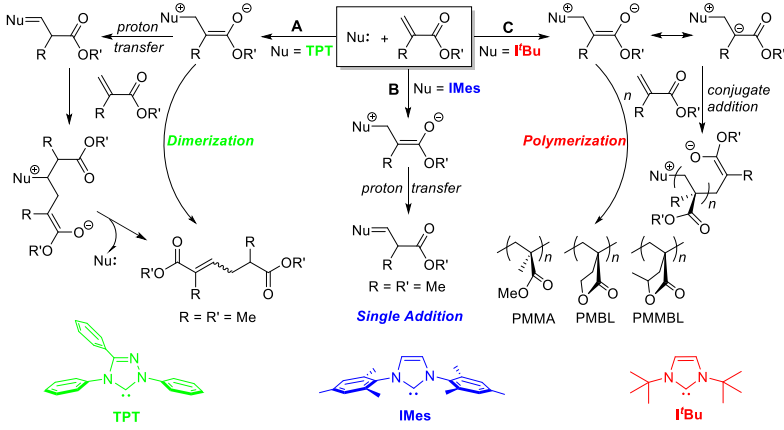

Figure 29. Outlined three distinctive reaction pathways involved in the reaction of NHCs and acrylic monomers.

Accordingly, the behavior of NHCs (IMes, ItBu, and TPT) as initiators or catalysts in the polymerization of MMA and MMBL was further investigated by density functional theory (DFT) calculations.

We investigated the general reactivity shown in Scheme 10. Upon addition of an NHC molecule to monomer **1**, leading to zwitterionic adduct **2**, two possible scenarios were considered. In the first scenario, indicated in Scheme 10 as the enamine/dimerization pathway, there is an overall H-transfer from the C_α to the C_β atom of **2**, leading to enamine **3**, followed by reaction of **3** with another monomer molecule, affording the dimerization product **4** with release of the NHC. In the second scenario, indicated in Scheme 10 as the polymerization pathway, the NHC adduct **2** directly reacts with another monomer molecule via classical 1,4-conjugate addition to start the polymerization process. The mechanisms of the

two pathways were investigated computationally both in toluene and DMF, considering all three NHCs, TPT, IMes, and ItBu, as depicted in Figure 29, and two monomers, the linear MMA and its cyclic analog MMBL.

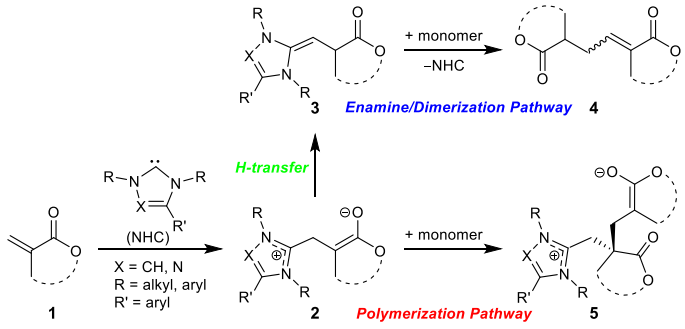

Scheme 10. Outlined two competing reaction pathways involving acrylic monomers (MMA, MMBL) and NHCs

Reactivity of NHCs towards MMA. Energetics relevant to the formation of the zwitterionic species **2** through NHC-addition to monomer is summarized in Table 8.

According to calculations, in either toluene or DMF the lowest energy NHC-MMA zwitterionic adduct **2** is that formed with IMes. Based on the data summarized in Table 8, the relative stability of the NHC-MMA adduct is IMes > TPT ≈ ItBu in toluene. This trend is not that expected based on the relative nucleophilicity of the NHCs (ItBu > IMes > TPT), but rather it correlates with the relative steric demand of the NHCs, as quantified by the buried volume (%V_{Bur}) of the NHC moiety in the MMA adduct, ItBu = 36.1 ≈ TPT = 36.8% > IMes = 32.3%. The rather large %V_{Bur} of TPT is consequence of the rotation of the phenyl rings next to the carbene C atom that assume a conformation nearly coplanar with the NHC ring. In IMes, the ortho Me groups prevent this rotation. On the other hand, the in-plane orientation of the phenyl rings in TPT allows extending the conjugation of the NHC ring, further stabilizing the free TPT molecule. A more polar solvent, DMF,

appears to have a rather small impact on the energy values of the enamine/dimerization manifold reported in Table 8.

Table 8. Energy, reported in kcal/mol and relative to NHC + free MMA, of the species shown in Schemes 3–5, with MMA as the monomer. X-Y denotes transition state (TS) from species X to species Y.

	IMes	ItBu	TPT	IMes	ItBu	TPT
	Toluene			DMF		
1	0	0	0	0	0	0
2	-7.3	0.4	-2.9	-8.1	-1.4	-1.2
	Enamine/Dimerization					
2-2’	4.3	27.4	9.4	6.6	27.7	10.0
2’	-12.4	16.3	-17.2	-10.3	15.3	-15.4
2’-3	-5.9	29.0	-3.8	-1.4	29.9	-1.7
3	-21.9	-5.3	-19.2	-19.9	-4.4	-18.8
3-3’	-2.5	9.9	2.1	-2.0	9.7	1.9
3’	-6.1	6.0	0.9	-7.7	5.4	0.1
4	-19.6	-19.6	-19.6	-18.8	-18.8	-18.8
	Polymerization					
2-5	-3.7	3.6	4.5	-5.5	0.6	2.8
5	-9.4	0.4	-3.6	-12.4	-4.0	-6.1

Zwitterionic adduct **2** is the branching point for dimerization vs polymerization. In the dimerization branch the first step is the H-transfer reaction to form enamine **3**, which reacts with a second MMA monomer to form the dimerization product **4** accompanied by NHC elimination (Scheme 10). Regarding the H-transfer step, owing to the expected high energy of the direct C_α to C_β 1,2-shift, we focused on the two-step, bimolecular mechanism proposed in Scheme 11. In the first step, one H atom (H^1 in Scheme 11) is transferred from the C_α of a first NHC-MMA adduct to the C_β of a second one, leading to the formation of the tightly bound ion pair **2’**. In the second step, the resulting intermediate **2’** undergoes a

further H-transfer reaction where another H atom (H^2 in Scheme 11) is transferred from the C_α of the second moiety to the C_β of the first moiety, generating two molecules of enamine product **3**. A similar two-step bimolecular proton transfer mechanism was proposed for the Stetter reaction in non-protic media involving 1,4-addition of aldehydes and Michael acceptors.

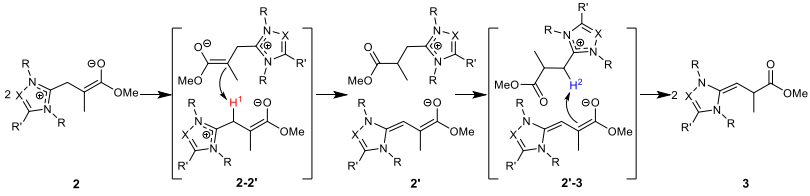

Scheme 11. Proposed two-step bimolecular H transfer mechanism involving the ion pair intermediate

The energetics of the species in Scheme 11 is reported in Table 8.
Starting with TPT, the TPT-MMA adduct **2** undergoes a first H-transfer through TS **2-2'** with a barrier of ~11-12 kcal/mol, leading to the charged intermediate **2'**, roughly 14 kcal/mol below **2**. The second H-transfer, through TS **2'-3**, also has a barrier of about 13 kcal/mol and leads to the final enamine **3**, which is clearly more stable than the initial adduct **2** (by ~16 kcal/mol) and also of **2'** (by ~2 kcal/mol). The enamine product **3** can react with a further MMA monomer via a classical monomer addition step (Scheme 11), through TS **3-3'** with a barrier of about 20 kcal/mol, leading to the high energy TS **3'**. A final H-transfer step converts **3'** into dimerization product **4** with release of TPT and an energy gain of only 0.4 kcal/mol in toluene relative to **3**, and basically thermo-neutral in DMF.
These yielded mechanistic features for the TPT-catalyzed MMA dimerization, including bimolecular (or intermolecular) proton transfer and the rate-limiting step being the addition of the enamine intermediate to the second MMA (which exhibits the highest activation barrier of ~21 kcal/mol), agree well with the most recent

results of experimental mechanistic studies by Matsuoka and co-workers.[221]

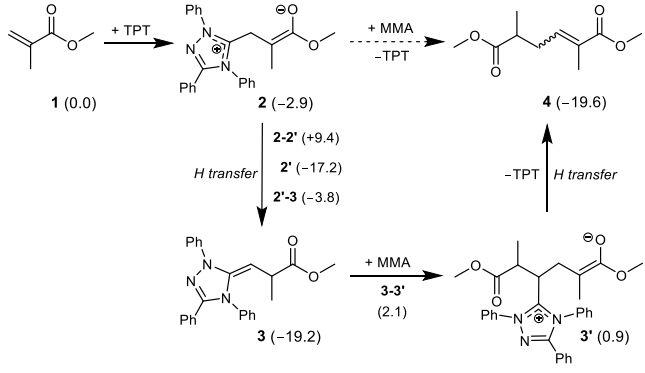

Scheme 11. Energetics of MMA dimerization catalyzed by TPT.

Moving to IMes, we found that the energy profiles of IMes are rather similar to those of TPT, with all TSs being of reasonably close energy. However, there is a relevant difference in the relative stability of enamine **3** with respect to product **4**. In fact, according to calculations, enamine **3** is the most stable species in the IMes promoted reactivity of MMA, whereas for TPT the most stable species is dimer **4**. This difference suggests that in the presence of IMes MMA dimerization is unfavored because dimer **4** is 2.3 kcal/mol higher in energy than enamine **3**. Finally, ItBu is unable to promote MMA dimerization, due to the high-energy barrier for the first H transfer, 27 kcal/mol. All these computational results are consistent with the experimental findings.

Next we examined the behavior of the NHC-MMA zwitterionic adduct **2** in promoting polymerization, through addition of a second MMA to **2** (Scheme 20). Analysis of the data reported in Table 8 indicates that addition of a second MMA molecule to any of the NHC-MMA adducts, through TS **2-5**, is a rather feasible process with a barrier smaller than 10 kcal/mol, whatever NHC and solvent is considered. The product of the first propagation step (i.e., the second monomer addition), **5**, is only slightly more stable than the

starting species, making addition of MMA to the NHC-MMA adduct reversible. Comparison of the H transfer with the polymerization pathway, that is TS **2-2'** vs **2-5**, indicates that for TPT the barrier for the second monomer addition, roughly 4-7 kcal/mol, is about one half of that for the H-transfer converting **2** into enamine species 3 and finally the dimer product **4**. However, the overall product of the H transfer, dimer 4, is the thermodynamically more stable species, in agreement with the experimental evidence that the TPT-MMA adduct undergoes H transfer and then dimerizes. Moving to IMes, the energy profiles of TPT and IMes promoted polymerization are again rather similar, with the difference being that IMes, in agreement with the experimental results, stops at the more stable enamine product 3 without reaching to dimer **4**. These conclusions are independent of the solvent polarity.

Lastly for ItBu, the computational data are different from those for IMes and TPT, and further are different in toluene and in DMF. In fact, in toluene the H-transfer barrier leading to enamine **3** is too high (27 kcal/mol), preventing the reaction to move along this pathway, while the MMA addition barrier starting polymerization is low, but the addition product **5** is not stable. As consequence, ItBu is practically inactive towards MMA in toluene. Moving to DMF, the H-transfer reaction along the enamine/dimerization pathway is still inaccessible, but the ItBu-MMA adduct can add another monomer with a negligible energy barrier leading to stable addition product **5**, – 4.0 kcal/mol below MMA + ItBu. Obviously, the higher stability of the addition product (the zwitterionic propagating species) along the polymerization pathway in the more polar DMF is due to the electrostatic stabilization. Again, these computational data are in agreement with the experiments that showed that ItBu does not react with MMA in toluene, but it polymerizes MMA in DMF (vide supra).

Termination Reaction in MMA Polymerization. In this section we discuss a possible mechanism of termination operative in the

MMA polymerization promoted by ItBu in DMF. We investigated the pathway proposed in Scheme 12, and used two methyl groups to model the chain segment connecting the cationic and anionic moieties of the growing chain in the starting zwitterionic species (P = CH_3 in Scheme 12). This termination reaction corresponds to a H-transfer from the -CH_2- group bound to the ItBu to the enolate C atom of the chain end, through a TS with a barrier of 8.8 kcal/mol, leading to the termination product (an enamine) with chain ends shown in the Scheme 12. The resulting termination product is 13.1 kcal/mol lower in energy relative to the starting zwitterionic propagation species considered. However, the barrier for the propagation species to add another MMA (~ 2 kcal/mol) is much lower than that for this termination step, explaining why a medium-high MW polymer (33.2 kg/mol) is achieved by ItBu in DMF. We also considered the possibility of the enamine termination product to add another MMA molecule, but the energy barrier for this addition is calculated to 26.8 kcal/mol. Overall, these computational results are in agreement with experimental evidence for the observed enamine chain ends by ^{1}H NMR and MALDI-TOF MS (vide supra), and the MMA polymerization is non-catalytic (i.e., the terminated enamine species is not longer active for further MMA additions).

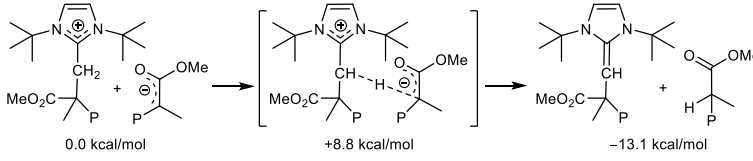

Scheme 12. Energetics for species involved in the termination step of MMA polymerization by ItBu in DMF. Note the cationic and anionic moieties of the growing chain are connected through two P sites.

Reactivity of NHCs towards MMBL. The same competing enamine/dimerization and polymerization pathways were explored for MMBL, the results of which are reported in Table 9. The overall

scenario emerging from Table 9 is rather similar to that discussed above for MMA; hence, the details are not discussed here, illuminating instead the differences.

In short, the energetic numbers reported in Table 9 indicate again that ItBu behaves differently with respect to IMes and TPT also in case of MMBL. The energy of TS 1-2 for the formation of the zwitterionic adduct **2** with ItBu is roughly 7-8 kcal/mol higher in energy than that with IMes and TPT and the energy barrier for the H-transfer step along the enamine/dimerization pathway is roughly 20 kcal/mol higher than that calculated for IMes and TPT. This barrier is high enough to conclude that ItBu is unable to promote reactivity along the enamine/dimerization pathway also for MMBL. Conversely, IMes and TPT result in a low energy barrier for the first H-transfer step, about 9-15 kcal/mol, and in stable products, about 18-23 kcal/mol below NHC + free MMBL, in both toluene and DMF. However, for both IMes and TPT enamine **3** is more stable than dimer **4**, which is in agreement with the experimental evidence that no dimer of MMBL is formed whatever NHC is considered.

Table 9. Energy, reported in kcal/mol and relative to NHC + free MMBL, of the species shown in Schemes 9 – 10, with MMBL as the monomer

	IMes	ItBu	TPT	IMes	ItBu	TPT
	Toluene			DMF		
1	0	0	0	0	0	0
1-2	6.1	14.4	7.1	7.8	12.9	8.7
2	-8.8	-0.6	-2.7	-9.9	-3.1	-2.6
	Enamine/Dimerization					
2-2’	4.1	24.5	6.7	5.3	24.8	8.7
2’	-18.6	4.7	-19.3	-15.6	4.8	-15.6
2’-3	-10.8	25.0	-6.8	-6.3	27.7	-3.0
3	-23.2	-5.0	-19.3	-20.2	-4.3	-18.6
3-3’	-7.0	9.6	-2.0	-6.8	-2.9	7.6
3’	-10.9	3.8	-5.1	-13.7	-1.2	-8.1
4	-18.7	-18.7	-18.7	-18.4	-18.4	-18.4
	Polymerization					
2-5	-4.8	1.8	0.7	-4.9	0.7	2.1
5	-10.0	-4.5	-7.0	-10.4	-6.7	-7.2

Next we focused on the first step of the polymerization pathway, in which the NHC-MMBL zwitterionic adduct **2** attacks the exocyclic CH_2 group of a MMBL molecule via 1,4-conjugate addition. As for MMA, the most stable NHC-monomer adduct is the one with IMes in both solvents, followed by the adduct with TPT in toluene and the one with ItBu in DMF. Again, the energy barrier for the NHC-MMBL adduct **2** to add another monomer molecule, through TS **2-5**, is quite small with all the three NHCs considered herein, 2.4 kcal/mol for ItBu, 3.4 kcal/mol for TPT and 4.0 kcal/mol for IMes

in toluene. A similar trend is seen in DMF. These computational data would suggest that the all the three NHC considered could promote MMBL polymerization. In fact, experimentally ItBu promotes extremely rapid polymerization of MMBL in both solvents, especially in DMF, and IMes also initiates MMBL polymerization in either solvent, albeit with much lower activity, while TPT is inactive for MMBL polymerization in DMF but in toluene it is active with even lower activity than IMes (vide supra).
The different reactivity trend towards MMBL polymerization among the three NHCs can be rationalized by relative aptitude in competing H-transfer and monomer-addition reactions involving the zwitterionic adduct **2**. Specifically, in the case of ItBu, the H-transfer reaction barrier along the enamine/dimerization pathway is much larger than the barrier along the polymerization pathway, permitting the reactivity only along the polymerization pathway and shutting down the enamine/dimerization pathway. In case of TPT and IMes, both the H-transfer reaction along the enamine/dimerization pathway and the MMBL addition along the polymerization pathway can occur, in principle, since they both show relatively low energy barriers. Although the barrier for the polymerization step is clearly lower than the barrier for the H-transfer, the most remarkable difference between the two pathways is in the stability of the products. In fact, the MMBL addition product **5** along the polymerization pathway is roughly 10 kcal/mol less stable than the H-transfer reaction product enamine **3**. Since MMBL addition from **2** to **5** can be reversed, the system can accumulate into the most stable enamine **3**, reducing the polymerization activity. However, the system with IMes is more biased toward the polymerization pathway, since the preference for the polymerization pathway, measured by the energy difference between TSs **2-2'** and **2-5**, increases by roughly 2 kcal/mol on going from TPT to IMes. This analysis explains the experimental evidence that the MMBL polymerization activity with IMes is somewhat between ItBu and TPT activities.

As the other general trend for ItBu and IMes, comparison of the energetics in toluene with that in DMF indicates that in the more polar DMF solvent the NHC-monomer adduct **2** tends to be more stable, and the energy barrier for the monomer addition becomes slightly lower; this observation is in agreement with the greater experimental activity of these two NHCs in DMF. However, the trend for TPT is opposite in the two solvents, in agreement with the experimental results showing that TPT is inactive for MMBL polymerization in DMF.

Considering that the data reported in Table 9 indicate that the TS **1-2** for the formation of ItBu-MMBL adduct is the highest in energy, and yet the experimental data showed that ItBu is the most active in the MMBL polymerization, we explored the alternative initiation pathway outlined in Scheme 13. In this pathway, an NHC serves as a strong base to abstract a proton of MMBL, forming a high-energy, highly reactive anion that initiates rapid polymerization. We examined abstraction of both β- and γ-protons of MMBL and found that abstraction of β-H costs 14.3 kcal/mol, while abstraction of γ-H costs 49.5 kcal/mol. Accordingly, the much preferred β-H abstraction generates an initiating species, anionic monomer **6** stabilized by electronic delocalization over the extend π-conjugated orbitals (Scheme 13). The first propagation step consists of addition of **6** to another MMBL molecule. The energetics of the alternative mechanism shown in Scheme 13 in DMF is report in Table 10.

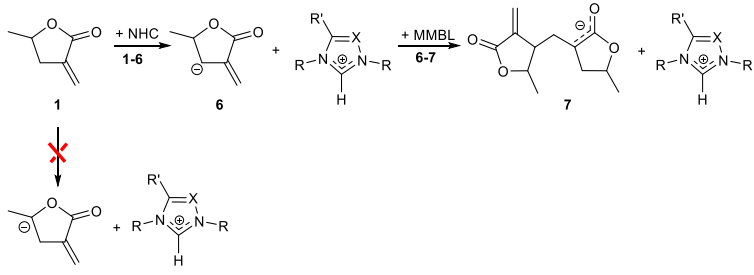

Scheme 13. A possible alternative initiation and propagation pathway for the MMBL polymerization by NHCs, where the NHC serves as a base

Table 10: Energy, reported in kcal/mol and relative to NHC + free MMBL, of the species shown in Scheme 13.

	IMes	ItBu	TPT
		DMF	
1	0	0	0
1-6	17.6	16.7	20.1
6	17.7	14.3	32.0
6-7*	-	-	-
7	-4.4	-7.8	+9.9

* No energy barrier

The rate-determining step for all the three NHCs is the formation of the active species **6** through abstraction of the β-proton from MMBL by an NHC base. In fact, once the anion **6** is formed, it can add a monomer molecule without any energy barrier. Thus, the highest energy barrier in the reaction pathway of Scheme 13, through TS **1-6** is roughly 17-20 kcal/mol for the three NHC systems. Comparing the energy of TS **1-6** in Table 10, and TS **1-2** in Table 9, it is clear that the mechanism of Scheme 13 is highly unfavored relative to the mechanism of Scheme 10 for both IMes and TPT. In fact, the energy barrier of TS 1-2 is 9.8 and 11.4 kcal/mol lower than TS **1-6** for IMes and TPT, respectively. For ItBu, the difference is lower, but with TS **1-2** being 3.8 kcal/mol lower in energy than TS **1-6**, the proton abstraction pathway outlined in Scheme 13 is still very unlikely.
This conclusion is further reaffirmed by the experiment that showed no reaction took place between ItBu and γ-valerolactone (1–5 equiv), a suitable non-polymerizable monomer model possessing even more acidic protons than the monomer MMBL.

Termination Reaction in MMBL Polymerization. To shed light on the termination mechanism operating in the MMBL

polymerization promoted by ItBu, we explored several different termination pathways. The first mechanism, consisting of SN_2 nucleophilic substitution reaction where the NHC is the leaving group, would lead to formation of a cyclic polymer, according to the two possible pathways schematized in Scheme 14. In the mechanism of Scheme 14a the nucleophile center is the C_α atom of the last MMBL unit and a new C–C bond is formed in **10**, while in that of Scheme 14b the nucleophile center is the enolate oxygen, where the major negative charge is localized, and an O–C bond is formed in **11**. In both cases two methyl groups were used to model the chain segment connecting the cationic and anionic moieties of the growing chain in the starting zwitterionic species **9** (P = CH_3 in Scheme 14). This treatment avoids the complication of modeling a long polymer chain joining the two reacting moieties. Nevertheless, both pathways showed of very high energy, with the mechanism of Scheme 14a resulting in a barrier higher than 40 kcal/mol, while for the mechanism in Scheme 14b the calculated barrier is ~ 50 kcal/mol, thus effectively ruling out these termination pathways. This analysis is consistent with our experimental result that showed no cyclic polymer formation.

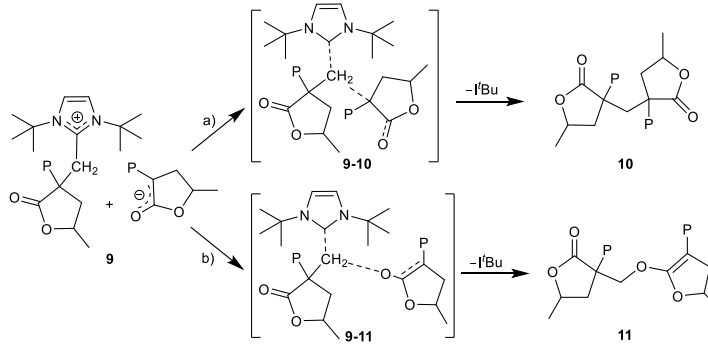

Scheme 14. Examined two possible termination pathways to a cyclic polymer

Keeping in mind the feasibility of H-transfer reactions with these systems, we investigated the possible chain termination pathways

outlined in Scheme 15 starting from the active zwitterionic propagating species **12**. The relative energetics of all species involved is summarized in Table 11. The first step of the termination sequence corresponds to a H-transfer from the -CH_2- group bound to the ItBu to the enolate C atom of the chain end in **12**, through TS **12-13** with a barrier of roughly 10 kcal/mol, leading to enamine type species 13 and chain end CE1 (Scheme 15). Chain end **CE1** could not be identified by NMR, due to its overlap with the main polymer peaks, but the enamine moiety in **13** can be readily identifiable by NMR and MALDI-TOF MS (vide supra). Interestingly, this reaction also allows for formation of an enamine type structure with ItBu, a step not possible by direct H-transfer between two ItBu-MMBL adducts (c.f., Table 9). Enamine species **13** can further react with another MMBL molecule through a classical 1,4-addition to give IM **14**, through TS **13-14** with an energy barrier of also roughly 10 kcal/mol (in DMF), and finally chain end, **CE2**, through a second H-transfer step. Alternatively, the reaction of enamine species **13** with another MMBL could proceed via a less favored 1,2-addition pathway to give IM **15**, through TS **13-15** with a barrier of roughly **15** kcal/mol. Subsequently, IM **15** could undergo another H transfer or nucleophilic substitution by the oxygen atom, leading respectively to chain end **CE3** or **CE4**. However, the TSs for the final nucelophilic attack or H-transfer have been calculated to be more than 40 kcal/mol higher in energy, making this termination pathways unlikely.

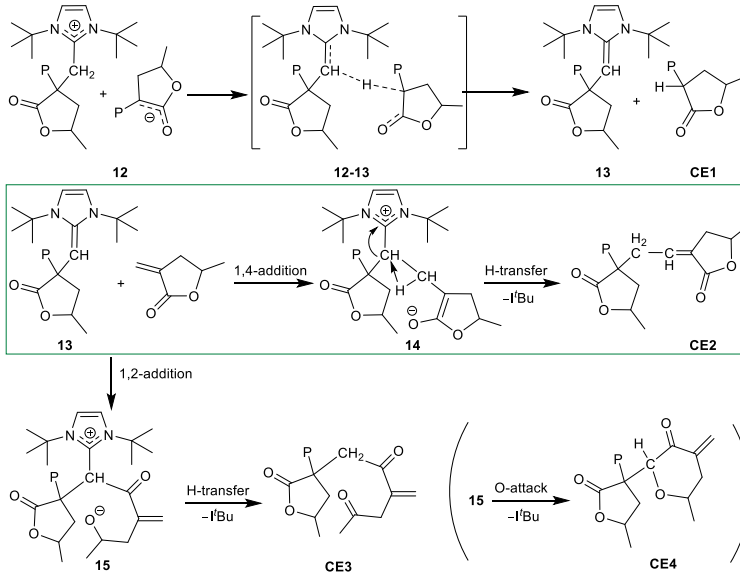

Scheme 15. Possible termination pathways through H-transfer and enamine intermediate 13.

Table 11. Energy, in kcal/mol, of the species shown in Scheme 15

	ItBu	ItBu
	Toluene	DMF
12	0	0
12-13	9.9	10.8
13 + CE1	-12.8	-10.7
13-14	2.1	-0.2
CE2	-31.2	-30.7
13-15	8.5	9.7
15	6.2	6.7
15-CE3	> 30	> 30
15-CE4	39.6	42.1
CE3	-18.2	-17.4
CE4	-9.8	-7.6

We further investigated the third possible chain termination pathway through chain transfer to monomer as outlined in Scheme 16. In this case the reactive enolate chain end abstracts a proton from the β-C of the monomer, with a barrier of only 6.8 kcal/mol. As result, the old chain P still has the $[NHC]^+$ attached to it as the polymeric counterion, paired with the monomer anion that re-initiates a new chain, effecting a catalytic polymerization.
Although the overall reaction seems to be not favored (i.e., the products are 1.6 kcal/mol higher in energy vs. the reactants), it is worth noting that the generated strong nucleophile (anionic monomer) can readily add a monomer without any energy barrier (Scheme 16), leading to formation of more favored products (with an energy gain of 20.5 kcal/mol for the addition of the second monomer).

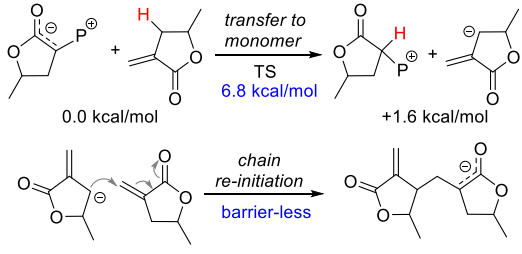

Scheme 16. Chain transfer to the monomer pathway

Overall, after having explored several different termination pathways, we found that only H-transfer/enamine addition and transfer to monomer pathways are energetically feasible. Between these two pathways, the chain termination, through an H-transfer reaction to generate the enamine type intermediate **13**, followed by an 1,4-addition to another MMBL molecule and subsequent second H-transfer to finally chain end **CE2** and release of the NHC catalyst (green box, Scheme 15), has an activation energy barrier of slightly higher than 10 kcal/mol, while the chain termination through chain transfer to monomer (Scheme 16) has an energy barrier of less than 7 kcal/mol. On the basis of experimental results (vide supra), the H-

transfer/enamine addition termination is effective only with a high NHC loading (e.g., the NMR signals relative to **CE1** and **CE2** were found with a [MMBL]0/[ItBu]0 ratio of 5:1 or similar). In other instances (e.g., high [MMBL]0/[ItBu]0 ratios) the chain-transfer termination to monomer, which is more favored from an energetic point of view (6.8 kcal/mol vs. 10 kcal/mol), takes place. Finally, these activation energies associated with the chain termination events are compared to a barrier of only ~3 kcal/mol for the active propagation species to add another MMBL, thereby explaining why a rather high MW polymer (up to ~ 90 kg/mol) can be achieved by ItBu.

Conclusions

The main goal of this PhD thesis has been providing a computational support to the development of new or better performing catalysts, leading to the synthesis of new materials.
In this context, it is worth remembering that catalysis is a topic of primary relevance in the academy as well as in the industry, due to the enormous impact of catalysis in every day life.
In particular, within this PhD project, attention has focused on catalytic systems based on N-heterocyclic carbene (NHC) ligands, which have emerged as useful ligands in the last ten years.
In the first part of this thesis, the development of new molecular descriptors for the quantification of steric and electronic effects in transition metal based catalysts has been pursued.
The final goal of this approach consists in rationalizing the highly disorganized and chaotic catalytic space, to orientate experimental efforts towards possibly well performing catalysts, and away from the ineffective ones. This would allow to pursue a catalysis by design approach, in alternative to the "trial and error" classical approach.
In particular, descriptors based on topographic steric maps have emerged as powerful tools that can be easily used and interpreted by the scientific community.
A user friendly web server has been implemented in order to allow the scientific community to build steric maps for the systems of interest. The web server has already achieved great success with a number of visitors all around the world.
In the second part of the thesis, attention was focused on developing and rationalizing new catalysts in strict collaboration with experimental groups.
The systems investigated represent advanced application of N-heterocyclic carbenes as ligand in Ru-catalyzed olefin metathesis, Pd-catalyzed C-C cross coupling reactions, and as catalysts in the organopolymerization of polar olefins.

The detailed mechanistic studies have offered a comprehensive understanding of the whole mechanisms, an achievement almost impossible to achieve with experimental techniques only.
The studies described in this work demonstrated that computational techniques can be of enormous value to screen novel catalyst architectures more rapidly, and to obtain insights that could help in the design and experimental synthesis of novel and improved catalysts.

References

[1] Kohn, W. and L. J. Sham (**1965**), *Physical Review* 140(4A): A1133.

[2] Frisch, M. J., et al. (**2009**), Gaussian 09. Pittsburgh PA, Gaussian, Inc.

[3] ADF 2012, SCM, Theoretical Chemistry, Vrije Universiteit, Amsterdam, The Netherlands, http://www.scm.com. Baerends, E. J.; Ziegler, T.; Autschbach, J.; Bashford, D.; Bérces, A.; Bickelhaupt, F. M.; Bo, C.; Boerrigter, P. M.; Cavallo, L.; Chong, D. P.; Deng, L.; Dickson, R. M.; Ellis, D. E.; van Faassen, M.; Fan, L.; Fischer, T. H.; Fonseca Guerra, C.; Ghysels, A.; Giammona, A.; van Gisbergen, S. J. A.; Götz, A. W.; Groeneveld, J. A.; Gritsenko, O. V.; Grüning, M.; Gusarov, S.; Harris, F. E.; van den Hoek, P.; Jacob, C. R.; Jacobsen, H.; Jensen, L.; Kaminski, J. W.; van Kessel, G.; Kootstra, F.; Kovalenko, A.; Krykunov, M. V.; van Lenthe, E.; McCormack, D. A.; Michalak, A.; Mitoraj, M.; Neugebauer, J.; Nicu, V. P.; Noodleman, L.; Osinga, V. P.; Patchkovskii, S.; Philipsen, P. H. T.; Post, D.; Pye, C. C.; Ravenek, W.; Rodríguez, J. I.; Ros, P.; Schipper, P. R. T.; Schreckenbach, G.; Seldenthuis, J. S.; Seth, M.; Snijders, J. G.; Solà, M.; Swart, M.; Swerhone, D.; te Velde, G.; Vernooijs, P.; Versluis, L.; Visscher, L.; Visser, O.; Wang, F.; Wesolowski, T. A.; van Wezenbeek, E. M.; Wiesenekker, G.; Wolff, S. K.; Woo, T. K.; Yakovlev.

[4] Baerends, E. J., D. E. Ellis and P. Ros (**1973**), *Chemical Physics* 2: 41.

[5] Becke, A. D. (**1988**), *Physical Review* 38: 3098.

[6] Perdew, J. P. (**1986**), *Phyical Review B* 34: 7406.

[7] Perdew, J. P. (**1986**), *Phyical Review B* 33: 8822.

[8] Weigend, F., Ahlrichs, R. (**2005**), *Chemical Physics 7*: 3297.

[9] Haeusermann, U., Dolg, M., Stoll, H., Preuss, H. (**1993**), *Molecular Physics* 78: 1211.

[10] Kuechle, W., Dolg, M., Stoll, H., Preuss, H. (**1994**), *Journal of Chemical Physics* 100: 7535

[11] Leininger, T, Nicklass, A., Stoll, H., Dolg, M.,Schwerdtfeger, P. (**1996**), *Journal of Chemical Physics* 105: 1052.

[12] Zhao, Y., Truhlar, D. G. (**2006**), *Journal of Chemical Physics* 125: 194101.

[13] Zhao, Y., Truhlar, D. G. (**2008**), *Theoretical Chemical Accounts* 120: 215.

[14] D. Rappoport, D., F. Furche, F. (**2010**), *Journal of Chemical Physics* 133: 134105.

[15] Tomasi, J., Mennucci, B., Cammi, R. (**2005**), *Chemical Review* 105: 2999.

[16] Barone, V., Cossi, M. (**1998**), *Journal of Physical Chemistry A* 102: 1995.

[17] Arduengo, A. J., et al. (**1991**), *Journal of the American Chemical Society* 113(1): 361.

[18] Huang, J., E. D. Stevens, S. P. Nolan and J. L. Petersen (**1999**), *Journal of The American Chemical Society* 121(12): 2674.

[19] Scholl, M., S. Ding, C. W. Lee and R. H. Grubbs (**1999**), *Organic Letters* 1(6): 953.

[20] Weskamp, T., F. J. Kohl, W. Hieringer, D. Gleich and W. A. Herrmann (**1999**), *Angewandte Chemie International Edition* 38: 2416.
[21] Trnka, T. M. and R. H. Grubbs (**2000**), *Accounts of Chemical Research* 34(1): 18.
[22] Fürstner, A. (**2000**), *Angewandte Chemie International Edition* 39: 3012.
[23] Samojłowicz, C., M. Bieniek and K. Grela (**2009**), *Chemical Reviews* 109: 3708.
[24] Grubbs, R. (**2003**), Handbook of olefin Metathesis. Wiley-VCH: Weinheim, Germany
[25] Rouhi, M. A. (**2002**), *Chemical Engineering News* 80: 29.
[26] Rybak, A. and M. A. R. Meier (**2007**), *Green Chemistry* 9: 1356.
[27] Malacea, R., C. Fischmeister, C. Bruneau, J. L. Dubois, J. L. Couturier and P. H. Dixneuf (**2009**), *Green Chemistry* 11: 152.
[28] Tsantrizos, Y. S., J.-M. Ferland, A. McClory, M. Poirier, V. Farina, N. K. Yee, X.-j. Wang, N. Haddad, X. Wei, J. Xu and L. Zhang (**2006**), *Journal of Organometallic Chemistry* 691(24-25): 5163.
[29] Kanada, R. M., D. Itoh, M. Nagai, J. Niijima, N. Asai, Y. Mizui, S. Abe and Y. Kotake (**2007**), *Angewandte Chemie International Edition* 46(23): 4350.
[30] Wallace, D. J., J. M. Goodman, D. J. Kennedy, A. J. Davies, C. J. Cowden, M. S. Ashwood, I. F. Cottrell, U.-H. Dolling and P. J. Reider (**2001**), *Organic Letters* 3(5): 671.
[31] Assen , E., et al. (**2007**), *Angewandte Chemie International Edition* 46(16): 2768.
[32] Miyaura, N. and A. Suzuki (**1995**), *Chemical Reviews* 95(7): 2457.
[33] Marion, N. and S. P. Nolan (**2008**), *Accounts of Chemical Research* 41(11): 1440
[34] Würtz, S. and F. Glorius (**2008**), *Accounts of Chemical Research* 41(11): 1523.
[35] Diez-Gonzalez, S., N. Marion and S. P. Nolan (**2009**), *Chemical Reviews* 109(8): 3612.
[36] Wolfgang, A. H., J. G. Lukas, K. Christian and R. J. A. Georg (**1996**), *Angewandte Chemie International Edition* 35(23-24): 2805.
[37] Laitar, D. S., P. Muller and J. P. Sadighi (**2005**), *Journal of the American Chemical Society* 127(49): 17196.
[38] Kleeberg, C., L. Dang, Z. Lin and T. B. Marder (**2009**), *Angewandte Chemie International Edition* 48(29): 5350.
[39] Danopoulos, A. A., D. Pugh and J. A. Wright (**2008**), *Angewandte Chemie International Edition* 47(50): 9765.
[40] Hanasaka, F., Y. Tanabe, K.-i. Fujita and R. Yamaguchi (**2006**), *Organometallics* 25(4): 826.
[41] Powell, M. T., D.-R. Hou, M. C. Perry, X. Cui and K. Burgess (**2001**), *Journal of the American Chemical Society* 123(36): 8878.
[42] Lee, C. W. and R. H. Grubbs (**2001**), *Journal of Organic Chemistry* 66(21): 7155.
[43] Nieto-Oberhuber, C., S. López, E. Jiménez-Núñez and A. M. Echavarren (**2006**), *Chemistry - A European Journal* 12: 5916.

[44] Añorbe, L., G. Domínguez and J. Pérez-Castells (**2004**), *Chemistry - A European Journal* 10: 4938.
[45] Scott, N. M., R. Dorta, E. D. Stevens, A. Correa, L. Cavallo and S. P. Nolan (**2005**), *Journal of the American Chemical Society* 127(10): 3516.
[46] De Frémont, P., N. M. Scott, E. D. Stevens, T. Ramnial, O. C. Lightbody, C. L. B. Macdonald, J. A. C. Clyburne, C. D. Abernethy and S. P. Nolan (**2005**), *Organometallics* 24(26): 6301.
[47] Fantasia, S., J. L. Petersen, H. Jacobsen, L. Cavallo and S. P. Nolan (**2007**), *Organometallics* 26(24): 5880.
[48] Kelly, R. A., III, H. Clavier, S. Giudice, N. M. Scott, E. D. Stevens, J. Bordner, I. Samardjiev, C. D. Hoff, L. Cavallo and S. P. Nolan (**2008**), *Organometallics* 27(2): 202.
[49] Leuthäußer, S., V. Schmidts, C. M. Thiele and H. Plenio (**2008**), *Chemistry - A European Journal* 14(18): 5465.
[50] Frey, G. D., C. F. Rentzsch, D. von Preysing, T. Scherg, M. Muehlhofer, E. Herdtweck and W. A. Herrmann (**2006**), *Journal of Organometallic Chemistry* 691: 5725.
[51] Khramov, D. M., V. M. Lynch and C. W. Bielawski (**2007**), *Organometallics* 26(24): 6042.
[52] Sanderson, M. D., J. W. Kamplain and C. W. Bielawski (**2006**), *Journal of the American Chemical Society* 128(51): 16514.
[53] Hu, X. L., I. Castro-Rodriguez, K. Olsen and K. Meyer (**2004**), *Organometallics* 23(4): 755.
[54] Chianese, A. R., A. Kovacevic, B. M. Zeglis, J. W. Faller and R. H. Crabtree (**2004**), *Organometallics* 23(10): 2461.
[55] Chianese, A. R., X. Li, M. C. Janzen, J. W. Faller and R. H. Crabtree (**2003**), *Organometallics* 22(8): 1663.
[56] Herrmann, W. A., Öfele, K., Elison, M., Kuhn, F. E. and Roesky, P. W. (**1994**), *Journal of Organomeallic Chemistry 480*, C7.
[57] Herrmann, W. A., Runte, O. and Artus, G.(**1995**), *Journal of Organometallic Chemistry 501*, C1.
[58] Boehme, C. and Frenking, G. (**1998**), *Organometallics 17*: 5801.
[59] Frenking, G. and Fröhlich, N. (**2000**), *Chemical Reviews 100*: 717.
[60] Garrison, J. C., Simons, R. S., Kofron, W. G., Tessier, C. A. and Youngs, W. J. (**2001**), *Chemical Communications* 1780.
[61] Schumann, H., Glanz, M., Gottfriedsen, J., Dechert, S. and Wolff, D. (**2001**), *Pure And Applied Chemistry* 73: 279.
[62] Tulloch, A. A. D., Danopoulos, A. A., Kleinhenz, S., Light, M. E., Hursthouse, M. B. and Eastham, G. (**2001**), *Organometallics* 20: 2027.
[63] Niehues, M., Erker, G., Kehr, G., Schwab, P., Fröhlich, R., Blacque, O. and Berke, H. (**2002**), *Organometallics* 21: 2905.
[64] Hillier, A. C., Sommer, W. J., Yong, B. S., Petersen, J. L., Cavallo, L. and Nolan, S. P. (**2003**), *Organometallics 22*: 4322.
[65] Hu, X. L., Tang, Y. J., Gantzel, P. and Meyer, K. (**2003**), *Organometallics 22*: 612.
[66] Tonner, R., Heydenrych, G. and Frenking, G. (**2007**), *Chemistry -An Asian Journal 2*: 1555.
[67] Tolman, C. A. (**1977**), *Chem. Rev*. 77(3): 313.

[68] Dunne, B. J., Morris, R. B. and Orpen, A. G. (**1991**), *Journal of the Chemical Society-Dalton Transactions* 653.
[69] White, D., Taverner, B. C., Leach, P. G. L. and Coville, N. J. (**1993**), *Journal Of Computational Chemistry* 14: 1042.
[70] White, D., Taverner, B. C., Coville, N. J. and Wade, P. W. (**1995**), *Journal Of Organometallic Chemistry* 495: 41.
[71] Taverner, B. C., (**1996**), *Journal Of Computational Chemistry* 17: 1612.
[72] Taverner, B. C., Smith, J. M., White, D. P. and Coville, N. J. (**1997**), *South Afrikan Journal of Chemistry* 50: 59.
[73] Cooney, K. D., Cundari, T. R., Hoffman, N. W., Pittard, K. A., Temple, M. D. and Zhao, Y. (**2003**), *Journal of the American Chemical Society* 125: 4318.
[74] Immirzi, A. and A. Musco (**1977**), *Inorganica Chimica Acta* 25(0): L41-L42.
[75] Ferguson, G., P. J. Roberts, E. C. Alyea and M. Khan (**1978**), *Inorganic Chemistry* 17(10): 2965.
[76] Huang, J., H.-J. r. Schanz, E. D. Stevens and S. P. Nolan (**1999**), *Organometallics* 18(12): 2370.
[77] Viciu, M. S., Navarro, O., Germaneau, R. F., Kelly, R. A., Sommer, W., Marion, N., Stevens, E. D., Cavallo, L. and Nolan, S. P. (**2004**), *Organometallics 23*, 1629.
[78] Cavallo, L., Correa, A., Costabile, C. and Jacobsen, H. (**2005**), *Journal of Organometallic Chemistry 690*, 5407.
[79] Dorta, R., Stevens, E. D., Scott, N. M., Costabile, C., Cavallo, L., Hoff, C. D. and Nolan, S. P. (**2005**), *Journal of the American Chemical Society 127*: 2485.
[80] Poater, A., Cosenza, B., Correa, A., Giudice, S., Ragone, F., Scarano, V. and Cavallo, L. (**2009**), *European Journal of Inorganic Chemistry* 13: 1759.
[81] Audic, N., H. Clavier, M. Mauduit and J.-C. Guillemin (**2003**), *Journal of the American Chemical Society* 125(31): 9248.
[82] Hillier, A. C., W. J. Sommer, B. S. Yong, J. L. Petersen, L. Cavallo and S. P. Nolan (**2003**), *Organometallics* 22(21): 4322.
[83] Mathew, J., Koga, N. and Suresh, C. H. (**2008**), *Organometallics* 27: 4666.
[84] Poater, A. and Cavallo, L. (**2010**), *Journal of Molecular Catalysis* 324: 75.
[85] Poater, A., Bahri-Laleh, N. and Cavallo, L. (**2011**), *Chemical Communication* 47: 6674.
[86] Poater, A., Ragone, F., Garrido, M., Pérez, S., Poch, M., Correa, A. and Cavallo, L. (**2011**), *Procedia Computer Science* 4: 1222.
[87] Seiders, T. J., D. W. Ward and R. H. Grubbs (**2001**), *Organic Let*ters 3: 3225.
[88] Funk, T. W., J. M. Berlin and R. H. Grubbs (**2006**), *Journal of the American Chemical Society* 128(6): 1840.
[89] Bexrud, J. and M. Lautens (**2010**), *Organic Letters* 12(14): 3160.
[90] Selim, K. B., Y. Matsumoto, K.-i. Yamada and K. Tomioka (**2009**), *Angewandte Chemie International Edition* 48(46): 8733.
[91] Wurtz, S., C. Lohre, R. FroÌˆhlich, K. Bergander and F. Glorius (**2009**), *Journal of the American Chemical Society* 131(24): 8344.
[92] Jacobsen, H., A. Correa, A. Poater, C. Costabile and L. Cavallo (**2009**), *Coordination Chemistry Reviews* 253: 687.
[93] Frenking, G., M. Solà and S. F. Vyboishchikov (**2005**), *Journal of Organometallic Chemistry* 690(24-25): 6178.

[94] Jacobsen, H., A. Correa, C. Costabile and L. Cavallo (**2006**), *Journal of Organometallic Chemistry* 691(21): 4350.
[95] Fröhlich, N., Pidun, U., Stahl, M. and Frenking, G. (**1997**), *Organometallics* 16: 442.
[96] Tafipolsky, M., W. Scherer, K. Öfele, G. Artus, B. Pedersen, W. A. Herrmann and G. S. McGrady (**2002**), *Journal Of The American Chemical Society* 124(20): 5865.
[97] Hu, X. L., Castro-Rodriguez, I. and Meyer, K. (**2003**), *Organometallics* 22: 3016.
[98] Altenhoff, G., Goddard, R., Lehmann, C. W. and Glorius, F. (**2004**), *Journal of the American Chemical Society* 126: 15195.
[99] Leuthäußer, S., Schwarz, D. and Plenio, H. (**2007**), *Chemistry - A European Journal* 13: 7195.
[100] Süßner, M. and H. Plenio (**2005**), *Angewandte Chemie International Edition* 44(42): 6885-6888.
[101] Süßner, M. and H. Plenio (**2005**), *Chemical Communications* (43): 5417-5419.
[102] Credendino, R., Falivene, L. and Cavallo, L.(**2012**), *Journal of the American Chemical Society* 134: 8127.
[103] Fernández, I., Lugan, N. and Lavigne, G. (**2012**), *Organometallics* 31: 1155.
[104] Calderon, N. (**1972**), *Accounts of Chemical Research* 5(4): 127-132.
[105] Calderon, N., H. Y. Chen and K. W. Scott (**1967**), *Tetrahedron Letters* 8(34): 3327.
[106] Eleuterio, H. S. (**1991**), *Journal of Molecular Catalysis* 65(1–2): 55-61.
[107] Banks, R. L. and G. C. Bailey (**1964**), *I&EC Product Research and Development* 3(3): 170.
[108] Casey, C. P. and T. J. Burkhardt (**1974**), *Journal of the American Chemical Society* 96(25): 7808.
[109] Katz, T. J. and J. McGinnis (**1975**), *Journal of the American Chemical Society* 97(6): 1592.
[110] Grubbs, R. H., P. L. Burk and D. D. Carr (**1975**), *Journal Of The American Chemical Society* 97(11): 3265.
[111] Grubbs, R. H., D. D. Carr, C. Hoppin and P. L. Burk (**1976**), *Journal of the American Chemical Society* 98(12): 3478.
[112] Katz, T. J. (2005), *Angewandte Chemie International Edition* 44(20): 3010.
[113] Lee, S. J., J. McGinnis and T. J. Katz (**1976**), *Journal of the American Chemical Society* 98(24): 7818.
[114] Kubas Gregory, J. (**1988**), *Accounts of Chemical Research* 21(3): 120.
[115] Huang, J., E. D. Stevens, S. P. Nolan and J. L. Petersen (**1999**), *Journal of the American Chemical Society* 121(12): 2674.
[116] Poulsen, C. S. and R. Madsen (**2003**), *Synthesis* (1): 1-18.
[117] Kulkarni, A. A. and S. T. Diver (**2003**), *Organic Letters* 5(19): 3463.
[118] Clark, D. A., J. R. Clark and S. T. Diver (**2008**), *Organic Letters* 10(10): 2055.
[119] Clark, D. A., B. S. Basile, W. S. Karnofel and S. T. Diver (**2008**), *Organic Letters* 10(21): 4927.
[120] Diver, S. T., D. A. Clark and A. A. Kulkarni (**2008**), *Tetrahedron* 64(29): 6909.
[121] Giessert, A. J. and S. T. Diver (**2005**), *Organic Letters* 7: 351.
[122] Smulik, J. A. and S. T. Diver (**2001**), *Tetrahedron Letters* 42(2): 171.

[123] Galan, B. R., A. J. Giessert, J. B. Keister and S. T. Diver (**2005**), *Journal of the American Chemical Society* 127: 5762.
[124] Schramm, M. P., D. S. Reddy and S. A. Kozmin (**2001**), *Angewandte Chemie International Edition* 40: 4274.
[125] Hoye, T. R., S. M. Donaldson and T. J. Vos (**1999**), *Organic Letters* 1(2): 277.
[126] J. Tornatzky, A. Kannenberg, S. Blechert (**2012**), *Dalton Trans*. 41: 8215.
[127] V. César, S. Bellemin-LAponnaz, L. H. Gade (**2002**), *Organometallics* 21: 5204.
[128] H. Ren, P. Yao, S. Xu, H. Song, B. Wang (**2007**), *Journal of Organometallic Chem*istry 692: 2092
[129] D. Meyer, M. A. Taige, A. Zeller, K. Hohlfeld, S. Ahrens, T. Strassner (**2009**), *Organometallics* 28: 2142.
[130] Arduengo, A. J., M. Kline, J. C. Calabrese and F. Davidson (**1991**), *Journal of the American Chemical Society* 113(25): 9704.
[131] Lund, C. L., M. J. Sgro and D. W. Stephan (**2012**), *Organometallics* 31(2): 580.
[132] Weskamp, T., W. C. Schattenmann, M. Spiegler and W. A. Herrmann (**1998**), *Angewandte Chemie International Edition* 37(18): 2490.
[133] Ledoux, N., B. Allaert, A. Linden, P. Van Der Voort and F. Verpoort (**2007**), *Organometallics* 26(4): 1052.
[134] Bantreil, X., T. E. Schmid, R. A. M. Randall, A. M. Z. Slawin and C. S. J. Cazin (**2010**), *Chemical Communications* 46(38): 7115.
[135] Zhang, W., C. Bai, X. Lu and R. He (**2007**), *Journal of Organometallic Chemistry* 692(16): 3563.
[136] Sashuk, V., L. H. Peeck and H. Plenio (**2010**), *Chemistry – A European Journal* 16(13): 3983.
[137] Wolf, S. and H. Plenio (**2010**), *Journal of Organometallic Chemistry* 695(22): 2418.
[138] Vorfalt, T., S. Leuthäußer and H. Plenio (**2009**), *Angewandte Chemie International Edition* 48(28): 5191.
[139] Bantreil, X., A. Poater, C. A. Urbina-Blanco, Y. D. Bidal, L. Falivene, R. A. M. Randall, L. Cavallo, A. M. Z. Slawin and C. S. J. Cazin (**2012**), *Organometallics* 31(21): 7415.
[140] Vougioukalakis, G. C. and R. H. Grubbs (**2009**), *Chemical Reviews* 110(3): 1746.
[141] Samojłowicz, C., M. Bieniek and K. Grela (**2009**), *Chemical Reviews* 109: 3708.
[142] Zirngast, M., E. Pump, A. Leitgeb, J. H. Albering and C. Slugovc (**2011**), *Chemical Communications* 47(8): 2261.
[143] Songis, O., A. M. Z. Slawin and C. S. J. Cazin (**2012**), *Chemical Communications* 48(9).
[144] Wang, H.-Y., W.-L. Yim, Y.-L. Guo and J. O. Metzger (**2012**), *Organometallics* 31(5): 1627.
[145] Ziegler, T. (**1991**), *Chemical Reviews* 91(5): 651.
[146] Martinho Simões, J. A. and J. L. Beauchamp (**1990**), *Chemical Reviews* 90: 629.
[147] Benitez, D., E. Tkatchouk and W. A. I. Goddard (**2008**), *Chemical Communications* 6194.

[148] Stewart, I. C., D. Benitez, D. J. O'Leary, E. Tkatchouk, M. W. Day, W. A. Goddard and R. H. Grubbs (**2009**), *Journal of the American Chemical Society* 131(5): 1931.
[149] Mariz, R., A. Poater, M. Gatti, E. Drinkel, J. J. Bürgi, X. Luan, S. Blumentritt, A. Linden, L. Cavallo and R. Dorta (**2010**), *Chemistry – A European Journal* 16(48): 14335.
[150] Sanford, M. S., M. Ulman and R. H. Grubbs (**2001**), *Journal of the American Chemical Society* 123(4): 749.
[151] Conrad, J. C., D. Amoroso, P. Czechura, G. P. A. Yap and D. E. Fogg (**2003**), *Organometallics* 22(18): 3634.
[152] Conrad, J. C., H. H. Parnas, J. L. Snelgrove and D. E. Fogg (**2005**), *Journal of the American Chemical Society* 127(34): 11882.
[153] Monfette, S. and D. E. Fogg (**2006**), *Organometallics* 25(8): 1940-1944.
[154] Denk, K., J. Fridgen and W. A. Herrmann (**2002**), *Advanced Synthesis & Catalysis* 344(6-7): 666.
[155] Jordaan, M. and H. C. M. Vosloo (**2007**), *Advanced Synthesis & Catalysis* 349(1-2): 184.
[156] Samec, J. S. M. and R. H. Grubbs (**2008**), *Chemistry - A European Journal* 14(9): 2686.
[157] Tanaka, K., V. P. W. Böhm, D. Chadwick, M. Roeper and D. C. Braddock (**2006**), *Organometallics* 25(24): 5696.
[158] Krause, J. O., O. Nuyken, K. Wurst and M. R. Buchmeiser (**2004**), *Chemistry – A European Journal* 10(3): 777.
[159] O'Hagan, D. (**2008**), *Chemical Society Reviews* 37(2): 308.
[160] Pagenkopf, B. L. and E. M. Carreira (**1999**), *Chemistry – A European Journal* 5(12): 3437.
[161] Dorta, R., P. Egli, F. Zürcher and A. Togni (**1997**), *Journal of the American Chemical Society* 119(44): 10857.
[162] Krüger, J. and E. M. Carreira (**1998**), *Tetrahedron Letters* 39(39): 7013-7016.
[163] Mezzetti, A. and C. Becker (**2002**), *Helvetica Chimica Acta* 85(9): 2686-2703.
[164] Baranger, A. M. and R. G. Bergman (**1994**), *Journal Of The American Chemical Society* 116(9): 3822-3835.
[165] Poulton, J. T., M. P. Sigalas, K. Folting, W. E. Streib, O. Eisenstein and K. G. Caulton (**1994**), *Inorganic Chemistry* 33(7): 1476-.
[166] Doherty, N. M. and N. W. Hoffmann (**1991**), *Chemical Reviews* 91(4): 553.
[167] Kiplinger, J. L., T. G. Richmond and C. E. Osterberg (**1994**), *Chemical Reviews* 94(2): 373.
[168] Murphy, E. F., R. Murugavel and H. W. Roesky (**1997**), *Chemical Reviews* 97(8): 3425.
[169] Coalter, J. N., J. C. Huffman, W. E. Streib and K. G. Caulton (**2000**), *Inorganic Chemistry* 39(17): 3757.
[170] Burch, R. R., R. L. Harlow and S. D. Ittel (**1987**), *Organometallics* 6(5): 982.
[171] Steffen, A., T. Braun, B. Neumann and H.-G. Stammler (**2007**), *Angewandte Chemie* 119(45): 8828.
[172] Kaspi, A. W., A. Yahav-Levi, I. Goldberg and A. Vigalok (**2007**), *Inorganic Chemistry* 47(1): 5.

[173] Cooper, A. C., K. Folting, J. C. Huffman and K. G. Caulton (**1997**), *Organometallics* 16(4): 505.
[174] Coleman, K. S., J. Fawcett, J. H. Holloway, E. G. Hope and R. Nassar (**2001**), *Journal Of Fluorine Chemistry* 112(2): 185.
[175] Coleman, K. S., J. Fawcett, D. A. J. Harding, E. G. Hope, K. Singh and G. A. Solan (**2010**), *European Journal Of Inorganic Chemistry* 2010(26): 4130.
[176] Fawcett, J., D. A. J. Harding, E. G. Hope, K. Singh and G. A. Solan (**2010**), *Dalton Transactions* 39(44): 10781.
[177] De Meijere, A., Diedrich, F. (**2004)** "Metal-Catalyzed Cross-Coupling Reactions", 2nd ed.;Weinheim, Germany
[178] Xue, L. and Z. Lin (**2010**), *Chemical Society Reviews* 39(5): 1692.
[179] Braga, A. A. C., G. Ujaque and F. Maseras (**2006**), *Organometallics* 25(15): 3647.
[180] García-Melchor, M., M. C. Pacheco, C. Nájera, A. Lledós and G. Ujaque (**2011**), *ACS Catalysis* 2(1): 135.
[181] García-Melchor, M., A. A. C. Braga, A. Lledós, G. Ujaque and F. Maseras (**2013**), *Accounts of Chemical Researc*h 46(11): 2626.
[182] Miyaura, N. and A. Suzuki (**1995**), *Chemical Reviews* 95(7): 2457.
[183] Stille, J. K. (**1986**), *Angewandte Chemie International Edition* 25(6): 508.
[184] Negishi, E., A. O. King and N. Okukado (**1977**), *The Journal of Organic Chemistry* 42(10): 1821.
[185] Navarro, O., R. A. Kelly and S. P. Nolan (**2003**), 125(52): 16194.
[186] Marion, N., O. Navarro, J. Mei, E. D. Stevens, N. M. Scott and S. P. Nolan (**2006**), *Journal of the American Chemical Society* 128(12): 4101.
[187] Diebolt, O., P. Braunstein, S. P. Nolan and C. S. J. Cazin (**2008**), *Chemical Communications* (27): 3190.
[188] Tang, W., A. G. Capacci, X. Wei, W. Li, A. White, N. D. Patel, J. Savoie, J. J. Gao, S. Rodriguez, B. Qu, N. Haddad, B. Z. Lu, D. Krishnamurthy, N. K. Yee and C. H. Senanayake (**2010**), *Angewandte Chemie* 122(34): 6015.
[189] Wu, L., E. Drinkel, F. Gaggia, S. Capolicchio, A. Linden, L. Falivene, L. Cavallo and R. Dorta (**2011**), *Chemistry – A European Journal* 17(46): 12886.
[190] Bexrud, J. and M. Lautens, *Organic Letters* 12(14): 3160.
[191] Würtz, S., C. Lohre, R. Fröhlich, K. Bergander and F. Glorius (**2009**), *Journal of the American Chemical Society* 131(24): 8344.
[192] Wu, L., L. Falivene, E. Drinkel, S. Grant, A. Linden, L. Cavallo and R. Dorta (**2012**), *Angewandte Chemie* 124(12): 2924.
[193] Kirk, K. L. (**2008**), *Organic Process Research & Development* 12(2): 305.
[194] Purser, S., P. R. Moore, S. Swallow and V. Gouverneur (**2008**), *Chemical Society Reviews* 37(2): 320.
[195] Qiu, X.-L., X.-H. Xu and F.-L. Qing (**2010**), *Tetrahedron* 66(4): 789.
[196] Wende, R. C. and P. R. Schreiner (**2012**), *Green Chemi*stry 14(7): 1821.
[197] Jacobsen, E. N. and D. W. C. MacMillan (**201**0), *Proceedings of the National Academy of Sciences* 107(48): 20618.
[198] Grondal, C.; Jeanty, M.; Enders, D. (**2010**), *Nature Chemi*stry 2: 167.
[199] Ahrendt, K. A., C. J. Borths and D. W. C. MacMillan (**2000**), *Journal of the American Chemical Society* 122(17): 4243.

[200] Zhang, Y.; Schmitt, M.; Falivene, L.; Caporaso, L.; Cavallo, L.; Chen, E. Y.-X. (**2013**), *Journal of the American Chemical Society*, 135(47): 17925.
[201] Brown, H. A.; Waymouth, R. M. (**2013**), *Accounts of Chemical Research* DOI:10.1021/ar400072z
[202] Fevre, M., J. Pinaud, Y. Gnanou, J. Vignolle and D. Taton (**2013**), *Chemical Society Reviews* 42(5): 2142.
[203] Kiesewetter, M. K., E. J. Shin, J. L. Hedrick and R. M. Waymouth (**2010**), *Macromolecules* 43(5): 2093.
[204] Kamber, N. E., W. Jeong, R. M. Waymouth, R. C. Pratt, B. G. G. Lohmeijer and J. L. Hedrick (**2007**), *Chemical Reviews* 107(12): 5813.
[205] Jeong, W., E. J. Shin, D. A. Culkin, J. L. Hedrick and R. M. Waymouth (**2009**), *Journal of the American Chemical Society* 131(13): 4884.
[206] Dove, A. P., H. Li, R. C. Pratt, B. G. G. Lohmeijer, D. A. Culkin, R. M. Waymouth and J. L. Hedrick (**2006**), *Chemical Communications* (27): 2881.
[207] Coulembier, O., B. G. G. Lohmeijer, A. P. Dove, R. C. Pratt, L. Mespouille, D. A. Culkin, S. J. Benight, P. Dubois, R. M. Waymouth and J. L. Hedrick (**2006**), *Macromolecules* 39(17): 5617.
[208] Shin, E. J., H. A. Brown, S. Gonzalez, W. Jeong, J. L. Hedrick and R. M. Waymouth (**2011**), *Angewandte Chemie International Edition* 50(28): 6388.
[209] Sau, S. C., S. Santra, T. K. Sen, S. K. Mandal and D. Koley (**2012**), *Chemical Communications* 48(4): 555-557.
[210] Kamber, N. E., W. Jeong, S. Gonzalez, J. L. Hedrick and R. M. Waymouth (**2009**), *Macromolecules* 42(5): 1634.
[211] Jeong, W., J. L. Hedrick and R. M. Waymouth (**2007**), *Journal of the American Chemical Society* 129(27): 8414.
[212] Raynaud, J., C. Absalon, Y. Gnanou and D. Taton (**2010**), *Macromolecules* 43(6): 2814.
[213] Raynaud, J., W. N. Ottou, Y. Gnanou and D. Taton (**2010**), *Chemical Communications* 46(18): 3203.
[214] Nederberg, F., B. G. G. Lohmeijer, F. Leibfarth, R. C. Pratt, J. Choi, A. P. Dove, R. M. Waymouth and J. L. Hedrick (**2006**), *Biomacromolecules* 8(1): 153.
[215] Rodriguez, M., S. Marrot, T. Kato, S. Stérin, E. Fleury and A. Baceiredo (**2007**), *Journal of Organometallic Chemistry* 692(4): 705.
[216] Lohmeijer, B. G. G., G. Dubois, F. Leibfarth, R. C. Pratt, F. Nederberg, A. Nelson, R. M. Waymouth, C. Wade and J. L. Hedrick (**2006**), *Organic Letters* 8(21): 4683.
[217] Guo, L., S. H. Lahasky, K. Ghale and D. Zhang (**2012**), *Journal of the American Chemical Society* 134(22): 9163.
[218] Guo, L. and D. Zhang (**2009**), *Journal of the American Chemical Society* 131(50): 18072.
[219] Zhang, Y., G. M. Miyake, M. G. John, L. Falivene, L. Caporaso, L. Cavallo and E. Y. X. Chen (**2013**). *Dalton Transactions* 41(30): 9119.
[220] Zhang, Y. and E. Y. X. Chen (**2012**), *Angewandte Chemie* 124(10): 2515.
[221] Kato, T.; Ota, Y.; Matsuoka, S.-I.; Takagi, K.; Suzuki, M. J. (**2013**), *Org. Chem*. 78, 8739.

List of Publications

1. R. Credendino, L. Falivene, L. Cavallo, "π-Face Donation from the Aromatic N-Substituent of N-Heterocyclic Carbene Ligands to Metal and Its Role in Catalysis." *Journal of the American Chemical Society*, **2012**, 134, 8127-8135.

2. Chartoire, M. Lesieur, L. Falivene, A. M. Z. Slawin, L. Cavallo, C. S. J. Cazin1, S. P. Nolan, "[Pd(IPr*)(cinnamyl)Cl]: An Efficient Pre-catalyst for the Preparation of Tetra-ortho-substituted Biaryls by Suzuki–Miyaura Cross-Coupling." *Chemistry – A European Journal*, **2012**, 18, 4517-4521.

3. L. Wu, E. Drinkel, F. Gaggia, S. Capolicchio, A. Linden, L. Falivene, L. Cavallo, R. Dorta, "Room-Temperature Synthesis of Tetra-ortho-Substituted Biaryls by NHC-Catalyzed Suzuki–Miyaura Couplings." *Chemistry – A European Journal* , **2011**, 17, 12886-12890.

4. X. Bantreil, A. Poater, C. A. Urbina-Blanco, Y. D. Bidal, L. Falivene, R. A. M. Randall, L. Cavallo, A. M. Z. Slawin, C. S. J. Cazin, "Synthesis and Reactivity of Ruthenium Phosphite Indenylidene Complexes." *Organometallics*, **2012**, 31, 7415-7426.

5. L. Wu, L. Falivene, E. Drinkel, S. Grant, A. Linden, L. Cavallo, R. Dorta,"Synthesis of 3-Fluoro-3-aryl Oxindoles: Direct Enantioselective α Arylation of Amides." *Angewandte Chemie*, **2012**, 124, 2924-2927.

6. P. Wucher, P. Roesle, L. Falivene, L. Cavallo, L. Caporaso, I. Göttker-Schnetmann, S. MeckingWucher, "Controlled Acrylate Insertion Regioselectivity in Diazaphospholidine-Sulfonato Palladium(II) Complexes." *Organometallics*, **2012**, 31, 8505-8515.

7. Y. Zhang , G. M. Miyake , M. G. John , L. Falivene , L. Caporaso , L. Cavallo, E. Y.-X. ChenZhang, "Lewis pair polymerization by classical and frustrated Lewis pairs: acid, base and monomer scope and polymerization mechanism." *Dalton Transactions*, **2012**, 41, 9119-9134.

8. L. Falivene , A. Poater , C. S. J. Cazin , C. Slugovc and L. Cavallo, "Energetics of the ruthenium-halide bond in olefin metathesis (pre)catalysts." *Dalton Transactions*, **2013**, 42, 7312-7317.

9. L. Falivene, L. Cavallo, H. Jacobsenc, "Electronic Bond Tuning with Heterocyclic Carbenes". *Dalton Transacations*, **2013**, 42, 7281-7286.

10. Albert Poater, Laura Falivene, César A. Urbina-Blanco, Simone Manzini, Steven P. Nolan and Luigi Cavallo, "How does the addition of steric hindrance on a typical IPr NHC ligand affect catalytic activity in olefin metathesis?" *Dalton Transacations*, **2013**, 42, 7433-7439.

11. Boris Neuwald, Laura Falivene, Lucia Caporaso, Luigi Cavallo, Stefan Mecking "Exploring Electronic and Steric Effects on the Insertion and Polymerization Reactivity of Phosphinesulfonato Pd(II) catalysts", *Chemistry - A European Journal*, **2013**, DOI: 10.1002/chem.201301365.

12. Albert Poater, Laura Falivene, Luigi Cavallo, Antoni Llobet, Montserrat Rodríguez, Isabel Romero, Miquel Solà, "Simple and cheap steric and electronic characterization of the reactivity of Ru(II) complexes containing oxazoline ligands as epoxidation catalysts", *Chemical Physics Letters*, **2013**, 577, 142-146.

13. Alba Collado, János Balogh, Sebastien Meiries,Alexandra M. Z. Slawin, Laura Falivene, Luigi Cavallo, Steven P. Nolan, " Steric and Electronic Parameters of a Bulky yet Flexible N-HeterocyclicCarbene:1,3-Bis(2,6-bis(1-ethylpropyl)phenyl)imidazol-2-ylidene(IPent)", *Organometallics*, **2013**, 32, 3249–3252.

14. Albert Poater, Laura Falivene, César A. Urbina-Blanco, Simone Manzini, Steven P. Nolanc, Luigi Cavallo "Steric Maps to Evaluate the Role of Steric Hindrance on the IPr NHC Ligand", *Procedia Computer Science*, **2013,** 845-854.

15. Yuetao Zhang, Meghan Schmitt, Laura Falivene, Lucia Caporaso, Luigi Cavallo, Eugene Y.-X. Chen "Organocatalytic Conjugate-Addition Polymerization of Linear and Cyclic Acrylic Monomers by N-Heterocyclic Carbenes: Mechanisms of Chain Initiation, Propagation, and Termination", *Journal of the American Chemical Society*, **2013**, 135 (47), 17925–17942.

16. Meghan Schmitt, Laura Falivene, Lucia Caporaso, Luigi Cavallo, Eugene Y.-X. Chen "High-Speed Organocatalytic Polymerization of a Renewable Methylene Butyrolactone by a Phosphazene Superbase", *Polymer Chemistry*, DOI:10.1039/C3PY01579C.

17. Pierre Quevala, Claire Jahiera, Mathieu Rouena, Jean-Christophe Legeaya, Isabelle Artura, Laura Falivenec, Loic Toupetb, Christophe Crévisya, Luigi Cavallo, Olivier Baslé, Marc Mauduit “One-pot synthesis of (a)chiral Unsymmetrical Unsaturated N-Heterocyclic Carbene (U2-NHC) precursors and their related Transition-Metal Complexes”, *Angewandte Chemie*, accepted.

18. Maria Rosaria Acocella, Marco Mauro, Laura Falivene, Luigi Cavallo, Gaetano Guerra “Inverting the Diastereoselectivity of the Mukaiyama-Michael Addition with Graphite-based Catalysts.", *ACS Catalysis*, **2014**, 4, 492–496.

19. Albert Poater, Laura Falivene, Luigi Cavallo “Theoretical attempts: “In silico olefin metathesis”-how can computers help in understanding of metathesis mechanisms and in catalysts development?”, **2013**, chapter 5, Olefin Metathesis -Theory and Practice - a John Wiley & Sons, Inc.

Acknowledgements

Al termine di questo percorso un doveroso pensiero va alle persone che mi hanno accompagnato in questi anni ricchi di esperienze e di emozioni.
E' dire poco, dire grazie al Prof. Cavallo, che ha fatto sì che potessi fare tante esperienze costruttive, permettendomi di lavorare in collaborazione con università in tutta Europa e oltre, di rapportarmi ad altre realtà, anche culturalmente diverse da noi, di avermi fatta crescere anche come persona, aiutandomi a superare insicurezze e timidezza. E soprattutto grazie a tutto ciò che umanamente mi ha trasmesso per tutte le volte che è stato più di un professore.
Ringrazio la Dott. Caporaso, che mi segue amorevolmente fin dai tempi della tesi di laurea, che ha creduto in me, mi ha sostenuta negli inevitabili momenti di scoraggiamento, mi ha spronato a continuare nel campo della ricerca. Senza di Lei, cui sento di essere legata da un rapporto di profonda amicizia, probabilmente oggi non sarei qui.
Un pensiero per il Dott. Credendino, che mi ha seguito come un fratello e mi ha svelato i "misteri" della chimica computazionale.
Grazie al Dipartimento Di Chimica dell'Università di Salerno per il quale sono onorata di aver lavorato, a tutti i professori che mi hanno dato solide basi, e che hanno contribuito ad alimentare il mio amore per la chimica. Ovunque la vita mi porterà, spero di onorare sempre il Suo nome.
Un grazie "speciale" a Luca per avermi supportato e soprattutto sopportato in tutti i miei momenti di ansia e di agitazione.
Ed infine, ma non ultimo, un ringraziamento va alla mia famiglia: a mio madre, per essermi stata sempre vicina, per il suo sostegno morale e il suo immenso affetto; a mio padre, per le sue sagge e confortanti parole nei momenti di difficoltà; a mia sorella, per l'amore incommensurabile e incondizionato che mi dimostra ogni giorno. A queste tre persone che sono state e saranno sempre il mio punto di riferimento dedico questa tesi.